Applications of **Lock-in Amplifiers in Optics**

Tutorial Texts Series

- *Low-Level Light Therapy: Photobiomodulation*, Michael R. Hamblin, Ying-Ying Huang, Cleber Ferraresi, James D. Carroll, and Lucas Freitas de Freitas, Vol. TT115
- *Fiber Bragg Gratings: Theory, Fabrication, and Applications*, Marcelo M. Werneck, Regina C. Allil, and Fábio V. B. de Nazaré, Vol. TT114
- *Automatic Target Recognition, Second Edition*, Bruce J. Schachter, Vol. TT113
- *Powering Laser Diode Systems*, Grigoriy A. Trestman, Vol. TT112
- *Optics Using MATLAB®*, Scott W. Teare, Vol. TT111
- *Plasmonic Optics: Theory and Applications*, Yongqian Li, Vol. TT110
- *Design and Fabrication of Diffractive Optical Elements with MATLAB®*, A. Vijayakumar and Shanti Bhattacharya, Vol. TT109
- *Energy Harvesting for Low-Power Autonomous Devices and Systems*, Jahangir Rastegar and Harbans S. Dhadwal, Vol. TT108
- *Practical Electronics for Optical Design and Engineering*, Scott W. Teare, Vol. TT107
- *Engineered Materials and Metamaterials: Design and Fabrication*, Richard A. Dudley and Michael A. Fiddy, Vol. TT106
- *Design Technology Co-optimization in the Era of Sub-resolution IC Scaling*, Lars W. Liebmann, Kaushik Vaidyanathan, and Lawrence Pileggi, Vol. TT104
- *Special Functions for Optical Science and Engineering*, Vasudevan Lakshminarayanan and L. Srinivasa Varadharajan, Vol. TT103
- *Discrimination of Subsurface Unexploded Ordnance*, Kevin A. O'Neill, Vol. TT102
- *Introduction to Metrology Applications in IC Manufacturing*, Bo Su, Eric Solecky, and Alok Vaid, Vol. TT101
- *Introduction to Liquid Crystals for Optical Design and Engineering*, Sergio Restaino and Scott Teare, Vol. TT100
- *Design and Implementation of Autostereoscopic Displays*, Byoungho Lee, Soon-gi Park, Keehoon Hong, and Jisoo Hong, Vol. TT99
- *Ocean Sensing and Monitoring: Optics and Other Methods*, Weilin Hou, Vol. TT98
- *Digital Converters for Image Sensors*, Kenton T. Veeder, Vol. TT97
- *Laser Beam Quality Metrics*, T. Sean Ross, Vol. TT96
- *Military Displays: Technology and Applications*, Daniel D. Desjardins, Vol. TT95
- *Interferometry for Precision Measurement,* Peter Langenbeck, Vol. TT94
- *Aberration Theory Made Simple, Second Edition*, Virendra N. Mahajan, Vol. TT93
- *Modeling the Imaging Chain of Digital Cameras*, Robert D. Fiete, Vol. TT92
- *Bioluminescence and Fluorescence for* In Vivo *Imaging*, Lubov Brovko, Vol. TT91
- *Polarization of Light with Applications in Optical Fibers*, Arun Kumar and Ajoy Ghatak, Vol. TT90
- *Digital Fourier Optics: A MATLAB Tutorial*, David G. Voeltz, Vol. TT89
- *Optical Design of Microscopes*, George Seward, Vol. TT88
- *Analysis and Evaluation of Sampled Imaging Systems*, Richard H. Vollmerhausen, Donald A. Reago, and Ronald Driggers, Vol. TT87
- *Nanotechnology: A Crash Course*, Raúl J. Martin-Palma and Akhlesh Lakhtakia, Vol. TT86
- *Direct Detection LADAR Systems*, Richard Richmond and Stephen Cain, Vol. TT85
- *Optical Design: Applying the Fundamentals*, Max J. Riedl, Vol. TT84
- *Infrared Optics and Zoom Lenses, Second Edition*, Allen Mann, Vol. TT83
- *Optical Engineering Fundamentals, Second Edition*, Bruce H. Walker, Vol. TT82
- *Fundamentals of Polarimetric Remote Sensing*, John Schott, Vol. TT81
- *The Design of Plastic Optical Systems*, Michael P. Schaub, Vol. TT80
- *Radiation Thermometry: Fundamentals and Applications in the Petrochemical Industry*, Peter Saunders, Vol. TT78
- *Matrix Methods for Optical Layout*, Gerhard Kloos, Vol. TT77
- *Fundamentals of Infrared Detector Materials*, Michael A. Kinch, Vol. TT76
- *Practical Applications of Infrared Thermal Sensing and Imaging Equipment, Third Edition*, Herbert Kaplan, Vol. TT75
- *Bioluminescence for Food and Environmental Microbiological Safety*, Lubov Brovko, Vol. TT74
- *Introduction to Image Stabilization*, Scott W. Teare and Sergio R. Restaino, Vol. TT73

(For a complete list of Tutorial Texts, see http://spie.org/publications/books/tutorial-texts.)

Applications of **Lock-in Amplifiers in Optics**

Gerhard Kloos

Tutorial Texts in Optical Engineering
Volume TT117

SPIE PRESS
Bellingham, Washington USA

Library of Congress Cataloging-in-Publication Data

Names: Kloos, Gerhard, 1966- author.
Title: Applications of lock-in amplifiers in optics / Gerhard Kloos.
Other titles: Tutorial texts in optical engineering ; v. TT 117.
Description: Bellingham, Washington, USA : SPIE Press, [2018] | Series: Tutorial texts in optical engineering ; volume TT 117 | Includes bibliographical references and index.
Identifiers: LCCN 2017052017 | ISBN 9781510617087 (softcover ; alk. paper) | ISBN 1510617086 (softcover ; alk. paper) | ISBN 9781510617094 (PDF) | ISBN 1510617094 (PDF) | ISBN 9781510617100 (ePub) | ISBN 1510617108 (ePub) | ISBN 9781510617117 (Kindle) | ISBN 1510617116 (Kindle)
Subjects: LCSH: Lock-in amplifiers. | Optical instruments. | Signal processing.
Classification: LCC TK7871.58.L57 K56 2018 | DDC 621.36–dc23 LC record available at https://lccn.loc.gov/2017052017

Published by

SPIE
P.O. Box 10
Bellingham, Washington 98227-0010 USA
Phone: +1 360.676.3290
Fax: +1 360.647.1445
Email: books@spie.org
Web: http://spie.org

Printed in the United States of America.
First Printing.
For updates to this book, visit http://spie.org and type "TT117" in the search field.

Introduction to the Series

Since its inception in 1989, the Tutorial Texts (TT) series has grown to cover many diverse fields of science and engineering. The initial idea for the series was to make material presented in SPIE short courses available to those who could not attend and to provide a reference text for those who could. Thus, many of the texts in this series are generated by augmenting course notes with descriptive text that further illuminates the subject. In this way, the TT becomes an excellent stand-alone reference that finds a much wider audience than only short course attendees.

Tutorial Texts have grown in popularity and in the scope of material covered since 1989. They no longer necessarily stem from short courses; rather, they are often generated independently by experts in the field. They are popular because they provide a ready reference to those wishing to learn about emerging technologies or the latest information within their field. The topics within the series have grown from the initial areas of geometrical optics, optical detectors, and image processing to include the emerging fields of nanotechnology, biomedical optics, fiber optics, and laser technologies. Authors contributing to the TT series are instructed to provide introductory material so that those new to the field may use the book as a starting point to get a basic grasp of the material. It is hoped that some readers may develop sufficient interest to take a short course by the author or pursue further research in more advanced books to delve deeper into the subject.

The books in this series are distinguished from other technical monographs and textbooks in the way in which the material is presented. In keeping with the tutorial nature of the series, there is an emphasis on the use of graphical and illustrative material to better elucidate basic and advanced concepts. There is also heavy use of tabular reference data and numerous examples to further explain the concepts presented. The publishing time for the books is kept to a minimum so that the books will be as timely and up-to-date as possible. Furthermore, these introductory books are competitively priced compared to more traditional books on the same subject.

When a proposal for a text is received, each proposal is evaluated to determine the relevance of the proposed topic. This initial reviewing process has been very helpful to authors in identifying, early in the writing process, the need for additional material or other changes in approach that would serve to strengthen the text. Once a manuscript is completed, it is peer reviewed to ensure that chapters communicate accurately the essential ingredients of the science and technologies under discussion.

It is my goal to maintain the style and quality of books in the series and to further expand the topic areas to include new emerging fields as they become of interest to our reading audience.

James A. Harrington
Rutgers University

Contents

Preface

Lock-in amplifiers are key devices in numerous instruments used in the optical sciences and in optical equipment in industry. In many experimental configurations, they represent the means to reliably detect and record very small or weak signals that are superimposed by noise.

The purpose of this text is to provide a step-by-step introduction to the technique of phase-sensitive detection using lock-in amplifiers, and to provide examples of its applications in optical instruments. The book begins by explaining the basics of how modulation is used to extract a signal from noise. Different types of modulation are discussed in detail and are compared. The book then presents the various applications of lock-in amplifiers in optical instruments, and the focus shifts from electronics to optics.

Some of the covered optical applications of lock-in amplifiers are optical spectroscopy, including absorption spectroscopy, fluorescence spectroscopy, and phosphorescence spectroscopy; optical interferometry, including detailed presentations of the various spectrometers used with lock-in amplifiers; crystal research and technology, including explanations of magneto-optical, electro-mechanical, and electro-optical effects; infrared thermography; laser wavelength stabilization; and advanced microscopy.

The book is intended for readers who want to better understand instruments and experiments based on lock-in detection and/or to design (and perform) new experiments in which lock-in amplifiers are applied.

Gerhard Kloos
January 2018

Chapter 1
Introduction

Lock-in amplifiers are electronic devices that are often applied in the optical sciences. They represent versatile instruments that can be adapted to a variety of measurement tasks. The purpose of a lock-in amplifier is to recover small or weak signals that would otherwise be lost in noise. This device serves to detect the amplitude of a signal s that is superimposed by noise (Fig. 1.1). The instrument can be considered as a highly selective amplifier that operates as a bandpass filter, the central frequency of which is determined by the reference signal (Fig. 1.2).

A measurement can be affected by white noise and $1/f$ noise. These terms were coined considering the noise spectrum in the frequency domain. White

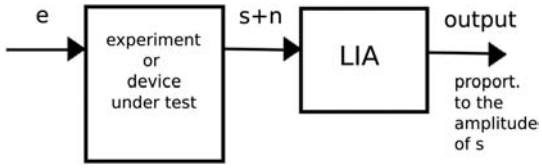

Figure 1.1 An excitation signal *e* serves as input to the experiment or to the device under test. The output signal is superimposed by noise *n*. The lock-in amplifier (LIA) generates an output signal that is proportional to the amplitude of the signal *s*.

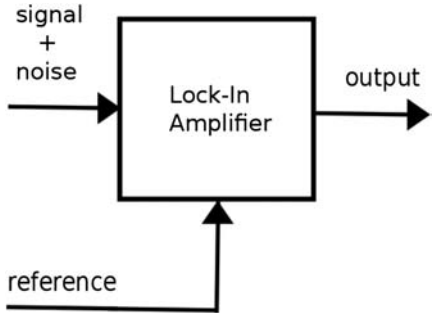

Figure 1.2 To be able to discriminate the signal from noise, it is essential to provide a reference signal to the lock-in amplifier that carries information on the signal *s*.

noise refers to the noise contribution that is constant with respect to frequency, whereas $1/f$ noise shows a steep decrease from low to high frequencies. It is advantageous to have a signal with a frequency outside of the range where $1/f$ noise is predominant. Lock-in detection allows the frequencies at which the amplifier operates to move away from regions dominated by $1/f$ noise. Noise rejection is performed using an electronic unit that mainly consists of a multiplier and an electronic filter, which acts as an integrator. It is essential to the operation of a lock-in amplifier that the signal and the reference be modulated periodically.

Lock-in detection can be applied to the measurement of nonperiodic quantities by introducing an additional device into the measurement setup. In the setup shown in Fig. 1.3, a chopper is used for this purpose. The chopper wheel interrupts the light path periodically. A signal is derived that bears information on the frequency and phase of the modulation. The signal is fed into the lock-in amplifier and serves as a reference (Fig. 1.4).

A lock-in unit detects the signal based on modulation at some known frequency. In a nutshell, a lock-in amplifier is an instrument that receives an input voltage

$$u_{in} = u_0 \sin(\omega t + \phi) + u_{noise} \tag{1.1}$$

and performs the operation of providing a DC output voltage

$$u_{out} \propto u_0 \cos(\phi) \tag{1.2}$$

that is proportional to the amplitude of the sinusoidal signal and the cosine of the phase. The lock-in amplifier serves to extract the signal from noise.

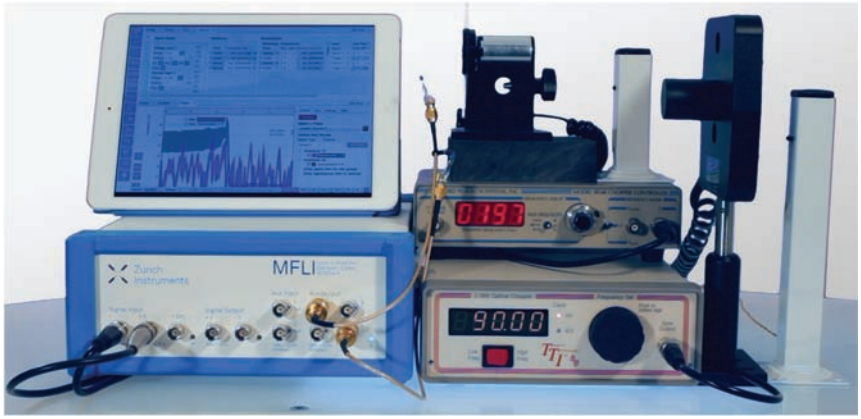

Figure 1.3 Measurement of the intensity of LEDs using lock-in amplifiers. (Courtesy of Zurich Instruments, used with permission.)

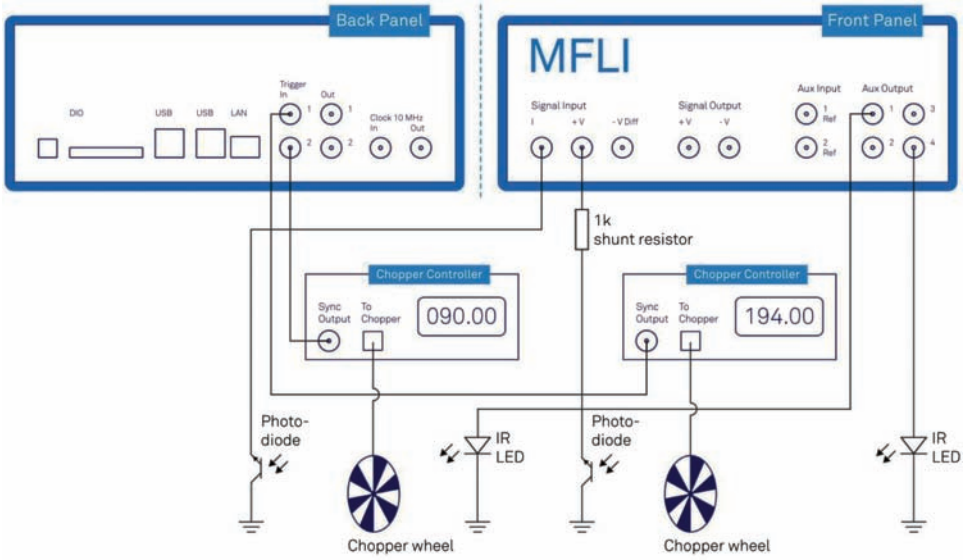

Figure 1.4 The measured signals and the corresponding references are fed into the lock-in amplifiers. (Courtesy of Zurich Instruments, used with permission.)

Chapter 2
Basic Concepts

Generating a reference signal is an important prerequisite for operation of a lock-in amplifier, and a phase-locked loop is usually employed for this purpose. Therefore, we look at this feedback system first and then consider the working principle of the multiplication-and-integration unit in detail.

In the signal path of the lock-in amplifier, the multiplication-and-integration unit is preceded by the front end, which comprises amplifiers and filters. In the reference path, the multiplication-and-integration unit is preceded by the reference channel, which comprises a phase-locked loop and a phase shifter.

2.1 Phase-Locked Loop

To detect the signal, the lock-in reference frequency has to be made the same as the signal frequency. In addition, the phase difference between the lock-in reference and the signal cannot change with time because a DC signal is to be obtained. To achieve this, the reference of the lock-in amplifier has to be phase-locked to the signal.

In lock-in amplifiers, a phase-locked loop (sometimes called a phase lock loop) is used to track the dominant frequency of the reference. The phase-locked loop[1] is a feedback system that has the purpose of synchronizing the frequency (and phase) of an oscillator to a given input signal. A phase-locked loop represents a core component of lock-in amplifiers and can also be found in other electronic devices, such as USB sticks, for example.

The phase-locked loop generates the reference signal in the lock-in unit. It "locks" the internal reference oscillator to the external reference, generating a sine wave with a fixed phase shift. It is this feature that has given the name to the lock-in technique. The phase-locked loop actively tracks the external reference. In other words, a phase-locked loop is used in lock-in amplifiers to generate a stable local oscillator that serves as a reference.

The feedback loop is shown schematically in Fig. 2.1. In the phase detector, the input signal (synchronization signal) and a reference signal are compared with respect to phase. The phase detector generates an error signal

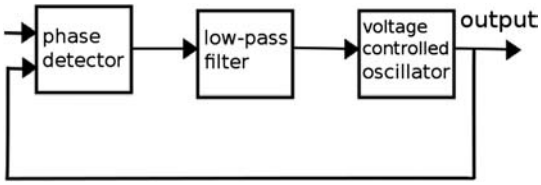

Figure 2.1 Phase-locked loop.

that (in a good approximation) is proportional to the phase difference between both signals. The error signal is a superposition of a DC component and an AC component. Because we are interested in the DC part, a low-pass filter is used to block the AC part.

The filtered signal is then fed back into the servo loop and serves as the input to a voltage-controlled oscillator. This signal is used to tune the frequency ω_2 of the voltage-controlled oscillator as described by

$$\omega_2 = \omega_0 + K \cdot (\phi_1 - \phi_2), \tag{2.1}$$

where ω_0 is a characteristic frequency of the oscillator, ϕ_1 is the phase of the input signal, ϕ_2 is the phase of the reference signal, and K is a proportionality constant. The second part of the sum represents the variable portion that is fed back into the servo loop. The loop can now be closed by taking the harmonic output signal of the voltage-controlled oscillator (VCO) as a reference signal and comparing it to the input signal using the phase detector.

To understand the working principle, let us now follow a signal around the loop: If both signals are not in phase when they enter the phase detector, a nonzero output of the low-pass filter causes the VCO to oscillate faster or slower, depending on the sign of the feedback signal. This changes the phase of the reference voltage accordingly. The process of tuning the frequency is continued until the VCO does not detect a difference in phase. At this point, the frequency of the VCO is the same as the frequency of the input signal.

To more clearly explain why locking the phase of the two signals implies equal frequencies, it might be helpful to make use of the race car analogy. Let us imagine a closed race car track on which different drivers compete in a race (Fig. 2.2). The number of laps per hour, which is a measure of a car's velocity,

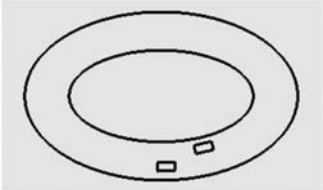

Figure 2.2 Race car analogy—closed track.

corresponds to the frequency in this analogy. In case of an accident, a pace car is employed to set a constant speed. The other drivers try to go fast, but they cannot to go faster than the pace car. After a while, they will go around the track at a constant distance from the pace car (phase). This implies that they will adopt the speed of this car (frequency).

An analogy can also be made between a tuning fork (Fig. 2.3) and a feature of a lock-in amplifier (Fig. 2.4). A tuning fork is a device used by musicians as a reference to tune the strings of their instruments (to a given frequency). Tuning a guitar string, the guitarist listens for the beat frequency between the tuning fork (the reference signal) and the guitar string. The tuning

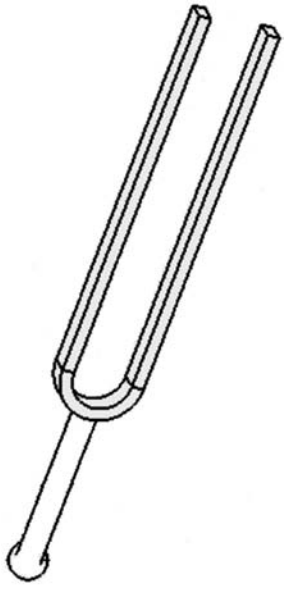

Figure 2.3 Tuning fork.

Figure 2.4 Compact lock-in amplifier. (Courtesy of Femto, used with permission.)

is repeated until the guitar string vibrates with the same frequency as the tuning fork.

2.2 Multiplication and Filtering

Figure 2.5 shows the circuit board of a lock-in amplifier, the core of which consists of a multiplier and a low-pass filter (Fig. 2.6). The signal (plus noise) and the reference signal are multiplied, and the resulting signal is then filtered to block off contributions from higher frequencies.[2–4]

Figure 2.7 shows the generic scheme involved in taking a measurement using a lock-in amplifier. The form of the periodic signal and of the reference can vary. The periodic signal from the oscillator forms the input (excitation) e of the experiment. This gives rise to an output s of the experiment that is superimposed by noise n.

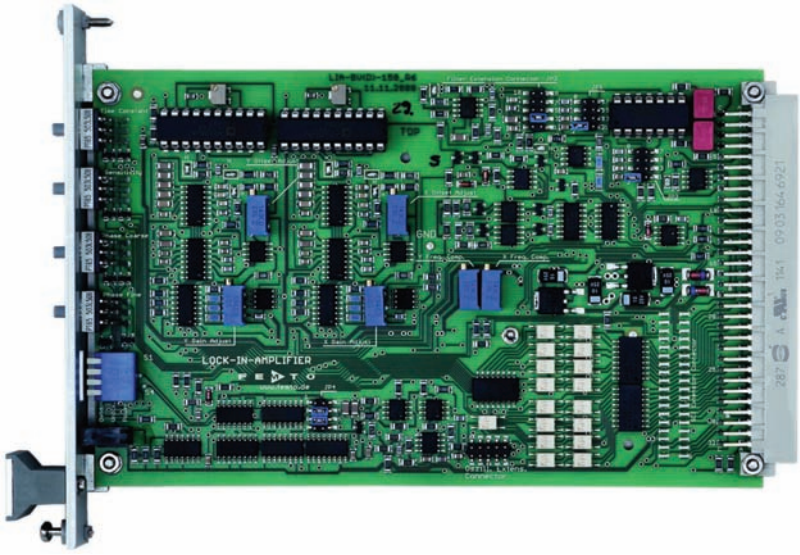

Figure 2.5 The electronic circuit board of a lock-in amplifier. (Courtesy of Femto, used with permission.)

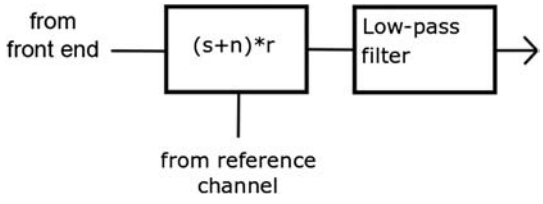

Figure 2.6 Multiplication unit and low-pass filter. Here, the signal (plus noise) from the front end and the reference from the reference channel (phase-lock loop, phase shifter) are combined.

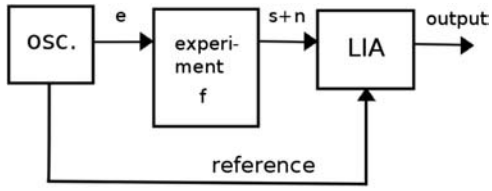

Figure 2.7 Measurement taken with a lock-in amplifier. The reference signal provides information on the frequency of the signal.

2.2.1 Sinusoidal signal and reference

The simplest case is when both the signal and the reference are sinusoidal, and the experiment can be represented by a linear transfer function. This experimental situation is depicted in Fig. 2.8: An oscillator provides a sinusoidal excitation to an experiment. The response that is fed to the lock-in amplifier is a superposition of a sinusoidal signal s and a noise contribution n. In order to be able to gain information on the signal s, a reference signal r is derived from the oscillator that is used as a second input signal to the lock-in amplifier. The reference signal contains information on the frequency of the excitation signal.

The reference signal r can be denoted as a function of time t:

$$r = A \sin \omega t, \tag{2.2}$$

where $\omega = 2\pi f$, and A is the amplitude of the reference signal. If the signal s features a phase shift ϕ with respect to the reference signal, then s can be written as

$$s = a_1 \sin(\omega t + \phi), \tag{2.3}$$

where a_1 denotes the amplitude of the reference signal.

The input of the lock-in amplifier is a superposition of the signal and noise. In the multiplication-and-filter unit (Fig. 2.6), the superposition of the

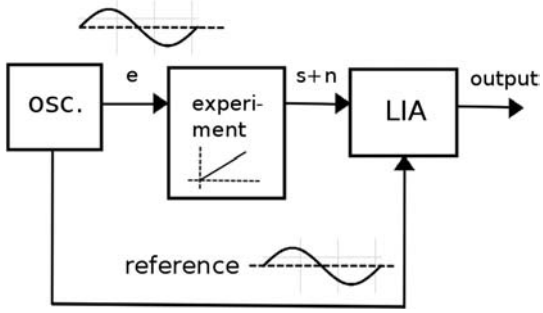

Figure 2.8 Lock-in detection experiment featuring a linear transfer function and a sinusoidal signal and reference.

signal and noise is combined with the reference. The low-pass filter corresponds to an averaging process. We can therefore describe the output u of the lock-in amplifier by

$$u = \frac{1}{\tau}\int_0^{\tau} (s+n)\cdot r\,dt, \tag{2.4}$$

where τ is the time constant of the low-pass filter. After multiplication, the noise is suppressed by the low-pass filter according to

$$\frac{1}{\tau}\int_0^{\tau} n\cdot r\,dt = 0. \tag{2.5}$$

This noise-rejection capability is a salient feature of a lock-in amplifier. The product of the signal and reference is

$$s\cdot r = a_1 A\sin(\omega t+\phi)\sin\omega t. \tag{2.6}$$

The trigonometric relation

$$\sin x\sin y = \frac{1}{2}[\cos(x-y)-\cos(x+y)]$$

is used to simplify Eq. (2.6) to

$$s\cdot r = \frac{a_1 A}{2}[\cos(-\phi)-\cos(2\omega t+\phi)]. \tag{2.7}$$

This product is then processed by the low-pass filter with the time constant τ:

$$u = \frac{1}{\tau}\int_0^{\tau} s\cdot r\,dt. \tag{2.8}$$

Therefore, we have as the output of the low-pass filter

$$u = \frac{a_1 A}{2\tau}\int_0^{\tau}\cos\phi\,dt - \frac{a_1 A}{2\tau}\int_0^{\tau}\cos(2\omega t+\phi)dt. \tag{2.9}$$

If the integration time is sufficiently long, the positive and negative contributions in the second integral will cancel out because the integrand is a periodic function. It must be stated that there is an idealization in this mathematical derivation. The response of the low-pass filter is described as a rectangular function even though in reality it has a more complicated form.

This is done to keep the derivation simple. The integrand in the first integral, on the other hand, is constant:

$$u = \frac{a_1 A}{2\tau} \int_0^{\tau} \cos\phi \, dt = \frac{a_1 A}{2} \cos\phi. \tag{2.10}$$

In this way, an output voltage is generated that is proportional to the amplitude a_1 of the signal and to the cosine of the phase shift between the reference and the signal.

Equation (2.10) reflects the situation in which the frequencies of the signal and the reference are the same. It is interesting to look at the more general case to see what happens if the two factors of the product in Eq. (2.7) have different frequencies. For this purpose, we introduce the symbol Ω into Eq. (2.2) for the reference:

$$r = A \sin \Omega t, \tag{2.11}$$

while the definition of the signal is kept unchanged:

$$s = a_1 \sin(\omega t + \phi). \tag{2.12}$$

Before integration, the phase term is separated into the product of the two functions:

$$s \cdot r = a_1 A \sin(\omega t + \phi) \sin \Omega t. \tag{2.13}$$

To this end, we make use of the trigonometric identity

$$\sin(x + y) = \sin x \cos y + \cos x \sin y$$

and apply it to the signal term. This gives

$$s \cdot r = a_1 A(\sin \omega t \cdot \cos\phi \cdot \sin \Omega t + \cos \omega t \cdot \sin\phi \cdot \sin \Omega t). \tag{2.14}$$

To proceed, we use two other trigonometric relations, namely,

$$\sin x \cdot \sin y = \frac{1}{2}[\cos(x - y) - \cos(x + y)]$$
$$\cos y \cdot \sin x = \frac{1}{2}[\sin(x - y) + \sin(x + y)].$$

In this way, we obtain a sum of two longer terms, in which the phase ϕ is separated:

$$s \cdot r = \frac{a_1 A}{2} \cos\phi[\cos(\omega - \Omega)t - \cos(\omega + \Omega)t] + \frac{a_1 A}{2} \sin\phi[\sin(\Omega - \omega)t + \sin(\omega + \Omega)t]. \quad (2.15)$$

With the product of the signal and reference thus re-arranged, integration with a sufficiently high time constant τ is performed:

$$u = \frac{1}{\tau} \int_0^\tau s \cdot r \, dt. \quad (2.16)$$

The periodic terms cancel out during this integration process. Only a nonzero DC part in the sum will contribute to the output voltage. This is the case where the argument of the cosine function is zero, i.e., where $\omega = \Omega$. Therefore, we obtain

$$u = \frac{a_1 A}{2\tau} \cos\phi \int_0^\tau \cos(0) \, dt \quad (2.17)$$

and, finally,

$$u = \frac{a_1 A}{2} \cos\phi. \quad (2.18)$$

Even though we considered the more general situation this time, we obtained the same result as when the frequency of the signal and the reference were the same.

2.2.2 Square-wave signal and reference

In the previous section, we looked at sine waves as signal and reference inputs of the instrument. Lock-in amplifiers can also be operated using square waves as the signal and reference. Different square waves are used in experimental setups; here we consider mark-space square waves and bipolar square waves.

2.2.2.1 Mark-space square wave

A mark-space square wave can be generated by repeatedly switching a DC signal on and off (Fig. 2.9). (The term mark-space square wave is used in the literature to distinguish it from a bipolar square wave.) A divided definition is necessary to describe such a function:

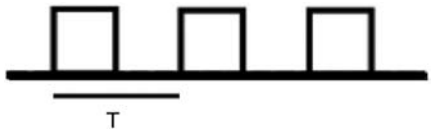

Figure 2.9 Mark-space square wave.

$$r = A\left\{\begin{array}{ll} +1 & \left[0, \frac{T}{2}\right] \\ 0 & \left[\frac{T}{2}, T\right] \end{array}\right\}, \tag{2.19}$$

where T is used to indicate a period of time; it represents the length of the time interval, which is repeated periodically to form the pulse train.

The function takes a value of 1 on the first interval and is 0 on the second interval. This pattern is repeated periodically. The pattern of the signal is similar. In the special case where the patterns coincide completely, the signal is denoted as

$$s = a_1\left\{\begin{array}{ll} +1 & \left[0, \frac{T}{2}\right] \\ 0 & \left[\frac{T}{2}, T\right] \end{array}\right\}. \tag{2.20}$$

We now consider the more general case where there is a time difference p between both pulses. To determine the lock-in amplifier output

$$u = \frac{1}{T}\int_0^T sr\,dt \tag{2.21}$$

it is convenient to distinguish between the two cases. In the first case, the time difference p of the rising edge of the square wave of the reference and the signal is smaller than $T/2$. This corresponds to the situation depicted in Fig. 2.10.

Because we are dealing with squares, the result of the integration can be directly concluded from Fig. 2.10:

$$u = \frac{1}{T}a_1 A\left(\frac{T}{2} - p\right) \text{ for } p \in \left[0, \frac{T}{2}\right]. \tag{2.22}$$

Interpreted as a function of p, u is a straight line with a negative slope on the given interval.

In the second case, the time difference p of the rising edge of the square wave of the reference and the signal is greater than $T/2$, as illustrated in Fig. 2.11. These results were derived for the interval $p \in [0, T/2]$. By an

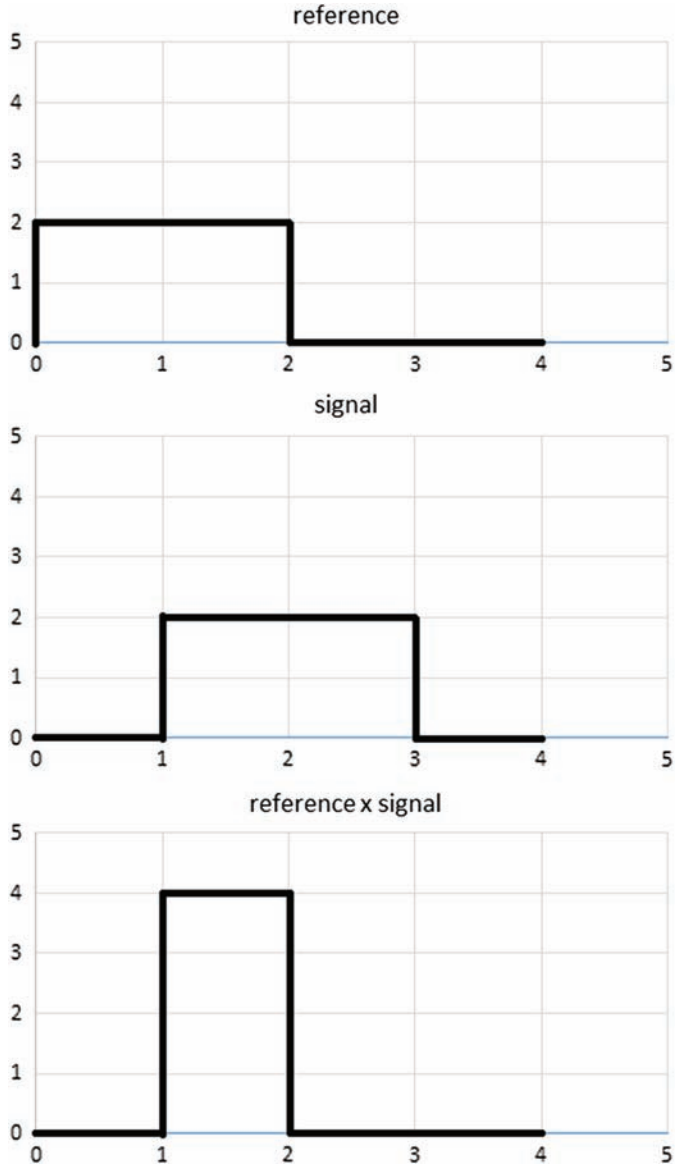

Figure 2.10 Multiplying mark-space square waves: first case.

analogous consideration, we obtain the following result for the other interval, where $p \in [T/2,\ T]$:

$$u = \frac{1}{T} a_1 A \left(p - \frac{T}{2} \right) \text{ for } p \in \left[\frac{T}{2}, T \right]. \tag{2.23}$$

This is again a straight line, but now with a positive slope. Equations (2.22) and (2.23) can be combined to obtain a result for the output signal generated by multiplying and integrating two mark-space square waves:

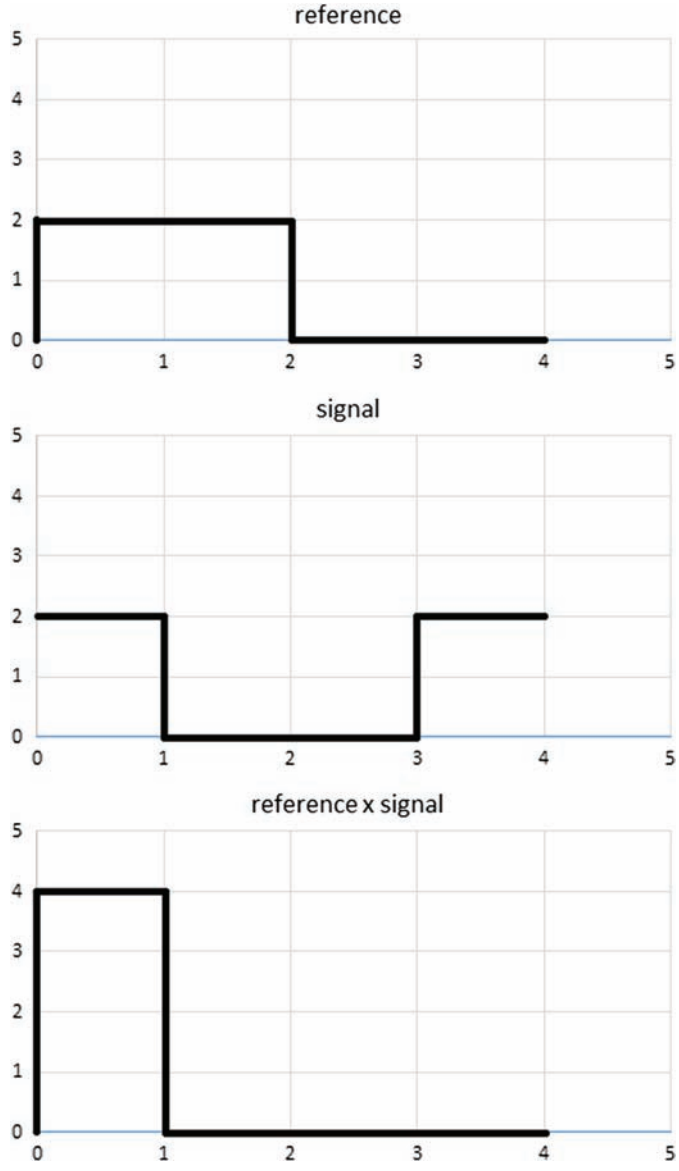

Figure 2.11 Multiplying mark-space square waves: second case.

$$u = \frac{a_1 A}{T} \left\{ \begin{array}{ll} \frac{T}{2} - p & \left[0, \frac{T}{2}\right] \\ p - \frac{T}{2} & \left[\frac{T}{2}, T\right] \end{array} \right\}. \tag{2.24}$$

The function is plotted in Fig. 2.12 for an interval that corresponds to one period.

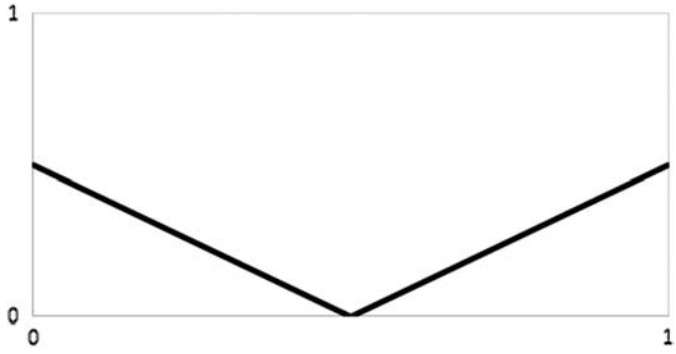

Figure 2.12 Multiplying mark-space square waves: output u versus phase parameter p. The amplitudes are normalized: $a_1 = 1$ and $A = 1$.

2.2.2.2 Bipolar square wave

A bipolar square wave is generated by repeatedly changing the polarity of a DC signal (Fig. 2.13). Again, a divided definition of the function on the interval [0, T] is used:

$$r = A\left\{\begin{array}{ll} +1 & \left[0, \frac{T}{2}\right] \\ -1 & \left[\frac{T}{2}, T\right] \end{array}\right\}. \tag{2.25}$$

This interval is the part of the square wave that is repeated periodically. A bipolar square wave might be considered as a mark-space square wave with twice the amplitude plus a negative DC offset.

To calculate the output of the lock-in amplifier for these slightly differing pulse forms, we distinguish between two different cases, as we did previously. Let us again choose as the first case the situation where the time difference p of the rising edge of the square wave of the reference and the signal is smaller than $T/2$. We can refer to Fig. 2.14 as the starting point of the integration.

We simply collect the contributions of the different rectangles; it is important to the take the correct sign into account:

$$u = \frac{1}{T}\left[(-a_1 A)p + a_1 A\left(\frac{T}{2} - p\right) + (-a_1 A)p + a_1 A\left(\frac{T}{2} - p\right)\right]$$
$$\text{for } p \in \left[0, \frac{T}{2}\right]. \tag{2.26}$$

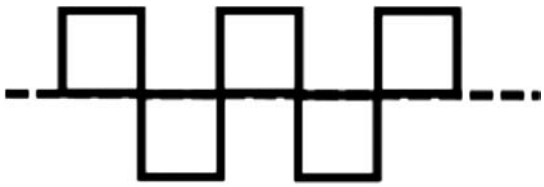

Figure 2.13 Bipolar square wave.

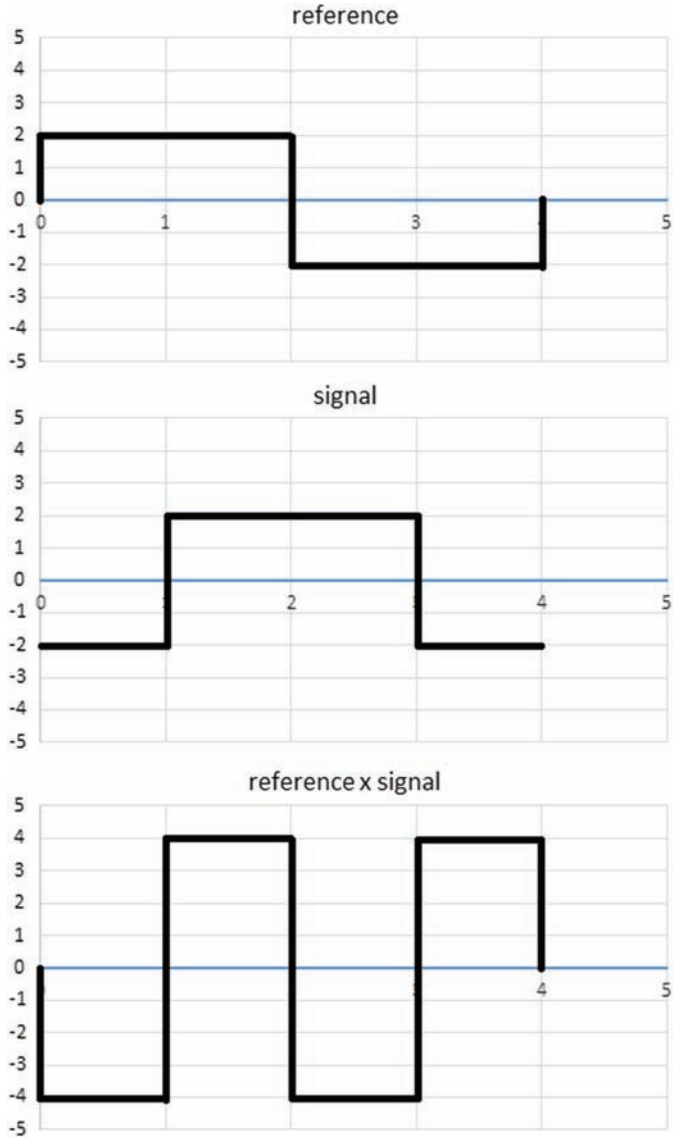

Figure 2.14 Multiplying bipolar square waves: first case.

This expression can be written in a more compact form:

$$u = \frac{1}{T} a_1 A(T - 4p) \quad \text{for } p \in \left[0, \frac{T}{2}\right]. \tag{2.27}$$

The complementary case is where the time difference p of the rising edge of the square wave of the reference and of the signal is greater than $T/2$. Fig. 2.15 illustrates this situation.

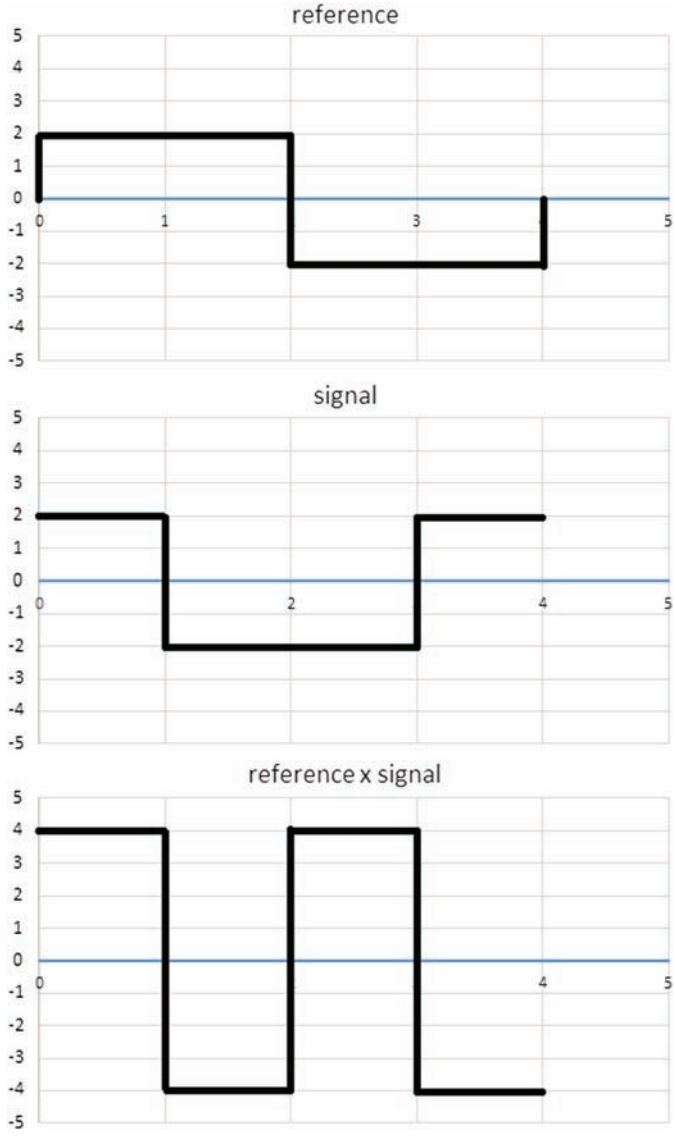

Figure 2.15 Multiplying bipolar square waves: second case.

Again, we can sum the rectangles to perform the integration:

$$u = \frac{1}{T} a_1 A \left[p - \frac{T}{2} - (T - p) + p - \frac{T}{2} - (T - p) \right] \text{ for } p \in \left[0, \frac{T}{2} \right]. \quad (2.28)$$

Some terms cancel out, and we obtain

$$u = \frac{1}{T} a_1 A(4p - 3T) \text{ for } p \in \left[0, \frac{T}{2}\right]. \tag{2.29}$$

The results for the separate intervals can be combined to describe the output on the complete interval:

$$u = \frac{a_1 A}{T} \left\{ \begin{array}{ll} T - 4p & \left[0, \frac{T}{2}\right] \\ 4p - 3T & \left[\frac{T}{2}, T\right] \end{array} \right\}. \tag{2.30}$$

This is again a combination of two straight lines with opposite slopes. Equation (2.30) is illustrated in Fig. 2.16.

2.2.2.3 Mark-space square wave and bipolar square wave

For completeness, the result obtained from a mark-space square wave as a signal, and a bipolar square wave as a reference, is also provided. This can be derived in the same way as before by adding the rectangles of the product function and taking the correct sign into account:

$$u = \frac{a_1 A}{T} \left\{ \begin{array}{ll} \frac{T}{2} - 2p & \left[0, \frac{T}{2}\right] \\ 2p - \frac{3T}{2} & \left[\frac{T}{2}, T\right] \end{array} \right\}. \tag{2.31}$$

A graph of this formula is provided in Fig. 2.17.

2.2.2.4 Comparison

At this point, it is convenient to compare the results obtained for the different types of square waves. This can be done using the graphical representation in Fig. 2.18. The solid lines show the dependence on parameter p for a combination of two mark-space square waves. The dashed lines represent the corresponding function when two bipolar square waves are combined. The

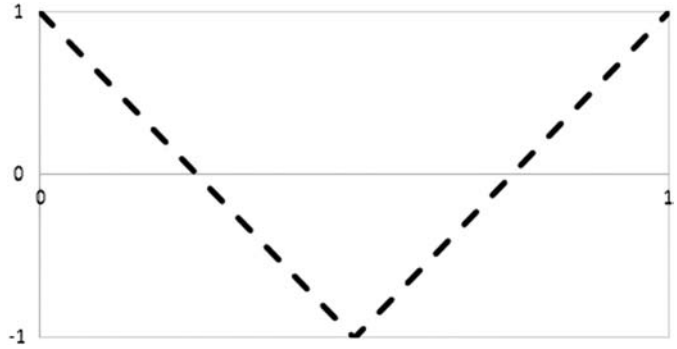

Figure 2.16 Multiplying bipolar square waves: output u versus phase parameter p. The amplitudes are normalized: $a_1 = 1$ and $A = 1$.

Figure 2.17 Multiplying mark-space and bipolar square waves: output u versus phase parameter p. The amplitudes are normalized: $a_1 = 1$ and $A = 1$.

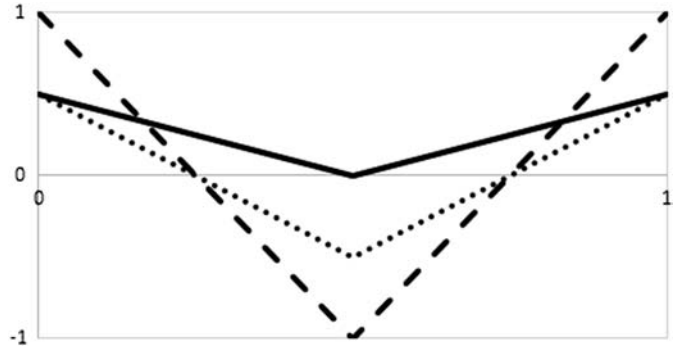

Figure 2.18 Multiplying square waves: output u versus phase parameter p. The amplitudes are normalized: $a_1 = 1$ and $A = 1$.

dotted lines between the solid and dashed lines show the relation if the signal is a mark-space square wave and the reference is a bipolar square wave. The graph is composed of straight lines with opposite slopes. In all three cases, the output of the lock-in amplifier is at its maximum if one of the conditions $p = 0$ or $p = T$ is met. Its output is at a minimum if $p = T/2$ holds.

2.2.3 Square-wave reference signal and comb-filter effect

Now we turn to the situation where the reference signal is a square wave and the signal is a sinusoidal function, as is encountered in some spectroscopic experiments. The square wave can be a bipolar function

$$r = A \cdot \left\{ \begin{array}{ll} +1 & \left[0, \frac{T}{2}\right] \\ -1 & \left[\frac{T}{2}, T\right] \end{array} \right\} \tag{2.32}$$

or a mark-space square wave

$$r = A \cdot \left\{ \begin{array}{ll} +1 & \left[0, \frac{T}{2}\right] \\ 0 & \left[\frac{T}{2}, T\right] \end{array} \right\}. \tag{2.33}$$

Both cases might appear in laboratory practice. We will treat the first case explicitly and give the result for the second case by referring to the first case. In subsections 2.2.3.1 and 2.2.3.2, the amplitude factor will be set to one, i.e., $A = 1$.

2.2.3.1 Bipolar square wave as a reference

Let us consider the experimental setup depicted in Fig. 2.19. The multiplication of the signal and reference is again of key importance to recover the signal from noise.

As a prerequisite for the integration step in the general case, it is advantageous to state the square-wave function as a superposition of harmonic functions. The function is therefore expanded into a Fourier series:

$$r = \left\{ \begin{array}{ll} +1 & \left[0, \frac{T}{2}\right] \\ -1 & \left[\frac{T}{2}, T\right] \end{array} \right\} = \frac{4}{\pi} \sum_{k=0}^{\infty} \frac{\sin[(2k+1)\Omega t]}{2k+1}. \tag{2.34}$$

Using this expansion, the product of the signal and reference reads as

$$s \cdot r = \frac{4a_1}{\pi} \sin(\omega t + \phi) \sum_{k=0}^{\infty} \frac{\sin[(2k+1)\Omega t]}{2k+1}. \tag{2.35}$$

In the first step, the phase is separated. To this end, the following trigonometric relation is used:

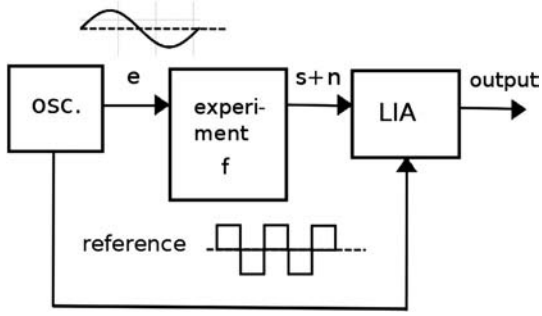

Figure 2.19 Sinusoidal excitation and bipolar square wave as a reference.

$$\sin(x+y) = \sin x \cos y + \cos x \sin y. \tag{2.36}$$

This gives the expression

$$s \cdot r = \frac{4a_1}{\pi} \cos\phi \sin(\omega t) \sum_{k=0}^{\infty} \frac{\sin[(2k+1)\Omega t]}{2k+1} + \frac{4a_1}{\pi} \sin\phi \cos(\omega t) \sum_{k=0}^{\infty} \frac{\sin[(2k+1)\Omega t]}{2k+1}. \tag{2.37}$$

In this step, we implicitly assume that the noise part in the lock-in amplifier input is successfully rejected by the multiplication-and-filtering process. Now the product of the two functions is integrated to obtain the output voltage of the lock-in amplifier:

$$u = \frac{1}{\tau} \int_0^{\tau} srdt. \tag{2.38}$$

We use two trigonometric relations to re-write the product, namely,

$$\sin x \sin y = \frac{1}{2}[\cos(x-y) - \cos(x+y)], \tag{2.39}$$

$$\cos y \sin x = \frac{1}{2}[\sin(x-y) + \sin(x+y)]. \tag{2.40}$$

The result turns out to be relatively lengthy. It reads

$$u = \frac{2a_1}{\pi\tau} \cos\phi \int_0^{\tau} dt \sum_{k=0}^{\infty} \frac{\cos[\omega - (2k+1)\Omega]t - \cos[\omega + (2k+1)\Omega]t}{2k+1} + \frac{2a_1}{\pi\tau} \sin\phi \int_0^{\tau} dt \sum_{k=0}^{\infty} \frac{\sin[-\omega + (2k+1)\Omega]t + \sin[\omega + (2k+1)\Omega]t}{2k+1}. \tag{2.41}$$

The periodic components of the sum vanish during integration. Only those components that are constant and nonzero contribute to the output voltage. This condition holds for the cosine term with a vanishing argument, i.e.,

$$\omega - (2k+1)\Omega = 0. \tag{2.42}$$

The lengthy sum therefore "shrinks" to the following expression:

$$u = \frac{2a_1}{\pi\tau}\cos\phi \int_0^{\tau} \frac{1}{2k+1}\,dt. \tag{2.43}$$

After integration, Eq. (2.43) reads as

$$u = \frac{2a_1}{\pi}\cos\phi\,\frac{1}{2k+1} \qquad k = 0, 1, 2, 3, \ldots. \tag{2.44}$$

Equation (2.44) implies that we will measure

$$u = \frac{2a_1}{\pi}\cos\phi \text{ at frequency } \omega = \Omega,$$

$$u = \frac{2a_1}{3\pi}\cos\phi \text{ at frequency } \omega = 3\Omega,$$

$$u = \frac{2a_1}{5\pi}\cos\phi \text{ at frequency } \omega = 5\Omega.$$

These lines correspond to the cases where $k = 0$, 1, 2 and can be continued in an analogous way.

2.2.3.2 Mark-space square wave as a reference

The situation where a mark-space square wave is used as a reference (Fig. 2.20) can be treated analogously. The difference between this situation and the situation where a bipolar square wave is employed is that here another Fourier-series expansion intervenes:

$$r = \left\{ \begin{array}{ll} +1 & \left[0, \frac{T}{2}\right] \\ 0 & \left[\frac{T}{2}, T\right] \end{array} \right\} = \frac{1}{2} + \frac{2}{\pi}\sum_{k=0}^{\infty} \frac{\sin[(2k+1)\Omega t]}{2k+1}. \tag{2.45}$$

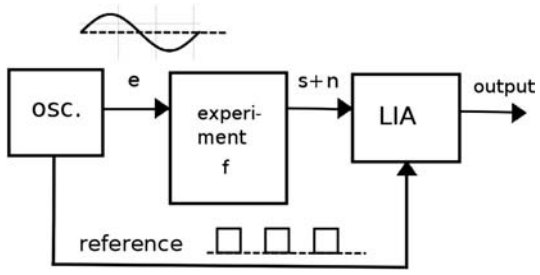

Figure 2.20 Sinusoidal excitation and mark-space square wave as a reference.

Equation (2.45) gives rise to an additional sine wave in the product. Being a periodic function, it will vanish during integration. The factor preceding the sum is slightly different from the first case. Taking this difference into account, we can directly conclude for the second case that

$$u = \frac{a_1}{\pi} \cos\phi \frac{1}{2k+1} \qquad k = 0, 1, 2, 3, \ldots . \tag{2.46}$$

As was the case when both the signal and the reference were periodic, the lock-in amplifier outputs a voltage that is proportional to the cosine of the phase difference.

2.2.3.3 Comb-filter effect

Two types of reference functions have been considered so far, namely, a bipolar square wave [Eq. (2.32)] and a mark-space square wave [Eq. (2.33)]. The salient feature in both cases is an amplitude function that differs from the situation when the reference is a pure sine wave. As expressed by Eq. (2.44) or Eq. (2.46), higher-order contributions with decreasing amplitude appear in the output voltage at higher frequencies. These contributions feature discrete distances in a plot of output voltage versus frequency (Fig. 2.21). This gives rise to the term comb-filter effect. (Note that the term comb filter is also used in the literature on signal processing to denote a filter, the frequency response of which consists of a series of regularly spaced notches.) Therefore, when using a lock-in amplifier with a bipolar square wave or a mark-space square wave as a reference to detect a sinusoidal signal, a comb-filter response is featured in the output of the lock-in amplifier.

2.2.4 Summary and overview

At this point, it is useful to collect the results obtained for the different combinations of signal and reference and represent them succinctly (Table 2.1).

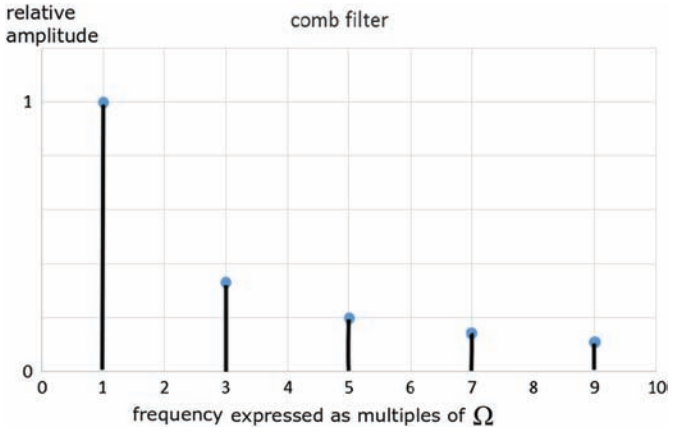

Figure 2.21 Comb-filter effect: normalized amplitude versus frequency $\omega = k\Omega$.

Table 2.1 Outputs obtained for different combinations of reference and signal.

Reference r	Signal s	Output u
Sine wave	Sine wave	$u = \frac{a_1 A}{2} \cos\phi$
Mark-space square wave	Mark-space square wave	$u = \frac{a_1 A}{T} \begin{cases} \frac{T}{2} - p & \left[0, \frac{T}{2}\right] \\ p - \frac{T}{2} & \left[\frac{T}{2}, T\right] \end{cases}$
Bipolar square wave	Bipolar square wave	$u = \frac{a_1 A}{T} \begin{cases} T - 4p & \left[0, \frac{T}{2}\right] \\ 4p - 3T & \left[\frac{T}{2}, T\right] \end{cases}$
Bipolar square wave	Mark-space square wave	$u = \frac{a_1 A}{T} \begin{cases} \frac{T}{2} - 2p & \left[0, \frac{T}{2}\right] \\ 2p - \frac{3T}{2} & \left[\frac{T}{2}, T\right] \end{cases}$
Bipolar square wave	Sine wave	$u = \frac{2a_1 A}{\pi} \cos\phi \frac{1}{2k+1}$, $k = 0, 1, 2, \ldots$
Mark-space square wave	Sine wave	$u = \frac{a_1 A}{\pi} \cos\phi \frac{1}{2k+1}$, $k = 0, 1, 2, \ldots$

2.3 Nonlinearities and Higher Harmonics

Thus far, a linear transfer function has been assumed. A transfer function that features nonlinearities gives rise to higher harmonics. Making use of this property, the lock-in technique can be used to explore these nonlinearities. We will later encounter applications of this approach to the characterization of optical materials. There is a variety of physical effects in materials that feature a quadratic dependence. Examples are the quadratic electro-optic Kerr effect and quadratic electrostriction. Here, we start with a consideration of a quadratic nonlinearity to motivate the use of lock-in detection at $2f$, i.e., the double frequency, and then generalize this reasoning to higher-order nonlinearities.

2.3.1 Detection at multiples of the frequency of the first harmonic

2.3.1.1 Detection at $2f$

In contrast to the situation previously considered, in the experimental arrangement depicted in Fig. 2.22., the transfer function of the experiment is

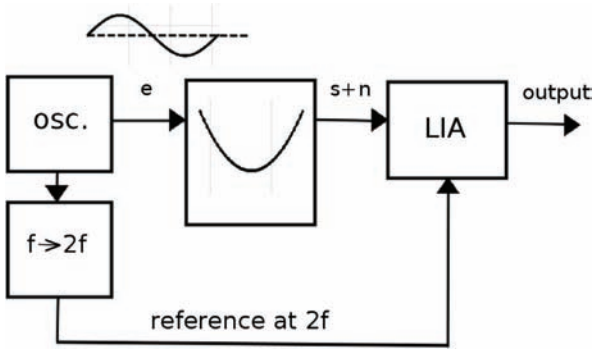

Figure 2.22 Experiment featuring a quadratic transfer function and detection at $2f$.

now nonlinear; i.e., it is a quadratic function. This implies that we obtain a significantly different measurement signal.

A sine wave is used as an input signal (excitation) for the experiment:

$$e = e_\omega \cos \omega t, \tag{2.47}$$

where $\omega = 2\pi f$. The transfer function is quadratic:

$$s = d_2 e^2. \tag{2.48}$$

The constant that precedes the square of the excitation is labelled d_2. Using the trigonometric identity $\cos^2 x = 1/2(1 + \cos 2x)$, we have

$$s = \frac{1}{2} d_2 e_\omega^2 + \frac{1}{2} d_2 e_\omega^2 \cos 2\omega t. \tag{2.49}$$

The first part of Eq. (2.49) is a DC signal, while the second part is a periodic signal at frequency $2f$. The nonlinearity described by the constant d_2 can therefore be quantified using a harmonic excitation signal and lock-in detection at $2f$.

2.3.1.2 Detection at higher-order harmonics

Let us now consider a more general case, namely, an experiment where the signal function can be described by the following expansion:

$$s = \sum_{k=1}^{4} d_k e^k = d_1 e^1 + d_2 e^2 + d_3 e^3 + d_4 e^4. \tag{2.50}$$

Again, we apply a harmonic input signal to probe the sample or device under investigation:

$$e = e_\omega \cos \omega t. \tag{2.51}$$

To obtain expressions of the system response in terms of higher frequencies, it is appropriate to apply the following trigonometric identities:

$$\cos^2 x = \frac{1}{2}(1 + \cos 2x), \tag{2.52}$$

$$\cos^3 x = \frac{1}{4}(3 \cos x + \cos 3x), \tag{2.53}$$

$$\cos^4 x = \frac{1}{8}(3 + 4 \cos 2x + \cos 4x). \tag{2.54}$$

The first and third of these equations can be interpreted as expansions into an even Fourier series, while the second one might be considered as an odd Fourier-series expansion.

Combining Eqs. (2.50) through (2.54) leads to a result for the response of the system:

$$
\begin{aligned}
s = {} & \frac{1}{2} d_2 \cdot e_\omega^2 + \frac{3}{8} d_4 \cdot e_\omega^4 \\
& + \cos \omega t \cdot \left(d_1 \cdot e_\omega + \frac{3}{4} d_3 \cdot e_\omega^3 \right) \quad \text{for detection at } f, \\
& + \cos 2\omega t \cdot \left(\frac{1}{2} d_2 \cdot e_\omega^2 + \frac{1}{2} d_4 \cdot e_\omega^4 \right) \quad \text{for detection at } 2f, \\
& + \cos 3\omega t \cdot \left(\frac{1}{4} d_3 \cdot e_\omega^3 \right) \quad \text{for detection at } 3f, \\
& + \cos 4\omega t \cdot \left(\frac{1}{8} d_4 \cdot e_\omega^4 \right) \quad \text{for detection at } 4f.
\end{aligned} \tag{2.55}
$$

In Eq. (2.55), the terms have been arranged according to different frequencies. As an example, we can conclude from Eq. (2.55) that we can measure the third-order coefficient in the expansion of the transfer function by lock-in detection at $3f$.

2.3.2 Intermodulation

This subsection can be skipped at first reading. It is included here to complement this section and can be used for reference, for example, related to troubleshooting.

If the input to the experiment contains more than one sine wave and the experiment features nonlinear characteristics, intermodulation may occur (see Fig. 2.23). This situation can arise if the excitation provided by the oscillator is distorted and contains higher harmonics in addition to the fundamental sine wave.

A simple example will illustrate this effect, namely, an experiment with a transfer function composed of a linear part and a quadratic part:

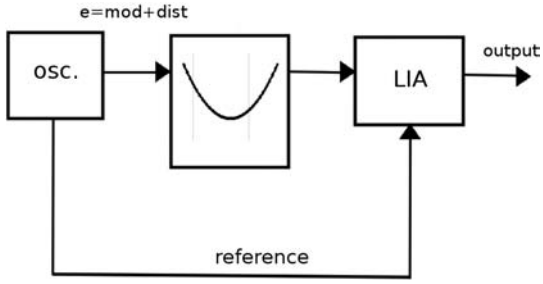

Figure 2.23 Intermodulation: The excitation signal is a superposition of the modulation signal and distortion.

$$s = d \cdot e + \gamma \cdot e^2. \tag{2.56}$$

As input to the experiment, we consider the superposition of a bias e_0 and three sinusoidal functions with different frequencies:

$$e = e_0 + e_1 + e_2 + e_3, \tag{2.57}$$

$$e_1 = e_\omega \cos \omega t, \tag{2.58}$$

$$e_2 = e_{2\omega} \cos 2\omega t, \tag{2.59}$$

$$e_3 = e_{3\omega} \cos 3\omega t. \tag{2.60}$$

The input e can be split into the fundamental modulation, $\text{mod} = e_1 = e_\omega \cos \omega t$, and a bias plus higher harmonics, $\text{dist} = e_1 + e_2 + e_3$. To obtain the intermodulated output s of the experiment in this situation, we first introduce the expression for the superimposed functions into Eq. (2.56):

$$s = d \cdot (e_0 + e_1 + e_2 + e_3) + \gamma \cdot (e_0 + e_1 + e_2 + e_3)^2. \tag{2.61}$$

To facilitate the interpretation, we arrange the result in a triangular shape, exploiting the symmetry:

$$\begin{aligned} s = {} & d \cdot e_0 + \gamma \cdot e_0^2 + (d + 2e_0\gamma)(e_1 + e_2 + e_3) + \gamma \cdot e_1^2 + 2\gamma e_1 e_2 + 2\gamma e_1 e_3 \\ & + \gamma \cdot e_2^2 + 2\gamma e_2 e_3 + \gamma \cdot e_3^2. \end{aligned} \tag{2.62}$$

To understand how intermodulation affects the output of the experiment at a given frequency, we note the trigonometric functions in a way that allows us to arrange them according to frequencies:

$$e_1^2 = \frac{1}{2} e_\omega^2 (1 + \cos 2\omega t), \tag{2.63}$$

$$e_2^2 = \frac{1}{2} e_{2\omega}^2 (1 + \cos 4\omega t), \tag{2.64}$$

$$e_3^2 = \frac{1}{2} e_{3\omega}^2 (1 + \cos 6\omega t). \tag{2.65}$$

The mixed terms read

$$2e_1 e_2 = 2e_\omega e_{2\omega} \cos \omega t \cdot \cos 2\omega t, \tag{2.66}$$

$$2e_1 e_3 = 2e_\omega e_{3\omega} \cos \omega t \cdot \cos 3\omega t, \tag{2.67}$$

$$2e_2e_3 = 2e_{2\omega}e_{3\omega}\cos 2\omega t \cdot \cos 3\omega t. \tag{2.68}$$

Using the trigonometric relation $2\cos x \cos y = \cos(x-y) + \cos(x+y)$, we can denote Eqs. (2.66)–(2.68) as

$$2e_1e_2 = e_\omega e_{2\omega}(\cos \omega t + \cos 3\omega t), \tag{2.69}$$

$$2e_1e_3 = e_\omega e_{3\omega}(\cos 2\omega t + \cos 4\omega t), \tag{2.70}$$

$$2e_2e_3 = e_{2\omega}e_{3\omega}(\cos \omega t + \cos 5\omega t). \tag{2.71}$$

With these prerequisites, we find that

$$\begin{aligned} s = {} & d \cdot e_0 + \gamma \cdot e_0^2 + (d + 2e_0\gamma)(e_\omega \cos \omega t + e_{2\omega} \cos 2\omega t + e_{3\omega} \cos 3\,\omega t) \\ & + \frac{1}{2}\gamma(e_\omega^2 + e_{2\omega}^2 + e_{3\omega}^2) + \gamma e_\omega e_{2\omega} \cos \omega t + \frac{\gamma}{2}e_\omega^2 \cos 2\omega t + \gamma e_\omega e_{2\omega} \cos 3\omega t \\ & + \gamma e_{2\omega}e_{3\omega} \cos \omega t + \gamma e_\omega e_{3\omega} \cos 2\omega t + R, \end{aligned} \tag{2.72}$$

where

$$\begin{aligned} R &= R(4\omega, 5\omega, 6\omega) \\ &= \frac{\gamma}{2}e_{2\omega}^2 \cos 4\omega t + \gamma e_\omega e_{3\omega} \cos 4\omega t + \gamma e_{2\omega}e_{3\omega} \cos 5\omega t + \frac{\gamma}{2}e_{3\omega}^2 \cos 6\omega t. \end{aligned}$$

The various terms in Eq. (2.72) have been arranged according to increasing frequencies. Obviously, there would be no intermodulation if nonlinearity did not exist, i.e., in the case where $\gamma = 0$ holds.

In the case of $e_{3\omega} = 0$, a measurement at $1f$ could be affected by the intermodulation

$$s_{1,2} = \gamma e_\omega e_{2\omega} \cos \omega t. \tag{2.73}$$

Under the same condition, a measurement at $2f$ could be affected by the following contribution due to intermodulation:

$$s_2 = (d + 2e_0\gamma)e_{2\omega} \cos 2\omega t. \tag{2.74}$$

The expressions for the case where $e_{3\omega} \neq 0$ follow accordingly, taking the third line of Eq. (2.72) into account.

2.4 Two-Phase Systems

2.4.1 Quadrature

Sometimes it is of interest to measure the in-phase and the quadrature components of a signal simultaneously. To this end, a two-phase lock-in

amplifier can be used. This basically consists of two combined lock-in amplifiers. The phase of the reference in the second unit is shifted by 90 deg with respect to the first unit. As shown in Fig. 2.24, the input signal of both lock-in amplifiers is the same. If $r = A \sin \Omega t$ is the reference of the first unit, then $r = A \sin(\Omega t + 90 \text{ deg}) = A \cos \Omega t$ is used as the reference of the second unit.

Assuming an input signal of the form $s = a_1 \sin(\omega t + \phi)$, we obtain the following equation for the in-phase component:

$$u_a = \frac{a_1 A}{2} \cos \phi. \tag{2.75}$$

For the quadrature component of the two-phase lock-in amplifier, which corresponds to the reference $r = A \sin(\Omega t + 90 \text{ deg})$, the product $s \cdot r$ reads as

$$s \cdot r = a_1 A \sin(\omega t + \phi) \cos \Omega t. \tag{2.76}$$

The lock-in operation ensures that $\omega = \Omega$ holds. Using the fact that $\sin x \cos y = (1/2)[\sin(x - y) + \sin(x + y)]$, Eq. (2.76) takes the form of

$$s \cdot r = \frac{a_1 A}{2} [\sin \phi + \sin(2\omega t + \phi)]. \tag{2.77}$$

During integration over many periods, the AC part cancels out, and only the DC part gives a contribution:

$$u_b = \frac{a_1 A}{2} \frac{1}{\tau} \int_0^\tau [\sin \phi + \sin(2\omega t + \phi)] dt = \frac{a_1 A}{2} \sin \phi, \tag{2.78}$$

which is the quadrature output of the two-phase lock-in amplifier.

2.4.2 Vector computer

Both signals can be further processed in a so-called vector computer (Fig. 2.25), which is incorporated into many lock-in amplifiers. This operation

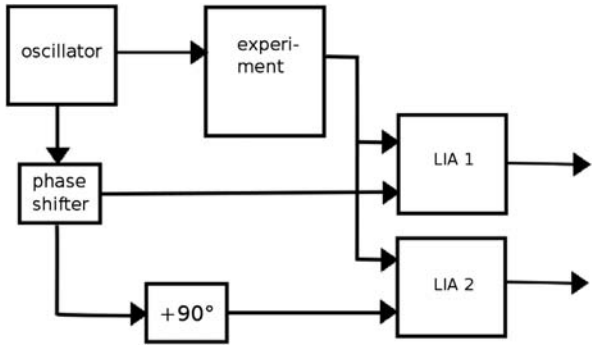

Figure 2.24 Two-phase lock-in detection.

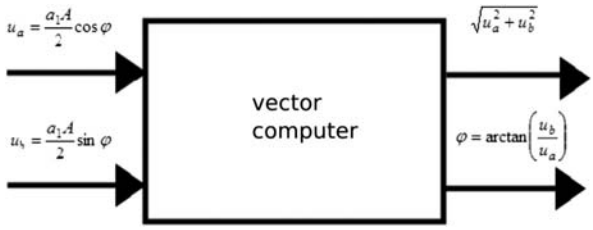

Figure 2.25 Vector computer.

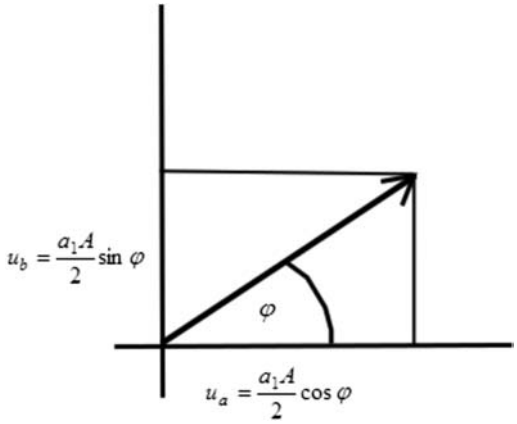

Figure 2.26 Change from Cartesian to polar coordinates.

corresponds to a change from Cartesian to polar coordinates (Fig. 2.26). Lock-in amplifiers are often provided with four separate outputs to simultaneously read out the signal in both representations.

2.4.3 Vector tracking

The output of the vector computer can be used as a feedback signal in a control loop. This feedback loop is depicted in Fig. 2.27. In this circuit, the information on the vector phase is used as input to a voltage-controlled phase shifter. In this way, the signal and reference are kept in phase at the output of the first unit (LIA 1).

2.5 Measuring Higher-Order Derivatives

In the technical and scientific literature on applications of lock-in amplifiers, it is often implicitly assumed that the reader is familiar with the idea that measuring at the frequency $n \cdot f$ is related to measuring the n^{th} derivative of the corresponding transfer function. This relation is not so obvious and will be derived in the following discussion.

The slope of a linear transfer function affects the amplitude of the output signal. In the case of a nonlinear transfer function, it is the local slope of the

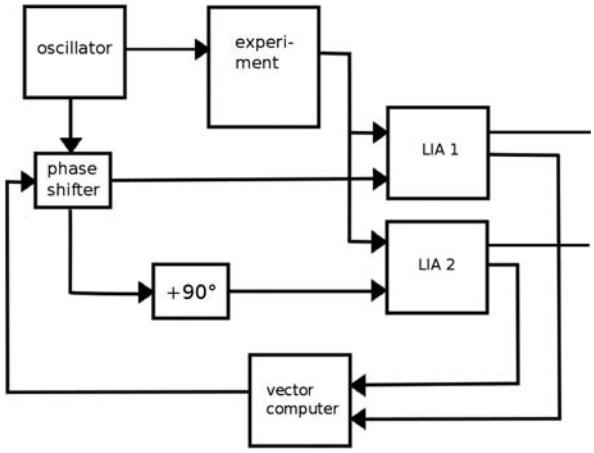

Figure 2.27 Vector tracking.

corresponding curve that directly influences the amplitude of the output voltage. A steeper slope of the transfer function results in a higher amplitude of the signal.

A formal derivation is based on Taylor's theorem, which states that some functions $f(x)$ that fulfill certain analytical conditions can be approximated at a point x_0 as

$$Tf(x, x_0) = \sum_{k=0}^{\infty} \frac{f^{(k)}(x_0)}{k!} (x - x_0)^k. \tag{2.79}$$

In this equation, $f^{(k)}(x_0)$ is used as an abbreviation for the k^{th}-order derivative of the function $f(x)$ at the point x_0:

$$f^{(k)}(x_0) = \left. \frac{d^k f}{dx} \right|_{x=x_0}. \tag{2.80}$$

To better understand the probing of a complicated function $f(x)$ by harmonic functions, we consider the situation where $f(x)$ is examined at point x_0 using

$$x = x_0 + a \cos \omega t. \tag{2.81}$$

Therefore, we have

$$Tf(x, x_0) = \sum_{k=0}^{\infty} \frac{f^{(k)}(x_0)}{k!} (a \cos \omega t)^k, \tag{2.82}$$

and our method of analysis will be based on this equation. In order to be able to treat most cases of practical interest, we consider a Taylor expansion of the transfer function to the fourth order:

$$s = \sum_{k=0}^{4} \frac{f^{(k)}(x_0)}{k!} (a \cos \omega t)^k. \tag{2.83}$$

Written more explicitly, Eq. (2.83) reads as

$$s = f(x_0) + f^{(1)}(x_0) a \cos \omega t + \frac{1}{2} f^{(2)}(x_0) a^2 \cos^2 \omega t + \frac{1}{6} f^{(3)}(x_0) a^3 \cos^3 \omega t + \frac{1}{24} f^{(4)}(x_0) a^4 \cos^4 \omega t. \tag{2.84}$$

As in Eqs. (2.52)–(2.54), we need expressions for the powers of trigonometric functions. Introducing them into Eq. (2.84) gives the result

$$\begin{aligned} s = {} & f(x_0) + \frac{a^2}{4} f^{(2)}(x_0) + \frac{3}{8}\frac{1}{4!} a^4 f^{(4)}(x_0) \\ & + \cos \omega t \cdot \left[a \cdot f^{(1)}(x_0) + \frac{3}{4 \cdot 6} a^3 \cdot f^{(3)}(x_0) \right] \quad \text{for detection at } f \\ & + \cos 2\omega t \cdot \left[\frac{1}{4} a^2 \cdot f^{(2)}(x_0) + \frac{1}{6}\frac{1}{8} a^4 f^{(4)}(x_0) \right] \quad \text{for detection at } 2f \\ & + \cos 3\omega t \cdot \left[\frac{1}{24} a^3 \cdot f^{(3)}(x_0) \right] \quad \text{for detection at } 3f \\ & + \cos 4\omega t \cdot \left[\frac{1}{4!}\frac{1}{8} a^4 \cdot f^{(4)}(x_0) \right] \quad \text{for detection at } 4f. \end{aligned} \tag{2.85}$$

When we consider the leading terms in Eq. (2.85), we recognize that they are all terms having the structure

$$+ \cos k\omega t \cdot [\ldots \cdot a^k \cdot f^{(k)}(x_0) + \ldots]. \tag{2.86}$$

This is why measuring at the frequency $k \cdot f$ is related (but not identical) to the measurement of the k^{th} derivative of the transfer function f. Recalling the discussion on nonlinearities and higher harmonics, we retrieve the result for a fourth-order polynomial by setting

$$s = f(x) = \sum_{k=1}^{4} d_k x^k = d_1 x^1 + d_2 x^2 + d_3 x^3 + d_4 x^4, \tag{2.87}$$

and by forming the derivatives of f that appear in Eq. (2.87) at $x_0 = 0$ and introducing them into the equation.

The measurement of higher-order derivatives using lock-in amplifiers is often applied in spectroscopy. This technique is sometimes designated as derivative spectroscopy.

2.6 Operating the Lock-in Amplifier

Lock-in amplifiers (Figs. 2.28 and 2.29) allow for different settings, making it possible to tailor the detection unit to the measurement task. They also feature an adjustable low-pass filter. The time constant of the low-pass filter is proportional to $1/f_{-3\mathrm{dB}}$, where $1/f_{-3\mathrm{dB}}$ is the -3-dB frequency of the filter and determines the bandwidth of the filter.

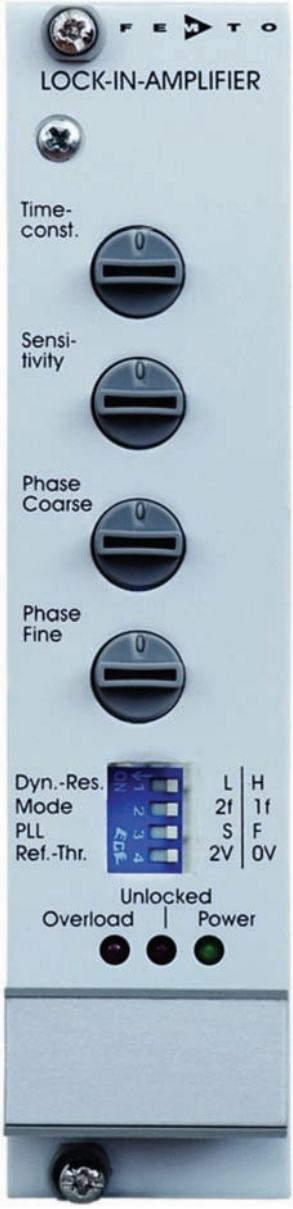

Figure 2.28 Compact lock-in amplifier. (Courtesy of Femto, used with permission.)

Figure 2.29 Lock-in amplifier. (Courtesy of Stanford Research Systems, used with permission.)

When choosing the correct bandwidth, the following trade-off has to be considered: A narrow bandwidth corresponds to a measurement with less noise but has the disadvantage of resulting in a slower measurement. A wider bandwidth implies a faster measurement but leads to more noise. In other words, there is a trade-off between the speed of a measurement and the tolerable low-frequency noise level.

Looking at Eq. (2.9), one would choose the time constant in such a way that the contribution of the term at the double frequency is just suppressed. It must be kept in mind that a low-pass filter has a more complex transfer function than implicitly assumed in the derivation, and care has to be taken that the bandwidth is sufficiently narrow. This is to avoid "leaking" of the $2f$ component into the output signal, which can lead to a measurement error.

Many lock-in amplifiers also allow one to choose the order of the filter, which determines the filter shape. Higher filter orders come closer to the rectangular shape of an idealized low-pass filter. Such a filter can therefore block more efficiently. On the other hand, the filter takes more time to settle, causing a phase delay. This is a disadvantage if higher speed requirements are to be met.

Equation (2.10) implies that the output voltage is at a maximum if the phase difference is adjusted to zero. Usually, lock-in amplifiers are calibrated in such a way that this maximum output voltage equals the root-mean-square (RMS) value of the desired signal. Equation (2.10) was obtained assuming a sinusoidal reference. In Fig. 2.18, the corresponding relationship is depicted for nonsinusoidal references. Looking at the graph lines, one arrives at the same conclusion, namely, that the output voltage can be maximized by adjusting the phase difference to zero. In addition to a phase shifter that can be adjusted manually, many lock-in units have an auto-phase button.

Generally speaking, if an interfering signal with a frequency f_i has to be rejected, it is advisable to arrange for a reference frequency that is incommensurate with f_i.

2.7 External Noise Sources

1/*f* noise and white noise stem from intrinsic noise sources. In addition to intrinsic noise sources, there might be external noise sources that can deteriorate an experiment and lead to measurement errors.

Capacitive coupling is one way that a noise source can unintendedly be coupled into the signal path. Capacitive coupling can occur if an AC voltage from another device is coupled to a detector via a stray capacitance. This can cause problems, especially if this noise is at the reference frequency. Countermeasures include measuring with low impedance and/or using capacitive shielding.

Another way in which noise might be coupled into the signal path is by inductive coupling. An AC current in another machine or instrument can couple to the loop that forms the connection of the detector to the experiment via a magnetic field. One countermeasure for this is magnetic shielding.

References

1. P. Horowitz and W. Hill, *The Art of Electronics*, Third Edition, Cambridge University Press, Cambridge (2015).
2. D. P. Blair and P. H. Sydenham, "Phase sensitive detection as a means to recover signals buried in noise," *J. Physics E: Scientific Instruments* **8**, 621–627 (1975).
3. M. L. Meade, "Advances in lock-in amplifiers," *J. Physics E: Scientific Instruments* **15**, 395–403 (1982).
4. B. Voigtländer, "Lock-in Technique," Chapter 6 in *Scanning Probe Microscopy: Atomic Force Microscopy and Scanning Tunnelling Microscopy*, Springer-Verlag GmbH, Berlin-Heidelberg, pp. 101–105 (2015).

Chapter 3
Optical Spectroscopy

Optical spectroscopy is a classical tool of scientific inquiry, and much effort has been devoted to the design of spectroscopic instruments.[1–3] Lock-in amplifiers play a prominent role when low-level signals need to be precisely detected.

3.1 Absorption Spectroscopy

Absorption can be described by the Beer–Lambert law. The intensity I of a light beam that passed through an absorbing specimen is

$$I = I_0 e^{-\alpha d}, \tag{3.1}$$

where I_0 is the intensity of the incident radiation, α is the absorption coefficient, which is a function of the wavelength of the incident light, and d is the thickness of the sample. The transmittance T of a solution is the fraction of incident light that is transmitted by a transparent specimen:

$$T = \frac{I}{I_0}. \tag{3.2}$$

The absorbance A is defined as the negative decadic logarithm of this ratio, i.e.,

$$A = -\log_{10} T. \tag{3.3}$$

Details on the experimental practice of absorption spectroscopy can be found in, e.g., the book *Standards and Best Practice in Absorption Spectrometry*.[4]

The absorption coefficient (or the absorbance) of a substance depends on the wavelength of the radiation that is used to probe the sample. A key component of an absorption spectrometer, which records spectra, is a dispersive element. This can be, e.g., a prism[5] or a grating.[6,7] Optical gratings used for spectroscopy can be ruled or holographic.

Figure 3.1 shows a symmetric prism, and Fig. 3.2 shows a Littrow prism, which can be derived from a symmetric prism. A Littrow prism reflects a light beam back onto itself.

Figure 3.3 depicts a Czerny–Turner arrangement that features a grating in transmission. Figure 3.4 depicts a Czerny–Turner configuration for an optical grating used in reflection. Both configurations are related by a symmetry operation. The geometry of Fig. 3.3 can be obtained from the geometry of Fig. 3.2 by using the plane of the grating (which is used in transmission) as the

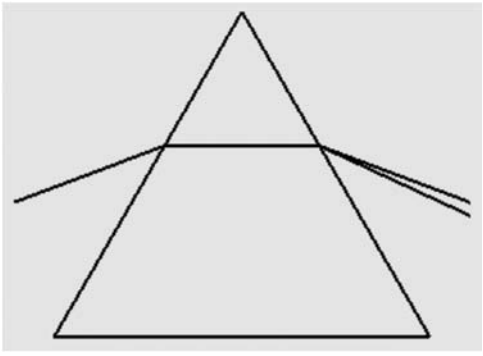

Figure 3.1 Symmetric prism as a dispersive element.

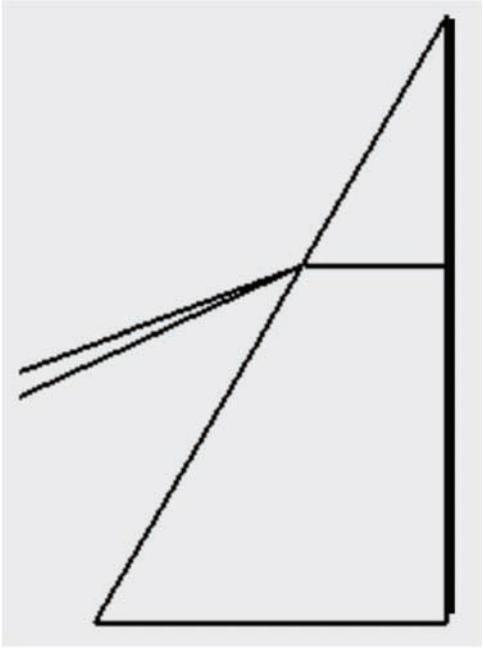

Figure 3.2 Littrow prism as a dispersive element.

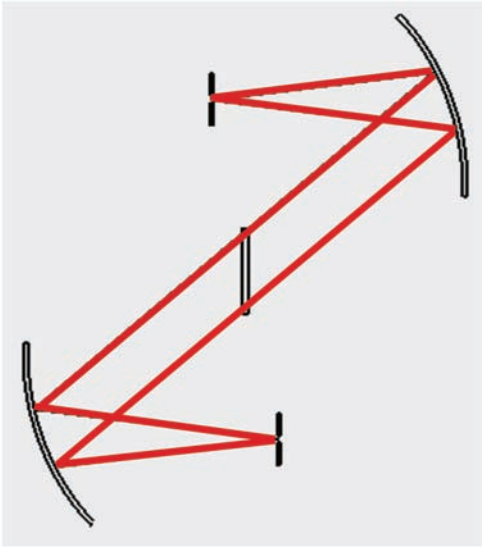

Figure 3.3 Czerny–Turner arrangement with a grating used in transmission.

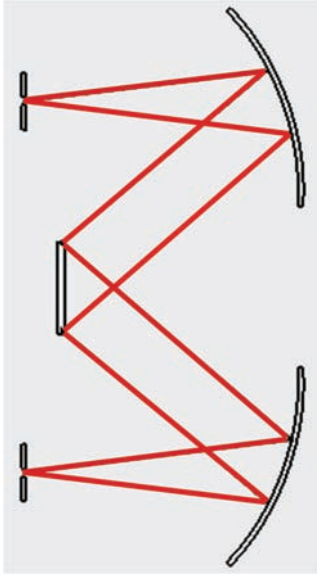

Figure 3.4 Czerny–Turner arrangement with a grating used in reflection.

reflection plane: If the lower part of the Czerny–Turner arrangement in Fig. 3.3 is reflected with respect to that plane, Fig. 3.4 is obtained.

3.1.1 Single-beam spectrometers

A wide variety of experimental setups and instrument configurations has been devised to measure absorption. A simple experimental arrangement consists of

a light source, a dispersive element, and a detector. The sample and reference sample are introduced between the dispersive element and the detector, and are measured in two consecutive steps [Figs. 3.5(a) and (b)]. In a third step, both measurement values are divided to obtain the ratio of the light intensities.

Frequently, the light source used for spectroscopic experiments emits light in a continuous way. If lock-in detection is to be applied, the light has to be modulated. A device used for this purpose is a rotating sector blade (Fig. 3.6). This device, often called a chopper, interrupts the light beam in a controlled and periodic manner.

Again, two consecutive steps are necessary to measure the specimen (the substance under test in solution, for example) and the reference specimen (the pure solution) [Figs. 3.7(a) and (b)]. The advantages of this approach are

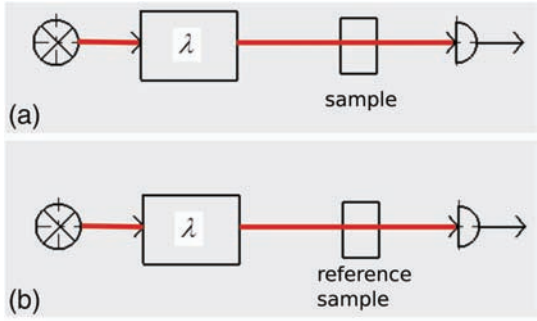

Figure 3.5 Experimental setup for absorption measurement in two steps. The setup consists of a light source, a dispersive element, a sample that is probed in transmission, and an optical detector, which generates an electronic signal.

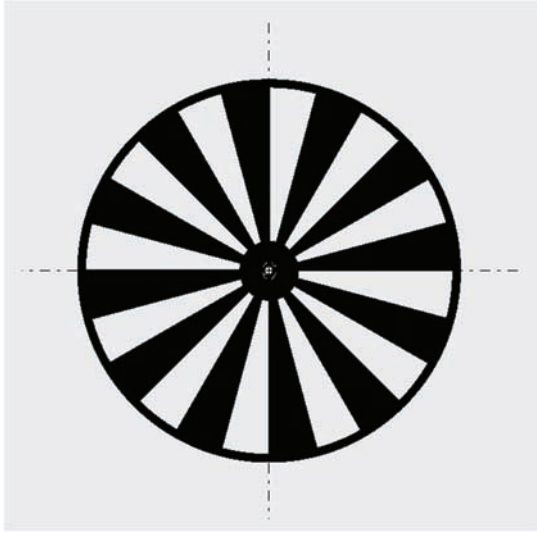

Figure 3.6 Rotating sector blade (chopper).

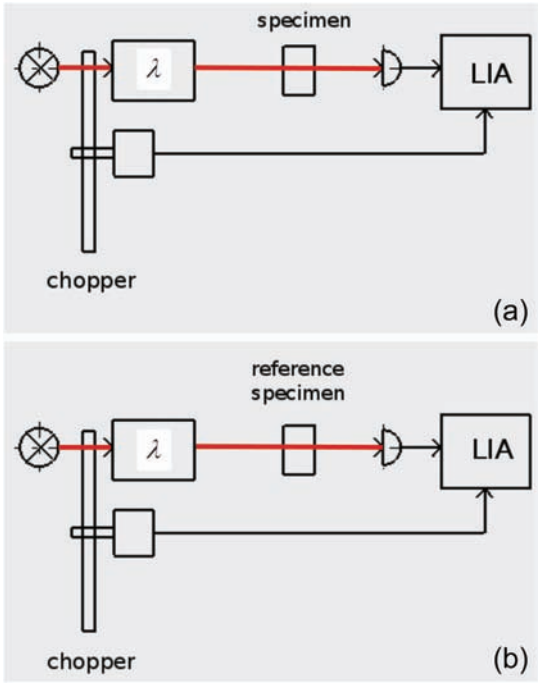

Figure 3.7 Setup for absorption measurement using a chopper (rotating sector blade) and a lock-in amplifier.

improvement of the signal-to-noise ratio and suppression of a zero-point drift. Furthermore, the influence of DC stray light is eliminated.

An alternative way to introduce modulation into the experiment involves modulating the light source. To obtain the ratio of the light intensities, two consecutive measurements have to be performed [Figs. 3.8(a) and (b)]. This experimental arrangement has the advantage that no moving mechanical parts are needed for modulation.

3.1.2 Two-beam spectrometers

To address the problem of temporal intensity variations of the light source, two-beam spectrometers can be used. These spectrometers provide compensation for the intensity variations. Figure 3.9 shows a setup that uses a beamsplitter to divide the incoming light beam into two separate beams. Beam A passes through the optical path in which the sample can be placed, and beam B propagates through another optical path that serves as an optical reference.

To obtain a modulated signal that makes lock-in detection possible, it is convenient to introduce a rotating sector blade into the light path. Figures 3.10 and 3.11 show two possible locations for placement of the blade in the setup.

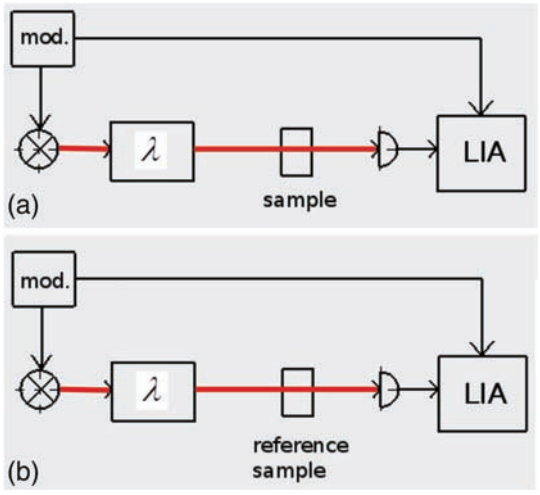

Figure 3.8 Setup for absorption measurement using electronic modulation of the light source and a lock-in amplifier.

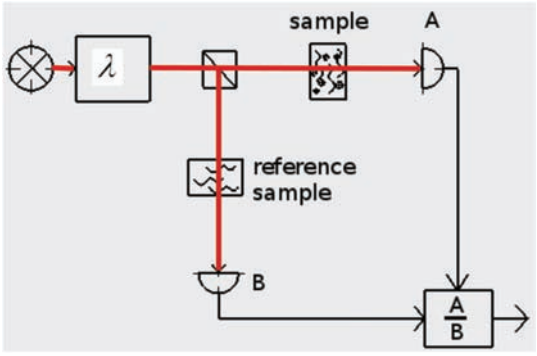

Figure 3.9 Setup for a two-beam spectrometer.

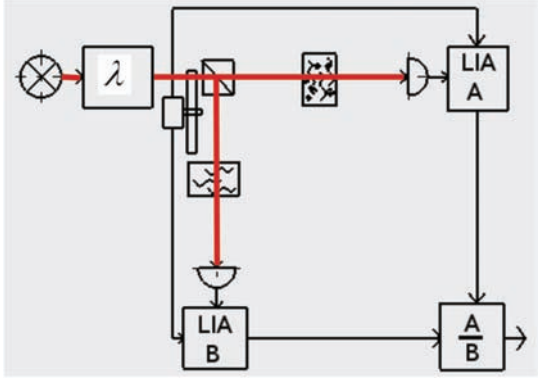

Figure 3.10 Setup for a two-beam spectrometer with chopper and two lock-in amplifiers.

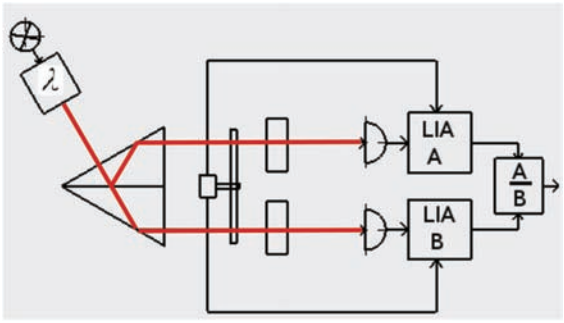

Figure 3.11 Setup for a two-beam spectrometer with modulation of both paths and two lock-in amplifiers.

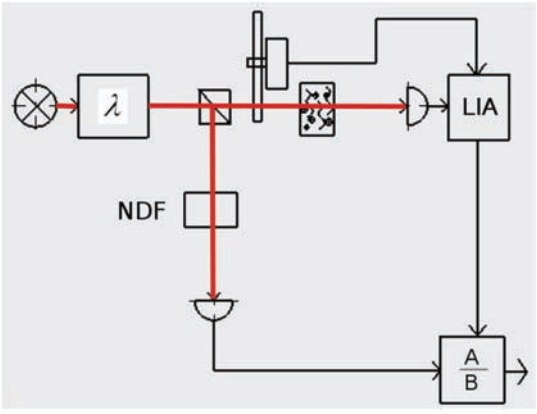

Figure 3.12 Setup for a two-beam spectrometer setup with a neutral-density filter.

Figure 3.12 shows a related experimental setup that features modulation in only one arm of the spectrometer. The intensity of the light beam in the reference path is kept continuous and is not interrupted. A neutral-density filter (NDF) is placed in the reference path.

An optical configuration that is analogous to that in Fig. 3.10 but uses electronic modulation of the light source is shown in Fig. 3.13. An electronic signal provided by the modulation unit serves as a reference signal for the lock-in amplifier.

The two-beam spectrometers discussed so far are equipped with two different detectors, one in the measurement arm and the other in the reference arm. This can give rise to differing variations in detector sensitivities. To avoid this problem, it can be advantageous to re-combine the light beams that passed through the sample and through the reference sample and guide them to a single detector (Fig. 3.14). The rotating sector blade that modulates the light intensity is positioned after the beamsplitter.

In the experimental arrangement shown in Fig. 3.14, the beamsplitter that precedes the chopper causes the light flux to be divided into two equal parts.

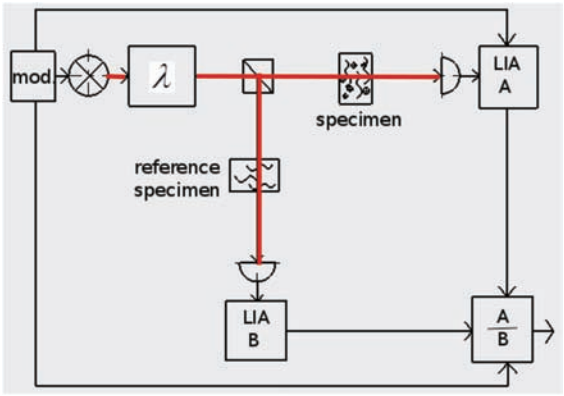

Figure 3.13 Setup for a two-beam spectrometer with electronic modulation.

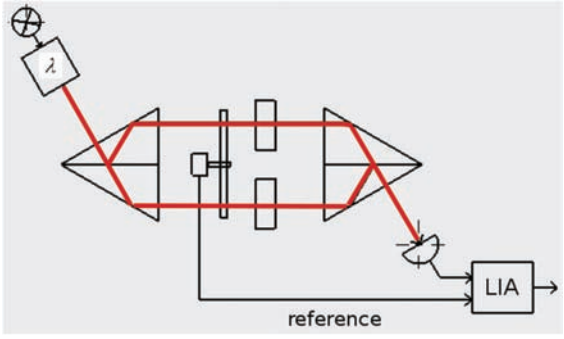

Figure 3.14 Setup for a two-beam spectrometer with a chopper.

To improve the throughput of the spectrometer, it is advantageous to use a device that combines the functions of a beamsplitter and a rotating sector blade. The rotating sectioned mirror shown in Fig. 3.15 distributes the light flux to both arms of the instruments in an alternating sequence. In one position, the full flux passes through the measurement arm of the instrument; in the other position, the (almost) complete light flux is reflected into the

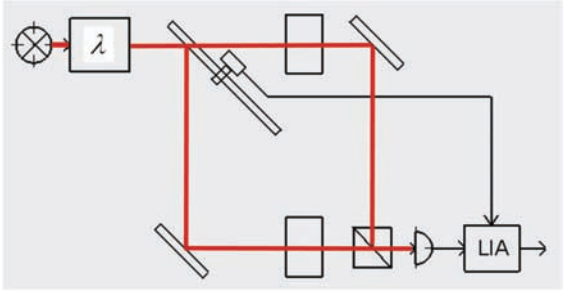

Figure 3.15 Setup for a two-beam spectrometer with a rotating sectioned mirror.

reference arm of the instrument. In this way, the (almost) full light flux is alternatingly available for the measurement light path and for the reference light path.

Figures 3.16 and 3.17 show rotating sector blades that have a twofold division, namely, into sectors (type A) and into an inner and an outer region (type B), respectively. In Fig. 3.18, the type-A chopper of Fig. 3.16 is introduced into the light path as shown. The purpose of adding the chopper is that the measurement light path can now be modulated with a chopping frequency f, while the modulation frequency of the reference light path is $2f$.

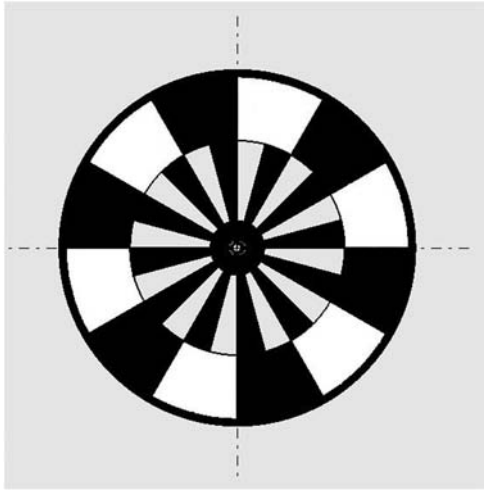

Figure 3.16 Structured rotating sector blades: type A.

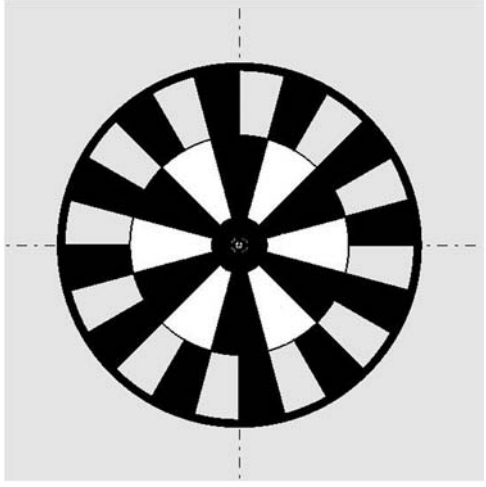

Figure 3.17 Structured rotating sector blades: type B.

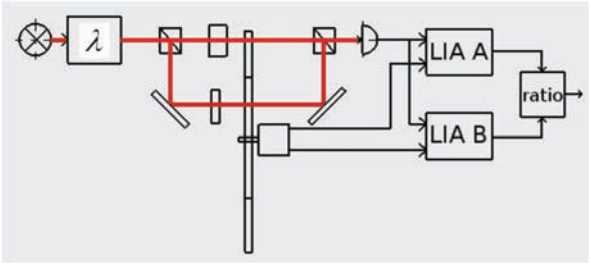

Figure 3.18 Setup for a two-beam spectrometer with modulation at *f* and 2*f*.

Other frequency ratios are of course possible, depending on the experiment and on the available equipment.

To realize modulation at two different frequencies, it is also possible to install two different rotating sector blades. One, operating at *f*, for example, interrupts the measurement light path, and the other, operating at 2*f*, for example, interrupts the reference arm in a periodic manner. The motors of both sector blades are controlled by the same electronic unit (so that the phase is locked).

Looking back, we can make the following distinction: The two-beam spectrometers sketched in Figs. 3.14 and 3.15 separate the two beams electronically by making use of information on their relative phase. The spectrometric configuration presented in Fig. 3.18, on the other hand, exploits information on the different modulation frequencies to discriminate the two optical paths.

Mechanical modulation is not adequate if fast phenomena, such as fast chemical reactions, for example, have to be monitored. In this case, electronic modulation is a necessity.

3.1.3 Frequency modulation

As an alternative to modulating the intensity, it is sometimes also possible to modulate the frequency[8] of the light that probes the sample. Here we discuss an application in which a tunable laser is controlled by a frequency modulator (Fig. 3.19). The frequency modulator provides the reference for the lock-in amplifier.

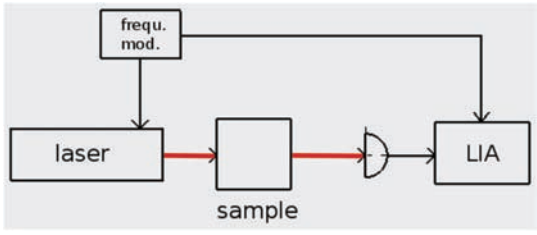

Figure 3.19 Setup for laser frequency modulation.

The laser frequency ω_L is modulated at ω_b with a modulation amplitude a:

$$\omega_L = \omega_b + a\cos\Omega t. \tag{3.4}$$

Let us designate the transmitted laser intensity using the notation $I_T(\omega_L)$ and assume that it can be expanded as a Taylor series at ω_b:

$$TI_T(\omega_L,\omega_b) = \sum_{k=0}^{\infty} \frac{1}{k!} I_T^{(k)}(\omega_L)(\omega_L - \omega_b)^k. \tag{3.5}$$

Combining Eqs. (3.4) and (3.5) gives

$$TI_T(\omega_L) = \sum_{k=0}^{\infty} \frac{1}{k!} I_T^{(k)}(\omega_b)(a\cos\Omega t)^k. \tag{3.6}$$

At this point, it is helpful to observe that Eqs. (3.4) and (3.6) are analogous to Eqs. (2.81) and (2.82) of Chapter 2:

$$x = p(t) + a\cos\omega t, \quad Tf(x,x_0) = \sum_{k=0}^{\infty} \frac{f^{(k)}(x_0)}{k!}(a\cos\omega t)^k.$$

In a sense, the equations from the two chapters are wearing the same mathematical "dress," but their physical content is different. This observation allows us to take a result from Chapter 2, namely Eq. (2.86), and to apply it to frequency modulation. In Eq. (2.86), we make the following substitutions:

$$\begin{aligned} &x \leftarrow \omega_L, \\ &p(t) = x_0 \leftarrow \omega_b, \\ &\omega \leftarrow \Omega, \\ &f(x) \leftarrow I_T(\omega_L), \end{aligned}$$

and obtain the typical product term of the following form:

$$+\cos k\Omega t \cdot [\ldots \cdot a^k \cdot I_T^{(k)}(\omega_L) + \ldots] \quad \text{with } k = 1, 2, 3, \ldots,$$

which expresses that the k^{th} derivative of the transmitted laser frequency can be measured with a lock-in amplifier tuned to $k\Omega$. Assuming that this is the dominant term, it is implied that the following equations hold for detection at the modulation frequency and higher harmonics:

$$I_T(\Omega) = \cos\Omega t \cdot [a \cdot I_T^{(1)}(\omega_L)] \quad \text{for detection at } f, \tag{3.7}$$

$$I_T(2\Omega) = \cos 2\Omega t \cdot \left[\frac{1}{4}a^2 \cdot I_T^{(2)}(\omega_L)\right] \quad \text{for detection at } 2f, \tag{3.8}$$

$$I_T(3\Omega) = \cos 3\Omega t \cdot \left[\frac{1}{24}a^3 \cdot I_T^{(3)}(\omega_L)\right] \quad \text{for detection at } 3f. \tag{3.9}$$

To relate these equations to the absorption coefficient, we start with the absorption law:

$$I_T = I_0 e^{-\alpha d}, \tag{3.10}$$

where d is the absorption length. Under the assumption that $d\alpha \ll 1$ holds, I_T can be approximated as

$$I_T \approx I_0[1 - \alpha(\omega_L)d]. \tag{3.11}$$

This implies for the k^{th} derivative of the intensity that

$$I_T^{(k)} = -I_0 d\alpha^{(k)}(\omega_L) \tag{3.12}$$

holds approximately for $k = 1, 2, 3$. Introducing this into Eqs. (3.7)–(3.9), we find that

$$I_T(\Omega) = -I_0 d\cos\Omega t \cdot [a \cdot \alpha^{(1)}(\omega_L)] \quad \text{for detection at } f, \tag{3.13}$$

$$I_T(2\Omega) = -I_0 d\cos 2\Omega t \cdot \left[\frac{1}{4}a^2 \cdot \alpha^{(2)}(\omega_L)\right] \quad \text{for detection at } 2f, \tag{3.14}$$

$$I_T(3\Omega) = -I_0 d\cos 3\Omega t \cdot \left[\frac{1}{24}a^3 \cdot \alpha^{(3)}(\omega_L)\right] \quad \text{for detection at } 3f, \tag{3.15}$$

where $\alpha^{(k)}(\omega_L)$ is the k^{th} derivative of the absorption curve with respect to the laser frequency ω_L. Equations (3.13)–(3.15) are the output of a lock-in amplifier tuned to Ω, 2Ω, and 3Ω, respectively. An absorption curve with a Lorentzian shape is a typical line profile that is scanned with frequency modulation.

The literature[8] states that frequency modulation techniques are superior to intensity modulation techniques with respect to both the signal-to-noise ratio and the sensitivity that can be achieved. Further information on frequency modulation may be found in the contributions by Bjorklund[9] and Silver.[10]

3.2 Fluorescence Measurements

3.2.1 Fluorescence spectroscopy

Fluorescence is the re-emission of absorbed light with a luminescence that ceases almost immediately when the light source is shut off. The corresponding time is smaller than 10^{-6} sec.[11] Fluorescence occurs in gaseous, liquid, and solid substances. Precise measurements of fluorescence have significance in many branches of science as well as in medicine.[12,13] Some chemical substances that feature fluorescence are benzene,[11] fluorescein, anthracene, coumarin, and rhodamine dyes (Figs. 3.20–3.22).

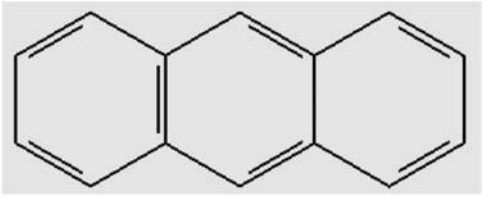

Figure 3.20 Anthracene.

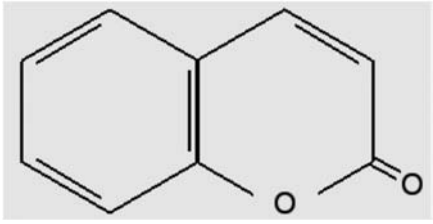

Figure 3.21 Coumarin.

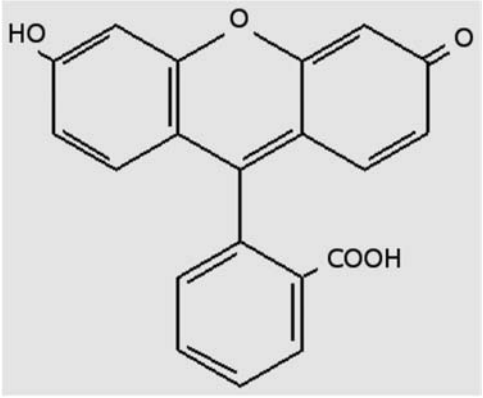

Figure 3.22 Rhodamine.

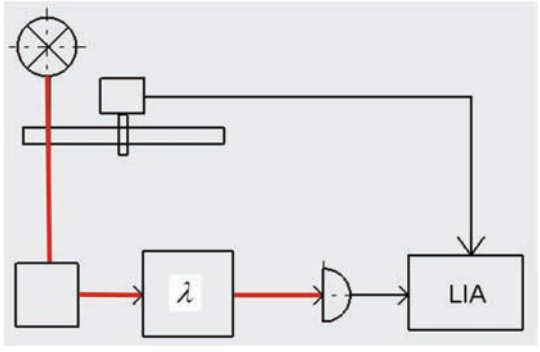

Figure 3.23 Setup for fluorescence measurement using mechanical modulation.

A typical property of the instrument configurations used for fluorescence detection is 90-deg geometry. Figure 3.23 shows an experimental setup that uses a rotating sector blade to periodically interrupt the light path. A representation of the corresponding configuration that features electronic modulation of the light source is given in Fig. 3.24. Alternatively, an electro-optic modulator (EOM) can be placed between the light source and the specimen under test. Such an experimental arrangement is shown in Fig. 3.25.

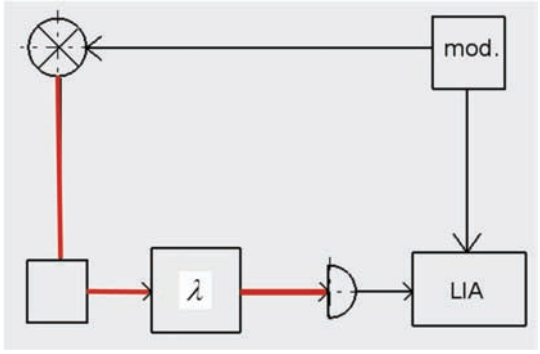

Figure 3.24 Setup for fluorescence measurement using electronic modulation.

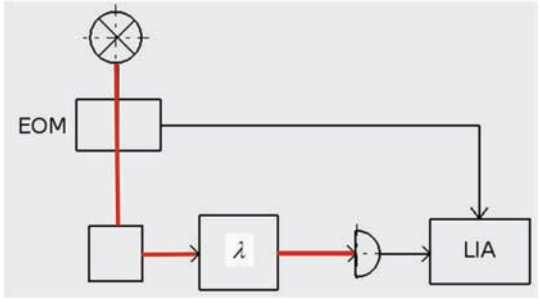

Figure 3.25 Setup for fluorescence measurement equipped with an electro-optical modulator.

3.2.2 Fluorescence lifetime imaging

Lock-in amplifiers are also used for fluorescence lifetime imaging.[14,15] The technique is based on the following phenomenon: The fluorescent light of a fluorophore excited by sinusoidally modulated light is delayed by a certain phase angle compared with the excitation light. The corresponding instrument configurations do not necessarily feature a dispersive element to select the excitation wavelength. A study on pH imaging of microscopic samples[15] uses an argon-ion laser that emits light at a wavelength of 488 nm. In order to be able to apply lock-in detection, the laser beam intensity is modulated with an EOM. This light beam is then directed to the sample under investigation (Fig. 3.26). A scanner unit is employed to target the light beam at different spots on the specimen. Between this scanning unit and the sample, the light passes through the lenses of a confocal microscope. The light emitted by fluorescence is guided into the optical detection path. An electronic signal generated by the control unit of the EOM serves as a reference for the lock-in amplifier.

In an earlier contribution,[14] Carlsson and Liljeborg describe how an experimental setup comprising a krypton-ion laser emitting at 568 nm as well as an argon-ion laser emitting at 488 nm can be realized. This experimental configuration can be used to simultaneously image lifetimes of different fluorophores (Fig. 3.27).

3.3 Phosphorescence Spectroscopy

Phosphorescence is another form of photoluminescence that is distinguished from fluorescence by the fact that the absorbed radiation is not immediately

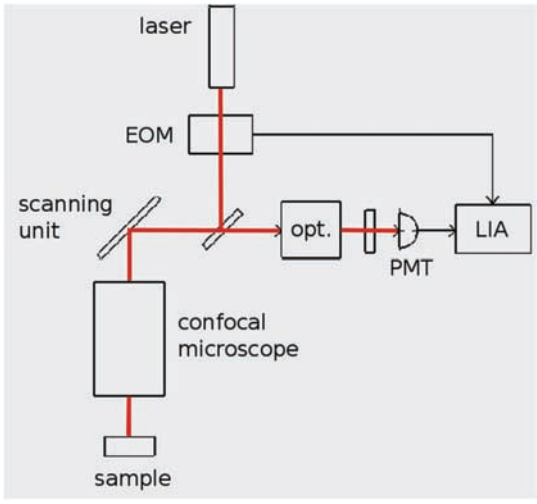

Figure 3.26 Setup for fluorescence measurement equipped with an EOM and a photomultiplier tube (PMT).

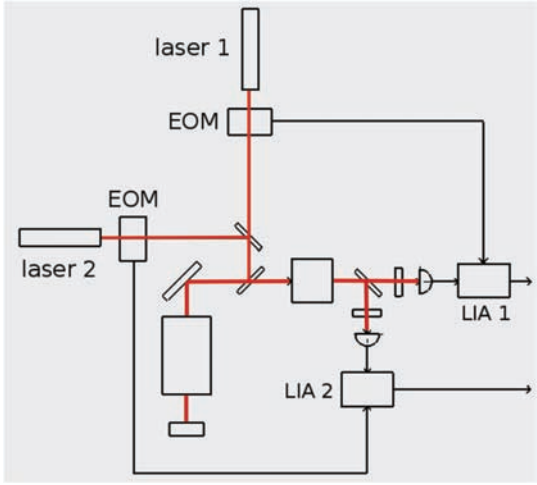

Figure 3.27 Setup for fluorescence measurement using two lasers at different wavelengths.

re-emitted in the former. The afterglow of phosphorescent materials can last for part of a second up to several hours. Substances featuring this property, or constituents of these substances, are designated as luminophores because they seem to store light.

In a nutshell, one might say that a luminescent material glows in the dark, while a fluorescent material does not emit light when the light source is switched off. Substances that show the phenomenon of phosphorescence are, e.g., zinc sulfide and strontium aluminate.

An instrumental configuration for the measurement of phosphorescence is depicted in Fig. 3.28. A special device often found in phosphorescence spectrometers is the mechanism of two rotating blades having a characteristic geometry (Figs. 3.29 and 3.30). The blades are positioned with respect to each other such that the excitation light is blocked from the specimen when light emitted from it falls onto the detector.

3.4 Outlook: Advanced Laser Spectroscopy

Many of the experimental configurations presented in this chapter can be viewed as laser experiments by interpreting the light source, which is depicted schematically in the drawings as a laser. Laser spectroscopy[16] is a growing field of modern science. Lock-in amplifiers have many applications in sophisticated instruments for laser spectroscopy.[8] Advanced techniques of spectroscopic research are built on these scientific instruments.

Saturation spectroscopy is such an advanced technique. A probe beam and a saturating beam, both of which are taken from a tunable laser, are

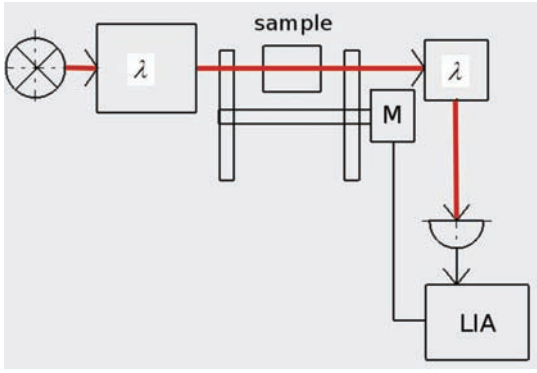

Figure 3.28 Setup for phosphorescence measurement using two rotating sector blades on an axis.

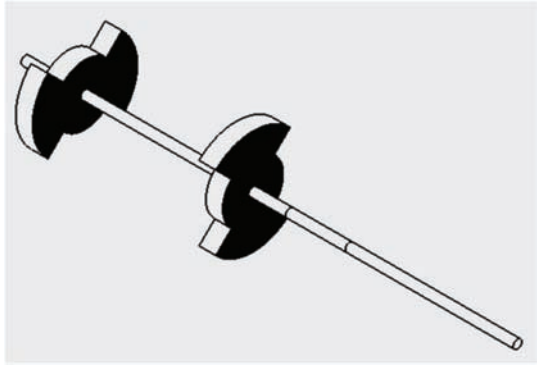

Figure 3.29 Two sector blades on an axis.

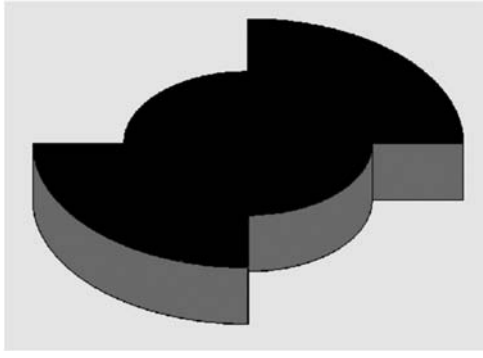

Figure 3.30 Single sector blade.

superimposed inside a specimen. The saturating beam is modulated by a chopper, and the probe beam is recorded using a lock-in amplifier.[17] A theoretical account of this technique can be found in the book by Meystre and Sargent.[18]

To observe Doppler-free, laser-induced dichroism and birefringence,[19] a pump beam generated by a dye laser is modulated by making use of a chopper. The probe beam, which stems from the same source of light, is passed through the same neon discharge cell as the pump beam and is then divided into two different states of polarization by a Wollaston prism. The corresponding signals are monitored by two lock-in amplifiers.

In one of the experimental arrangements of optical–optical double resonance spectroscopy, a dye laser provides the pump beam, which is periodically interrupted by a chopper. Another dye laser delivers the probe beam, which also interacts with a laser beam generated from an argon sodium laser. This interaction is observed using an ion detector, the output of which is the input signal to a lock-in amplifier.

These advanced techniques are mentioned here in the way of a future outlook. It is beyond the scope of this introductory text to treat them in detail.

References

1. R. Kingslake, Ed., *Applied Optics and Optical Engineering V: Optical Instruments* Part II, Academic Press, New York (1969).
2. J. F. James and R. S. Sternberg, *The Design of Optical Spectrometers*, Chapman and Hall, London (1969).
3. G. A. Vanasse, *Spectrometric Techniques*, Academic Press, New York (1977).
4. C. Burgess and T. Frost, Eds., *Standards and Best Practice in Absorption Spectrometry*, Blackwell Science Ltd., Oxford (1999).
5. A. P. Thorne, *Spectrophysics*, Chapman and Hall, London-New York (1988).
6. S. P. Davis, *Diffraction Grating Spectrographs*, Holt, Rinehart & Winston, New York (1970).
7. M. C. Hutley, *Diffraction Gratings*, Academic Press, London-New York (1982).
8. W. Demtröder, *Laser Spectroscopy: Basic Concepts and Instrumentation*, Springer-Verlag GmbH, Berlin-Heidelberg-New York (1996).
9. G. C. Bjorklund, "Frequency-modulation spectroscopy: a new method for measuring weak absorptions and dispersions," *Optics Letters* **5**(1), 15–17 (1980).
10. J. A. Silver, "Frequency-modulation spectroscopy for trace species detection: theory and comparison among experimental methods," *Applied Optics* **31**(6), 707–717 (1992).
11. D. A. Skoog, *Principles of Instrumental Analysis*, Saunders College Publishing, Philadelphia (1985).
12. W. Rettig, B. Strehmel, S. Schrader, and H. Seifert, Eds., *Applied Fluorescence in Chemistry, Biology, and Medicine*, Springer-Verlag GmbH, Berlin-Heidelberg (1999).

13. J. R. Lakowicz, *Principles of Fluorescence Spectroscopy*, Third Edition, Springer Science+Business Media, New York (2006).
14. K. Carlsson and A. Liljeborg, "Simultaneous confocal lifetime imaging of multiple fluorophores using the intensity-modulated multiple wavelength scanning (IMS) technique," *J. Microscopy* **191**(Pt 2), 119–127 (1998).
15. K. Carlsson, A. Liljeborg, R. M. Andersson, and H. Brismar, "Confocal pH imaging of microscopic specimens using fluorescence lifetimes and phase fluorometry: influence of parameter choice on system performance," *J. Microscopy* **199**(Pt 2), 106–114 (2000).
16. I. V. Hertel and C.-P. Schulz, "Molecular Spectroscopy," Chapter 5 in *Atoms, Molecules and Optical Physics 2—Molecules and Photonics: Spectroscopy and Collisions*, Springer-Verlag GmbH, Berlin-Heidelberg, pp. 289–381 (2015).
17. B. Henderson, "Optical Spectrometers," in *Handbook of Optics II: Devices, Measurements, and Properties*, M. Bass, E. W. Van Stryland, D. R. Williams, and W. L. Wolfe, Eds., McGraw-Hill, New York, pp. 20.24–20.26 (1995).
18. P. Meystre and M. Sargent, III, "Saturation Spectroscopy," Chapter 9 in *Elements of Quantum Optics*, Springer-Verlag GmbH, Berlin-Heidelberg, pp. 223–248 (2007).
19. C. Delaert and J. C. Keller, "Doppler-Free Laser-Induced Dichroism and Birefringence," in *Laser Spectroscopy III*, J. L. Hall and J. L. Carlsten, Eds., Springer-Verlag GmbH, Berlin-Heidelberg, pp. 154–159 (1976).

Chapter 4
Optical Interferometry

Interferometers are valuable instruments of measurement technology, and a wide variety of different interferometric configurations is used in science and industry.

Traditionally, interferometers are divided into those featuring amplitude division and those based on wavefront division. In this chapter, only amplitude-division interferometers are discussed.

Amplitude-division interferometers are again subdivided into two-beam interferometers and multiple-beam interferometers. Michelson interferometers, Kösters interferometers, Mach–Zehnder interferometers, Jamin interferometers, and many others are examples of two-beam interferometers. Fabry–Pérot interferometers, for example, belong in the multiple-beam category.

In the first group, we can make a further distinction in interferometric arrangements: those in which the device for dividing and re-combining the amplitude is the same, namely, Michelson and Kösters interferometers, and those that have separate optical means to separate and re-combine the amplitude, i.e., Mach–Zehnder and Jamin interferometers.

A broad branch of optical interferometry is devoted to examining and assessing the shape of surfaces by processing interferometric patterns.[1] Another branch, which might be designated as modulation interferometry, involves monitoring periodic phenomena (such as vibrations) and retrieving information on small amplitudes from modulated fringes. It is the latter branch of optical interferometry that we turn to in this chapter.

The technical literature contains a wealth of interferometric instruments that feature one or more lock-in amplification systems in their detection units. Sometimes the lock-in detection units help to improve the performance of an existing system, but in many cases, lock-in amplification is the very technique that makes possible the recovery of small or weak signals from noise.

We start with the basic equations that are useful to describe interference patterns. The phenomenon is characterized by the appearance of an additional interference term in the intensity equation. When two waves with

an identical frequency are superimposed, the intensity is proportional to the modulus of the (time-averaged) square of the sums of the corresponding electric fields:

$$I = |E_1 + E_2|^2. \tag{4.1}$$

This leads to an equation that features two quadratic expressions and an additional interference term:

$$I = A_1^2 + A_2^2 + 2A_1A_2\cos(\phi_1 - \phi_2). \tag{4.2}$$

The maxima (minima) of intensity in the interference pattern are called fringes.

The quadratic expressions can be identified with the intensities of the corresponding waves:

$$I = I_1 + I_2 + 2\sqrt{I_1 I_2}\cos(\phi_1 - \phi_2). \tag{4.3}$$

The intensities sum to the mean intensity $I_0 = I_1 + I_2$, which corresponds to the intensity in the case where no interference term appears. Equations (4.1) and (4.2) describe a striking feature of optical interference: Dark lines appear on an illuminated surface when two light waves are superimposed. To characterize observed fringes, it is useful to introduce a quantity called contrast or modulation:

$$\gamma = 2\frac{\sqrt{I_1 I_2}}{I_1 + I_2}. \tag{4.4}$$

Making reference to maximum and minimum intensities, Eq. (4.4) can be rewritten as

$$\gamma = \frac{I_{\max} - I_{\min}}{I_{\max} + I_{\min}} \quad \in [0,1]. \tag{4.5}$$

The modulation parameter can take values between 0 and 1, giving an alternative form of the interferometer equation in terms of mean intensity and contrast:

$$I = I_0 + \gamma\cos d. \tag{4.6}$$

In modulation interferometry, the optical path length difference of one arm is modulated in a periodic manner:

$$d = \phi_d + x\sin\omega t. \tag{4.7}$$

A combination of the formula that describes the interference intensity [Eq. (4.6) and an argument that represents modulation [Eq. (4.7)] leads to a relatively complicated nested function:

$$I = I_0 + \gamma \cos(\phi_d + x \sin \omega t). \tag{4.8}$$

Bessel functions are useful mathematical tools for dealing with expressions of nested trigonometric functions. One way to represent/introduce Bessel functions of the first kind is as Fourier expansions of trigonometric functions:

$$\cos(x \sin s) = J_0(x) + 2 \sum_{k=1}^{\infty} J_{2k}(x) \cos(2ks), \tag{4.9}$$

$$\sin(x \sin s) = 2 \sum_{k=1}^{\infty} J_{2k+1}(x) \sin[(2k-1)s], \tag{4.10}$$

where J_k indicates the Bessel function of the order k.

To proceed, a generalization of Eq. (4.9) is used:[2]

$$\cos(\phi_d + x \sin s) = \cos \phi_d \left[J_0(x) + 2 \sum_{k=1}^{\infty} J_{2k}(x) \cos(2k\omega t) \right] - \sin \phi_d \left\{ 2 \sum_{k=1}^{\infty} J_{2k+1}(x) \sin[(2k+1)\omega t] \right\}. \tag{4.11}$$

After low-pass filtering, it is the contribution at $1f$ that is detected:

$$I_{1f} = -2\gamma \sin \phi_d J_1(x). \tag{4.12}$$

Assuming that the trigonometric function can be approximated as $\sin \phi_d \cong \phi_d$, we have

$$I_{1f} \cong -2\gamma \phi_d J_1(x). \tag{4.13}$$

To express the Bessel function term, we make reference to another approximation used,[3] namely,

$$J_1(x) \cong \frac{x}{2}. \tag{4.14}$$

This leads to the following equation for the intensity:

$$I_{1f} \cong -\gamma \phi_d x. \tag{4.15}$$

This linearized equation [or Eq. (4.11)] is often used in optical interferometry[3] with lock-in detection. It links the measured intensity with the modulation parameter, the phase of the static optical path length difference, and the amplitude of the modulated part of the path length difference.

To apply techniques based on the use of lock-in amplifiers, it is necessary to generate a modulated measurement signal as well as a modulated reference

signal. There are at least two ways to realize this: (1) by periodically changing the transmission/phase in one arm of the interferometer, or (2) by periodically moving a mirror in one arm of the interferometer. We will consider these two methods in detail.

The derivation of the intensity equation is based on wave optics. However, a majority of this chapter deals with geometrical optics; i.e, a variety of optical interferometers are presented with emphasis on their geometrical realization. The purpose of this is twofold: On one hand, an overview of the many interferometric configurations that use lock-in amplifiers is given. Herein, emphasis is placed on generic geometries in order to provide access to the technical literature that presents and discusses many other and more-complex systems. On the other hand, this overview might indicate to an engineer and/or experimenter which toolbox would be useful for devising instruments for different applications. It will become clear that the combination of an optical interferometer and a lock-in detection system provides a unique versatility that allows one to adapt the geometry to different boundary conditions and measurement tasks. The overview might help readers choose the configuration that is most suitable for the measurement tasks at hand.

The availability of optical lasers as light sources has enabled the design and realization of interferometric instruments with lock-in detection of unprecedented precision and stability. Lock-in measurement units are often used to assess and measure the performance of actuators. Therefore, sensor configurations that allow one to probe the dynamic behavior of an actuator will be discussed. For applications in industry, these sensors can be implemented as compact measurement heads. They can perform long-term process monitoring and are suitable for integration into an automated quality control.

4.1 Michelson Interferometer

The Michelson interferometer is probably one of the most versatile interferometer configurations. A classical configuration of a Michelson interferometer is shown in Fig. 4.1.[4] It features a compensator plate to balance the optical path length difference in both arms of the interferometer. A more symmetric arrangement is depicted in Fig. 4.2, where a key component is the beamsplitter cube that divides the beams and also serves as beam combiner.

These configurations can be modified by replacing the plane mirrors with alternative optical components. In Figs. 4.3 and 4.4, roof prisms are depicted, but the use of corner-cube reflectors is also possible and probably more common.

The Michelson interferometer is a standard configuration used in Fourier spectroscopy.[5] Figure 4.5 shows a setup[6] implemented to measure small mechanical vibrations making use of a Michelson interferometer. To control

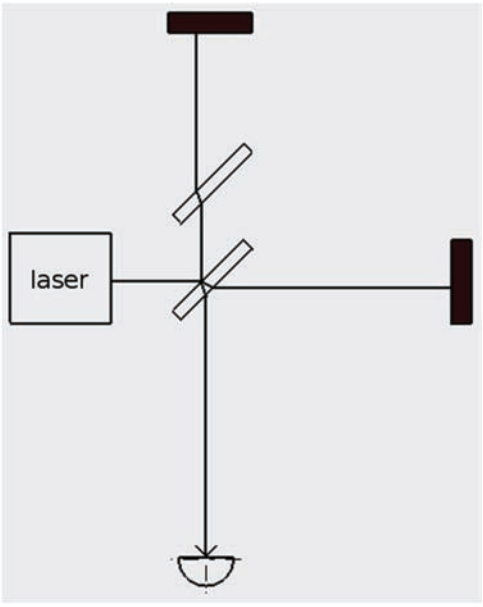

Figure 4.1 Setup for a Michelson interferometer.

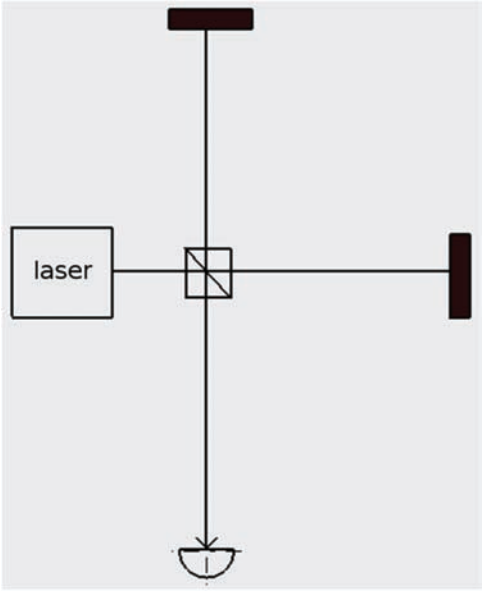

Figure 4.2 Setup for a Michelson interferometer with a symmetric beamsplitter.

the optical path length difference of the reference arm, an additional actuator can be introduced into that arm of the interferometer (Fig 4.6). This additional piezoelectric transducer can be, e.g., a $BaTiO_3$ crystal with a mirror mounted on it.[6]

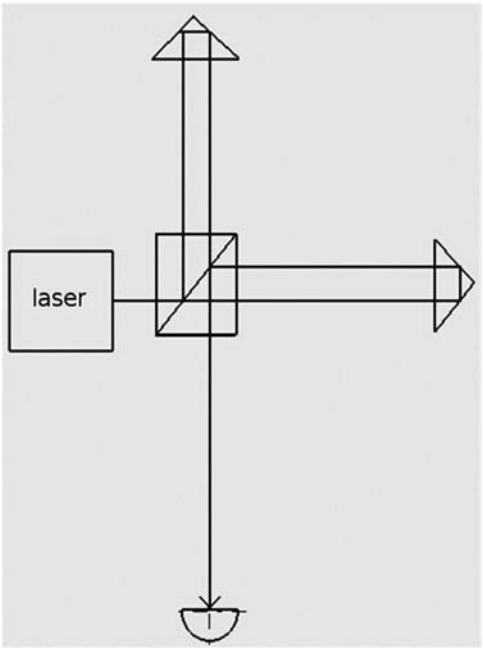

Figure 4.3 Setup for an interferometer with retroreflectors.

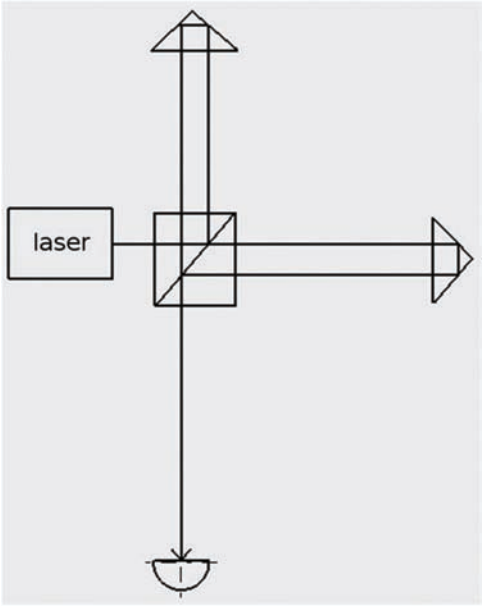

Figure 4.4 Alternative setup for an interferometer with retroreflectors.

A Michelson interferometer can be improved with polarizing optical components, an example[7] of which is given in Fig. 4.7. The beam of a linearly polarized laser is oriented 45 deg to the vertical. The polarization of the light

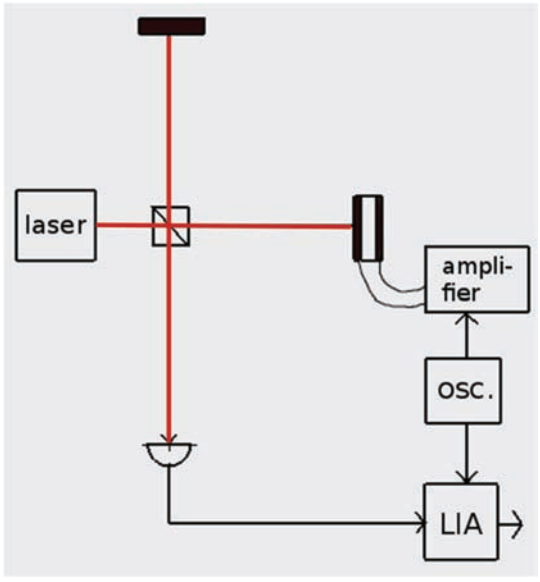

Figure 4.5 Setup for a lock-in technique to detect small voltage-induced vibrations. The voltage from the amplifier is connected to the electrodes on the vibrating sample.

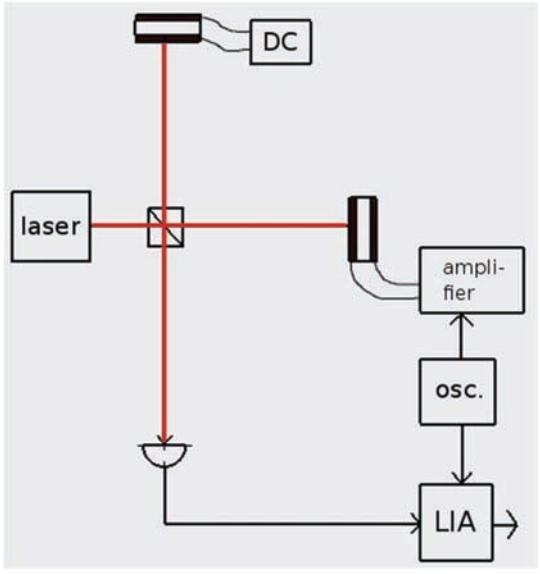

Figure 4.6 Setup for an interferometer with an additional piezoelectric transducer in the reference arm.

waves might be decomposed in directions parallel (Fig. 4.8) and perpendicular (Fig. 4.9) to the paper plane. The operating principle of the interferometer can be illustrated by considering the two orthogonal systems of polarization

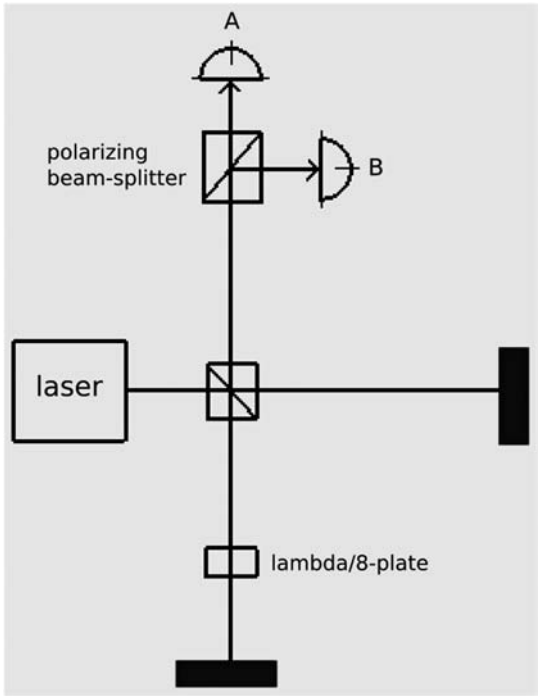

Figure 4.7 Setup for a Michelson interferometer with a polarizing optical readout.

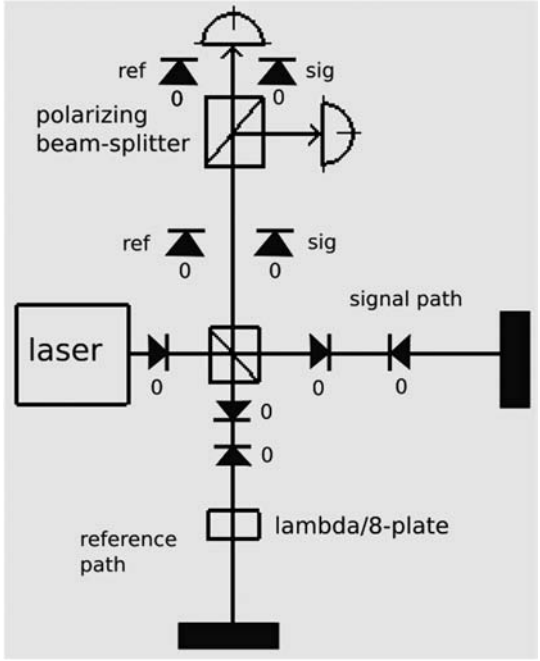

Figure 4.8 Setup in which the polarization direction is perpendicular to the slow axis of the λ/8 plate: No phase difference is induced between the signal and the reference, which are combined on detector A.

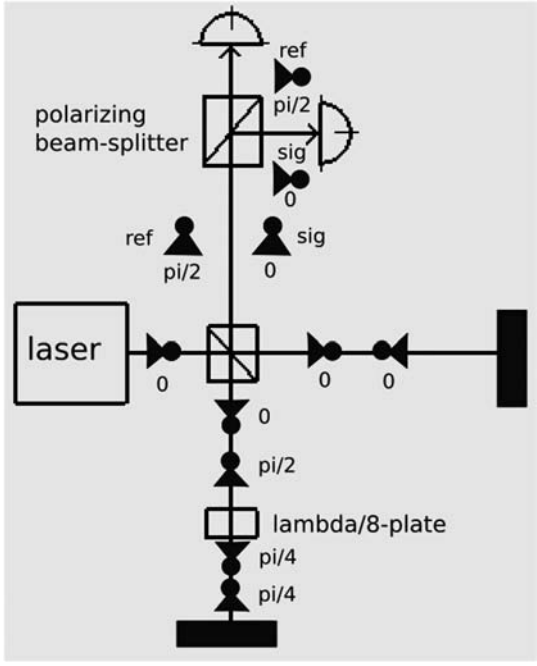

Figure 4.9 Setup in which the polarization direction is parallel to the slow axis of the λ/8 plate: A phase difference of π/2 is induced between the signal and the reference, which are combined on detector B.

separately. The slow axis of the λ/8 plate is aligned with one direction. The waves polarized perpendicular to this direction create an interference pattern on detector A, while the waves polarized parallel to this direction give rise to fringes at detector B. In this way, the experimenter can observe the output of the interferometer twice, i.e., with two detectors simultaneously. It is a salient feature of this opto-electronic instrument that both outputs are in phase quadrature. This provides the advantage that squaring and summing of the signals can be used to stabilize the interferometer at the operating point where it is most sensitive.

An advanced application of lock-in amplifiers can be found in interferometric gravitational wave detectors. Using a lock-in technique, it is possible to stabilize a suspended Michelson interferometer and use it to measure very small or weak signals.[8]

4.2 Kösters Interferometer

The key component of the Kösters interferometer[9,10] is the prism that bears the same name. The angle enclosed by the two opposite flat sides of the Kösters prism is 60 deg.[11] The prism beamsplitter is symmetric with respect to the horizontal plane, i.e., the plane where beamspitting occurs (Fig. 4.10). This component allows for a compact design of the interferometer. The measurement

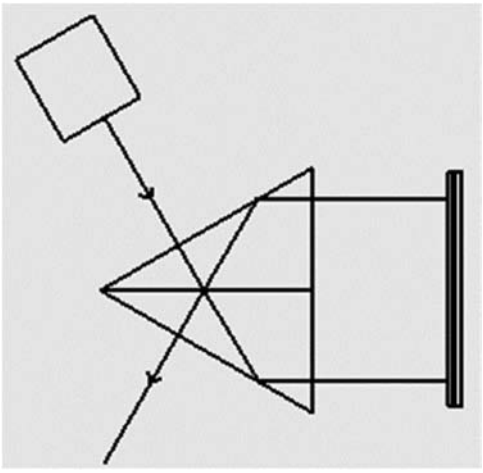

Figure 4.10 Setup for an interferometer with a Kösters prism as a beamsplitter.

and reference arms of the interferometer are parallel to each other, and the specimen and the reference specimen can be positioned close to one another.

A useful measurement application uses an interferometer based on a Kösters prism as an autocollimator.[12] In another type of optical interferometer[13] that uses a Kösters prism and a Porro prism instead of two plane mirrors, the light beam does not enter perpendicularly through the entrance surface of the Kösters prism but rather at an angle that differs by 90 deg. This configuration implies that the light beams in the interferometer arms are convergent and no longer parallel to each other. This type of interferometer is used to measure the deviation of a target device from a plane.

Figure 4.11 shows a symmetric experimental arrangement with two Kösters prisms. This configuration shows some similarity to that of a Mach–Zehnder interferometer.

Some interesting alternative geometries are in use that might be understood as modifications of the Kösters interferometer. The first geometry[4] can be derived by "splitting" the Kösters prism along its plane of symmetry and shifting the lower part in the direction of the optical axis. Figure 4.12 shows

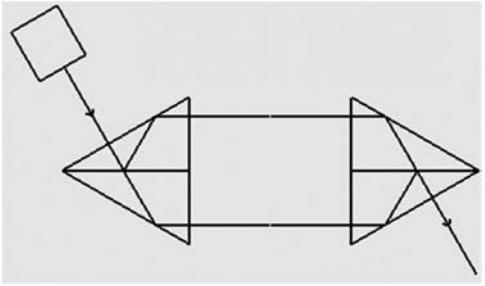

Figure 4.11 A symmetric interferometer geometry with two Kösters prisms.

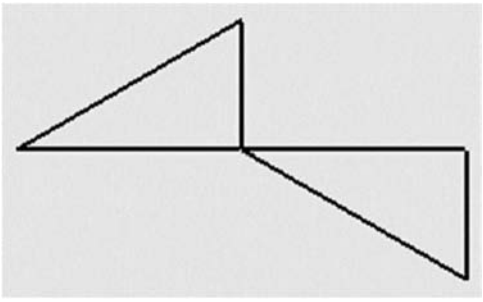

Figure 4.12 Geometry after splitting the Kösters prism.

the result of this operation. This geometry is now made "symmetric" with respect to a vertical plane that is perpendicular to the optic axis. In this way, a new component is derived (Fig. 4.13). An optical interferometer based on this component provides measurement and reference arms that point in opposite directions (Fig. 4.14).

The second geometry, which is shown in Fig. 4.15, has the property of providing inline input (and inline output). In comparison with the oblique geometry of the standard Kösters prism, this can be advantageous in some experimental situations. As in the case of the Michelson interferometer, the

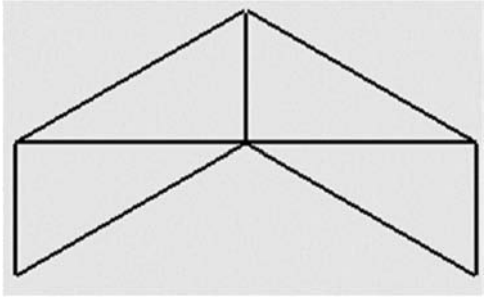

Figure 4.13 Geometry making the arrangement symmetric.

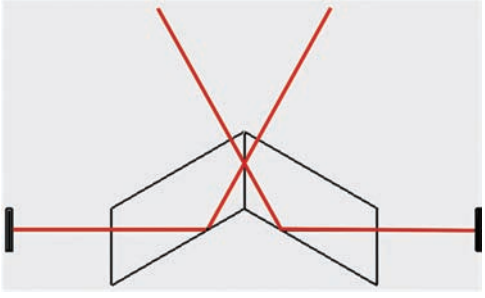

Figure 4.14 Interferometer geometry with measurement and reference arms pointing in opposite directions.

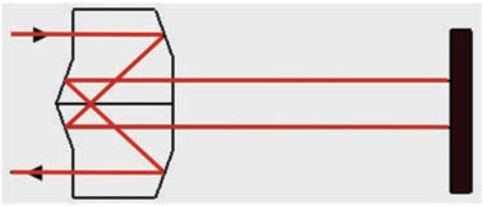

Figure 4.15 Interferometer geometry with inline input.

Kösters interferometer can be employed in modulation interferometry in several ways. If a vibrating mirror is introduced into the measurement arm of the device, small vibrations can be detected using a lock-in technique (Fig. 4.16). Another possibility is to operate a transparent modulating device in transmission in one arm of the interferometer.

4.3 Mach–Zehnder Interferometer

The geometry of the Mach–Zehnder interferometer provides a high degree of flexibility in the arrangement of instruments for measuring samples with varying sizes. This interferometer can host relatively large specimens. Figure 4.17 presents a standard configuration that consists of a beamsplitter, two mirrors, and a beam combiner.

Figure 4.18 shows an interesting modification of the Mach–Zehnder interferometer that was proposed by Hariharan.[14] It uses two pentaprisms in place of mirrors. Due to the different beam-pointing behavior of pentaprisms, the manual alignment of such an interferometer is a little different from that of an interferometer with plane mirrors and demands some practice.

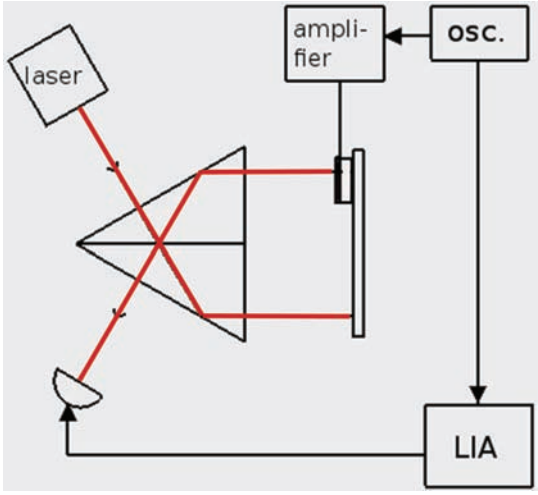

Figure 4.16 Setup of a Kösters interferometer and lock-in detection.

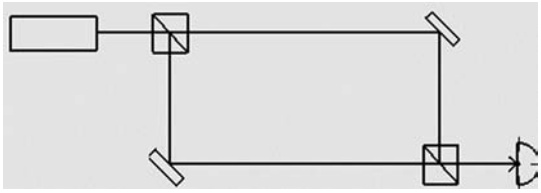

Figure 4.17 Setup of a Mach–Zehnder interferometer.

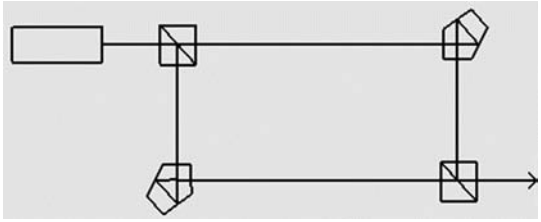

Figure 4.18 Setup of a Mach–Zehnder interferometer with pentaprisms.

Using a symmetry argument, we can establish a relation between the Mach–Zehnder interferometer and the Michelson interferometer, which was considered in Section 4.1. This relation is illustrated in Figs. 4.19 and 4.20.

Many applications of interferometers are based on the Mach–Zehnder configuration. In a polarization optical study, a liquid crystal spatial light modulator that is to be characterized can be introduced into the measurement arm of the interferometer.[15] An EOM is used to provide a time-varying shift between the electric field components of both arms, and a lock-in amplifier is employed to observe the phase delay.

Figure 4.19 A symmetry plane divides the interferometer configuration in two parts.

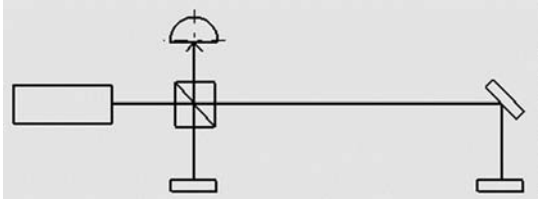

Figure 4.20 A new interferometer geometry is obtained by placing mirrors at positions on the symmetry plane.

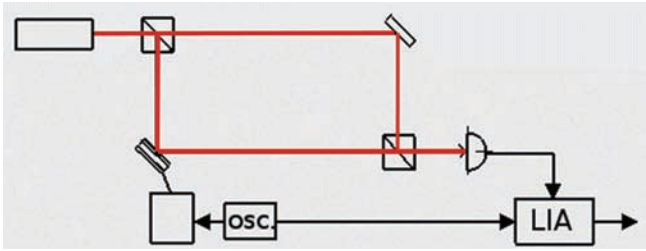

Figure 4.21 Setup of a Mach–Zehnder interferometer to measure piezoelectric samples.

A less sophisticated example is shown in Fig. 4.21. A piezoelectric specimen is characterized by providing it with a mirror and introducing it into the measurement arm. For samples that have to be investigated in transmission, the Mach–Zehnder interferometer offers ample space to introduce a modulating device in one arm of the interferometer (Fig. 4.22).

4.4 Jamin Interferometer

The Jamin interferometer,[16] which is named after the French scientist Jules Célestin Jamin,[17,18] comprises two plane-parallel transparent plates that serve as a beamsplitter and a beam combiner. Figure 4.23 shows these plates in a standard Jamin interferometry geometry. Figure 4.24 provides a closer look at the output of the interferometer. In order to obtain an unambiguous signal, some beams must be blocked before they reach the detector.

It could be considered a disadvantage for some applications that the lateral size of the samples to be introduced in the measurement path is limited by geometric conditions, as can be seen from Fig. 4.25. The separation of both arms is given by

$$s = d\frac{\sin(2\alpha)}{\sqrt{n^2 - \sin^2\alpha}}, \tag{4.16}$$

where the separation is a function of the refractive index, the angle α, and the thickness d of a plate.

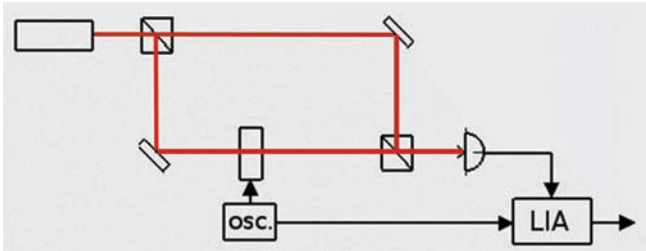

Figure 4.22 Setup of a Mach–Zehnder interferometer to measure transparent samples.

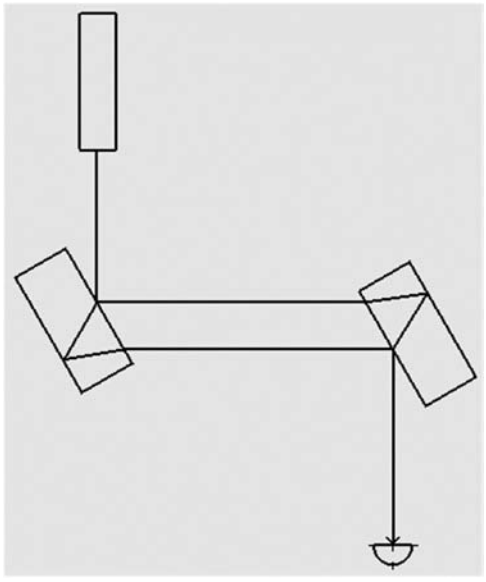

Figure 4.23 Setup of a Jamin interferometer.

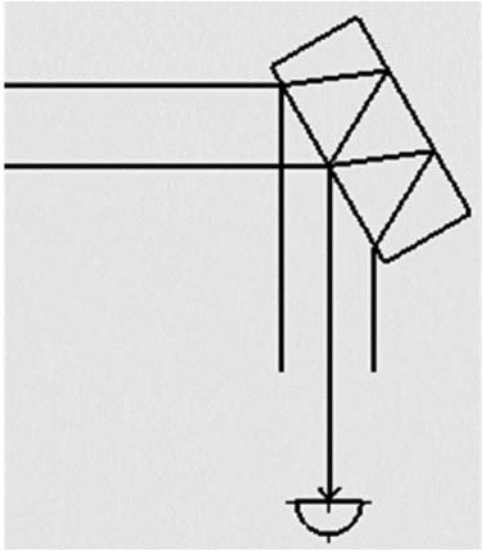

Figure 4.24 Setup of the beam combiner of a Jamin interferometer.

From the standard configuration of the Jamin interferometer (Fig. 4.23), a folded Jamin interferometer can be derived[19] by using a retroreflector. In Fig. 4.26, a roof prism is introduced into the optical path as a retroreflector. In this configuration, a single plane-parallel plate serves as both a beamsplitter and a beam combiner.

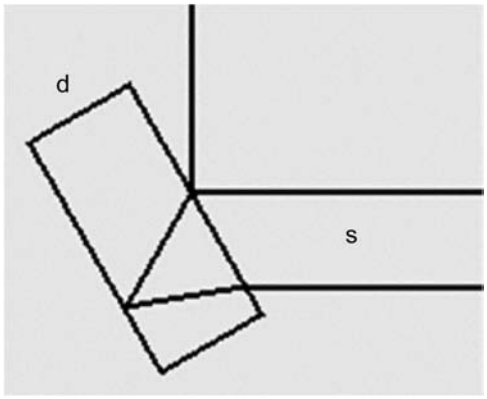

Figure 4.25 Illustration defining the separation *s* of the two arms and the thickness *d* of the plate.

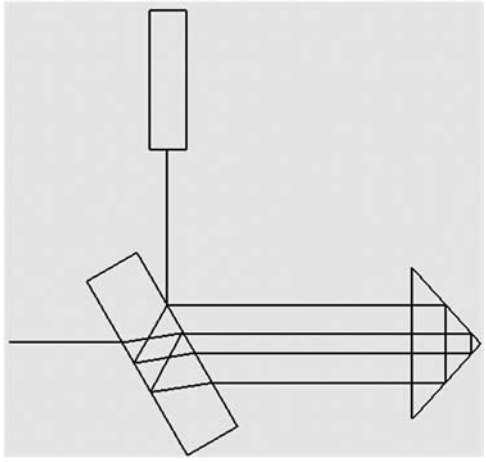

Figure 4.26 Folded Jamin interferometer.

Figure 4.27 shows a classical measurement setup for studying electro-optical coefficients of transparent crystals. The crystal under study is introduced into one arm of the interferometer. A periodic voltage is applied to the crystal, and the modulated signal is measured using a lock-in amplifier.

4.5 Spherical Fabry–Pérot Interferometer

An experimental apparatus for measuring piezoelectric oscillations has been suggested by Bruins and Garland.[20] The apparatus is based on a spherical Fabry–Pérot interferometer. The specimen under test is mechanically linked to one mirror of the Fabry–Pérot cavity. In this way, small vibrations of the piezoelectric sample cause small variations in the cavity length. These periodic changes are then detected using a lock-in amplifier. The measurement head of the interferometer can be placed in a temperature-controlled can.

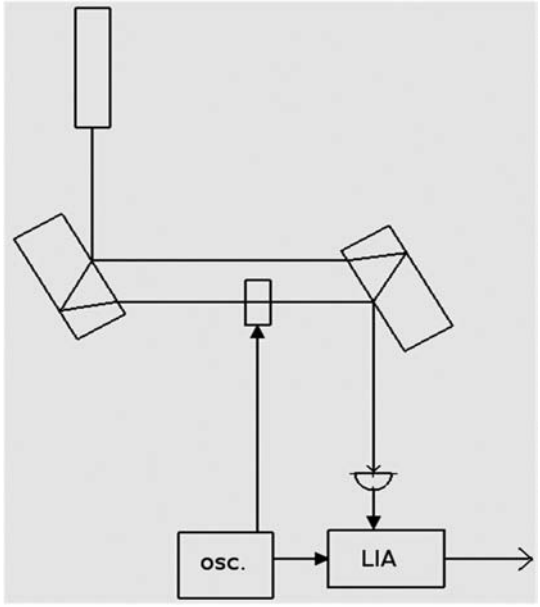

Figure 4.27 Setup of a Jamin interferometer with a lock-in technique.

4.6 Conclusion

This chapter provides an overview of the many technical configurations that are possible when an optical interferometer and a lock-in detection unit are combined to form a high-precision measurement system. Such a device can measure optical or mechanical properties and can operate in transmission or reflection mode. The geometry of the sensor can be adapted to the measurement task, providing a high degree of versatility. Examples provided include a 90-deg configuration, sensors probing with parallel beams, common-path interferometers, devices with measurement and reference arms pointing in opposite directions, sensors with inline input, devices with rectangular symmetry, as well as instruments with a folded configuration.

References

1. D. Malacara, Ed., *Optical Shop Testing*, John Wiley & Sons, New York-Chichester-Brisbane-Toronto (1978).
2. D. A. Jackson, "Monomode optical fibre interferometers for precision measurements," in *Current Advances in Sensors*, B. E. Jones, Ed., Adam Hilger, Bristol (1987).
3. D. P. Blair and P. H. Sydenham, "Phase sensitive detection as a means to recover signals buried in noise," *J. Physics E: Scientific Instruments* **8**, 621–627 (1975).
4. W. H. Steel, *Interferometry*, Cambridge University Press, Cambridge-New York-New Rochelle-Melbourne-Sydney, p. 109 (1987).

5. A. P. Thorne, *Spectrophysics*, Chapman and Hall, London-New York (1988).
6. S. Sizgoric and A. A. Gundjian, "An optical homodyne technique for measurement of amplitude and phase of sub-angstrom ultrasonic vibration," *Proc. IEEE* **57**(7), 1313–1314 (1969).
7. D. Vilkomerson, "Measuring pulsed picometer-displacement vibrations by optical interferometry," *Applied Physics Letters* **3**(1), 183–185 (1976).
8. F. Barone, E. Calloni, R. De Rosa, L. Di Fiore, F. Fusco, L. Milano, and G. Russo, "Fringe-counting technique used to lock a suspended interferometer," *Applied Optics* **33**(7), 1194–1197 (1994).
9. J. B. Saunders, "The Kösters interferometer," *J. Research of the National Bureau of Standards* **58**(1), 27–31 (1957).
10. G. H. Lovins, "High-precision pointing interferometer," *Applied Optics* **3**(7), 883–887 (1964).
11. J. Shamir, "Compact interferometer for accurate determination of optical constants of thin films," *J. Physics E; Scientific Instruments* **9**, 499–502 (1976).
12. E. J. Tew, Jr., "Measurement techniques used in the optics workshop," *Applied Optics* **5**(5), 695–700 (1966).
13. R. O. Naess, "A measuring interferometer for high accuracy alignment," *Applied Optics* **7**(11), 2315–2317 (1968).
14. P. Hariharan, "Modified Mach–Zehnder interferometer," *Applied Optics* **8**(9), 1925–1926 (1969).
15. M. Yamauchi, A. Márquez, J. A. Davis, and D. J. Franich, "Interferometric phase measurements for polarization eigenvectors in twisted nematic liquid crystal spatial light modulators," *Optics Communications* **181**, 1–6 (2000).
16. G. Bruhat, *Optique*, Masson, Paris-Milano-Barcelona, pp. 133–135 (1992).
17. J. C. Jamin, "Description d'un nouvel appareil de recherches, fondé sur les interférences," *Comptes rendus hebdomadaires des séances de l'Académie des sciences* **42**, 482–485 (1856).
18. J. Jamin, "Mémoires sur les variations de l'indice de refraction de l'eau à diverses pressions," *Annales de chimie et de physique* **52**, 163–171 + Fig. on p. 513 (1858).
19. A. J. Sedlacek, "Real-time detection of ambient aerosols using photothermal interferometry: Folded Jamin interferometer," *Review of Scientific Instruments* **77**, 064903 (2006).
20. D. E. Bruins and C. W. Garland, "New interferometric method for piezoelectric measurements," *Review of Scientific Instruments* **46**(9), 1167–1170 (1975).

Chapter 5
Crystal Research and Technology

The interest in crystal effects from the point of view of lock-in amplifier technology is twofold. On one hand, these effects are the subject of experimental studies that use delicate instruments equipped with lock-in amplifiers to detect small amplitudes. On the other hand, they form the basis of devices that are used to modulate light (electro-optic modulators and photo-elastic modulators, for example) or of solid state actuators that are used to periodically move mirrors.

Magneto-optic, electromechanical, and electro-optic crystal effects are introduced on a phenomenological basis. Quite often these effects are so small that the use of lock-in detection is mandatory to measure them. In many cases, the optical part of the measurement instrument is an interferometer.

5.1 Magneto-Optic Effects

Magneto-optic (MO) effects[1] are changes of optical material properties caused by a magnetic field. These effects can be described by introducing a dielectric constant that depends on magnetization. Because the induced anisotropy is a salient feature, it is helpful to start with the dielectric tensor and extend it by terms that depend on magnetization. The equation for the dielectric tensor is

$$\mathbf{D} = \varepsilon \mathbf{E}, \tag{5.1}$$

where $\mathbf{D}$ is the dielectric displacement vector, ε is the dielectric tensor in the presence of a magnetic field, and $\mathbf{E}$ is the vector of the applied electric field. In the presence of a magnetic field, $\mathbf{D}$ can be denoted as

$$\mathbf{D} = \left(\underbrace{\varepsilon_\Theta I + iQ \begin{bmatrix} 0 & -m_3 & m_2 \\ m_3 & 0 & -m_1 \\ -m_2 & m_1 & 0 \end{bmatrix}}_{\text{linear MO effects}} + \underbrace{\begin{bmatrix} R_1 m_1^2 & R_2 m_1 m_2 & R_2 m_1 m_3 \\ R_2 m_1 m_2 & R_1 m_2^2 & R_2 m_2 m_3 \\ R_2 m_1 m_3 & R_2 m_2 m_3 & R_1 m_3^2 \end{bmatrix}}_{\text{quadratic MO effects}} \right) \mathbf{E}, \tag{5.2}$$

where ε_Θ is the dielectric constant, the coefficients Q and R_k are material constants, and i is the unit of the imaginary axis in the complex plane. The magnetization vector **m** is chosen as a unit vector:

$$m_1^2 + m_2^2 + m_3^2 = 1. \tag{5.3}$$

The first term on the right-hand side of Eq. (5.2) corresponds to the dielectric tensor of an isotropic material in the absence of a magnetic field. The next term describes linear magneto-optic effects. This extension of the dielectric tensor has the form of a skew-symmetric matrix. The last term represents quadratic magneto-optic effects (the Voigt effect[2] or Cotton–Mouton effect[3,4]) and takes the form of a symmetric matrix. One material constant R_1 in this tensor relates to the diagonal entries, and the other material constant R_2 relates to the off-diagonal elements of the tensor. The tensor that describes the quadratic magneto-optic effects of an isotropic material can be decomposed into a diagonal part and a part that is also symmetric and has trace zero:

$$\begin{bmatrix} R_1 m_1^2 & R_2 m_1 m_2 & R_2 m_1 m_3 \\ R_2 m_1 m_2 & R_1 m_2^2 & R_2 m_2 m_3 \\ R_2 m_1 m_3 & R_2 m_2 m_3 & R_1 m_3^2 \end{bmatrix} = R_1 \begin{bmatrix} m_1^2 & 0 & 0 \\ 0 & m_2^2 & 0 \\ 0 & 0 & m_3^2 \end{bmatrix} + R_2 \begin{bmatrix} 0 & m_1 m_2 & m_1 m_3 \\ m_1 m_2 & 0 & m_2 m_3 \\ m_1 m_3 & m_2 m_3 & 0 \end{bmatrix}. \tag{5.4}$$

We now take a closer look at the linear magneto-optic effects. A fundamental distinction between types of linear effects is that the Faraday effect is observed in transmission, while the magneto-optic Kerr effect is measured in reflection. However, both of these linear effects can be described as magnetic circular birefringence.

5.1.1 Faraday effect

The Faraday effect[5] makes up part of the initial evidence of a physical link between light and magnetism. Nowadays, electromagnetic theory forms one of the pillars of classical physics, but at the time of its discovery, this link was by no means obvious.

One method to measure the Faraday effect is by letting a light beam pass through a Faraday cell. This is a device that consists of a specimen of a transparent, dielectric medium that is exposed to a strong magnetic field. The effect is based on circular birefringence, in which left and circularly polarized waves propagate at slightly different speeds through the transparent sample. This has the following consequence: After passing through the Faraday cell, the polarization plane of a linearly polarized wave is rotated by an angle β (Fig. 5.1). The angle of rotation β of the plane depends on the geometric path length d and the magnetic flux density B (the magnitude of the magnetic field):

$$\beta = V \cdot d \cdot B, \tag{5.5}$$

where the intervening material constant V is called the Verdet constant.

An important feature of the Faraday effect is that the rotation takes twice its value if the device is passed two times, first in one direction and then in the opposite direction. This is in contrast to passing through an optically active substance. In an optically active substance, the rotation is compensated after the second pass in the opposite direction. This different phenomenology of the Faraday effect is the reason that it can be used in so-called optical isolators.

To measure the effect using a lock-in technique, the magnetic field is modulated periodically. It is convenient to use a linearly polarized laser as a light source to define the plane of polarization, and to place a polarizer into the optical path before the detector (Fig. 5.2). Using the modulation signal that controls the magnetic field as a reference signal as well, the changes in light intensity can now be recorded with the lock-in unit.

5.1.2 Magneto-optic Kerr effect

The magneto-optic Kerr effect[6,7] is observed experimentally by measuring the light reflected from a sample. Due to the pronounced anisotropy, the magneto-optic Kerr effect (MOKE) is measured in three different experimental

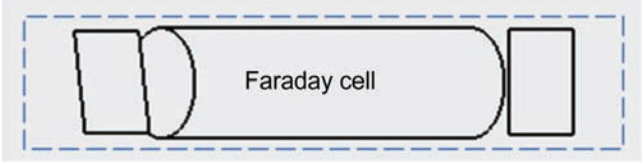

Figure 5.1 The plane of polarization of linearly polarized light is rotated after passing through a Faraday cell.

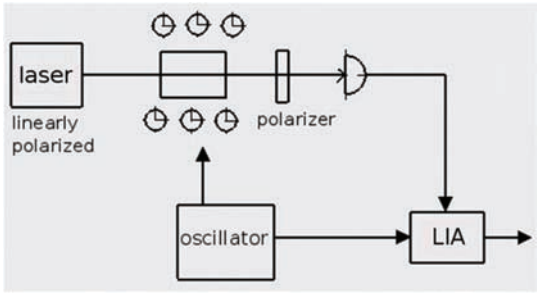

Figure 5.2 Faraday cell in a magnetic field used to modulate the intensity of a laser.

configurations. In the longitudinal configuration, the plane in which the incident and reflected beams propagate is parallel to the vector of magnetization (Fig. 5.3). In the transversal configuration, the vector of magnetization is perpendicular to the plane in which the incident and reflected light beams propagate (Fig. 5.4). The geometry in which to observe the polar MOKE is depicted in Fig. 5.5.

In a typical MOKE setup (Fig. 5.6), a light beam is modulated using a photo-elastic modulator (PEM) and directed toward a specimen. After passing through a polarizer, the beam impinges on the sample. From the surface of the specimen it is then reflected in the direction of the detector in front of which an analyzer has been placed. The phenomenon is interesting

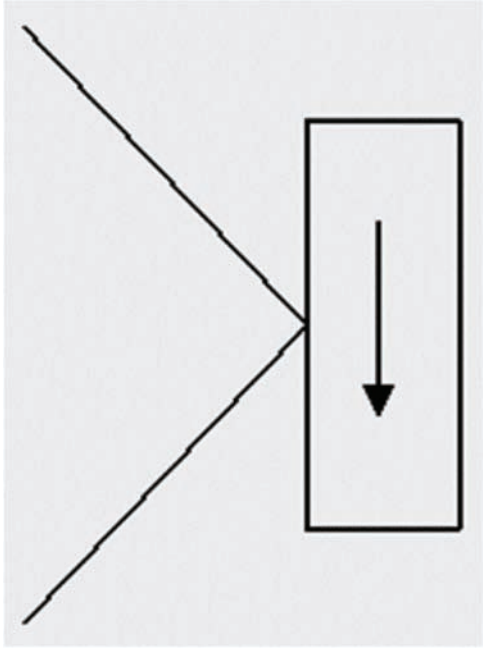

Figure 5.3 Longitudinal configuration.

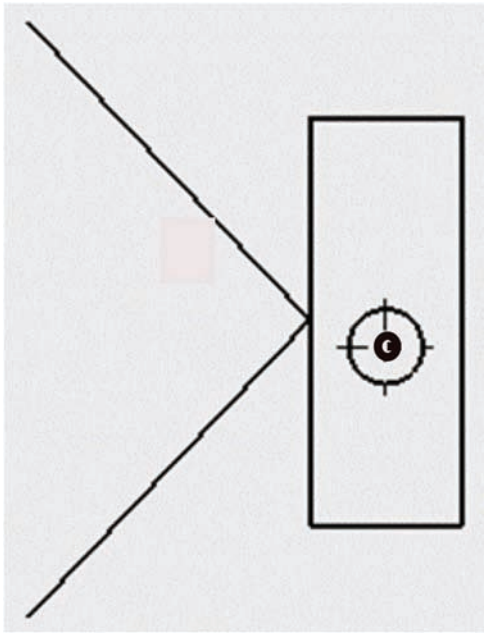

Figure 5.4 Transversal configuration.

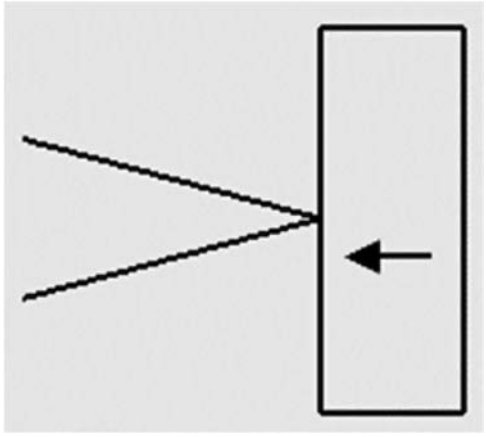

Figure 5.5 Polar configuration.

from a technological point of view because, e.g., the magneto-optic Kerr effect is exploited in magneto-optic systems for data storage.[8,9]

5.2 Electromechanical Cross-Effects

A dielectric sample becomes strained when exposed to an electric field. In most materials, these strains are so small that lock-in techniques have to

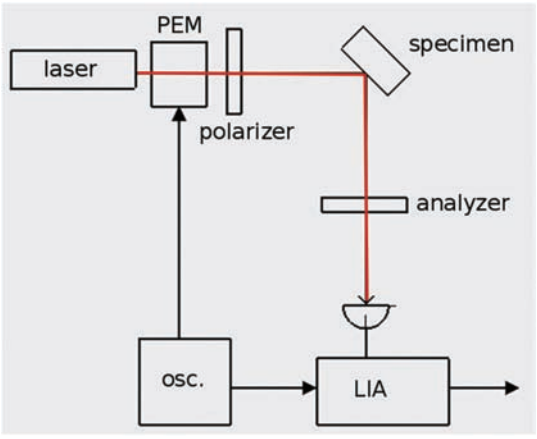

Figure 5.6 Experimental configuration for measuring the magneto-optic Kerr effect. The laser light is modulated using a photo-elastic modulator.

be applied to observe them. All dielectrics show electrostriction, an effect that is quadratic in the applied electric field. In some materials, the linear effect can also be observed; this is the piezoelectric effect. (Note that some authors use electrostriction as a term that comprises piezoelectricity as well as quadratic electrostriction.) The equation that describes piezoelectricity and electrostriction by linking the observed strain to the applied electric field can be written as

$$\varepsilon = d \cdot E + \gamma \cdot E^2, \tag{5.6}$$

where d and γ are material constants that are characteristic of the corresponding dielectric.

In a more general experimental situation, the anisotropy of the fields and of the material has to be taken into account, and the situation is described using tensor notation:

$$\varepsilon_{ij} = \sum_{k=1}^{3} d_{ijk} E_k + \sum_{k=1}^{3} \sum_{l=1}^{3} \gamma_{ijkl} E_k E_l, \tag{5.7}$$

where ε_{ij} is a component of the strain tensor, and E_k is the k^{th} component of the electric field strength vector. The material constants are expressed as coefficients of the corresponding tensors, namely, the tensor of piezoelectric coefficients and the tensor of electrostrictive coefficients.

A first step in exploring the material anisotropy expressed by the tensor equation [Eq. (5.7)] is to measure the longitudinal electromechanical effect (Fig. 5.7) and the transverse electromechanical effect (Fig. 5.8). In the first case, the direction of strain and the direction of the electric field are parallel. In the case of the transversal effect, the directions of strain and of the electric field are perpendicular to each other.

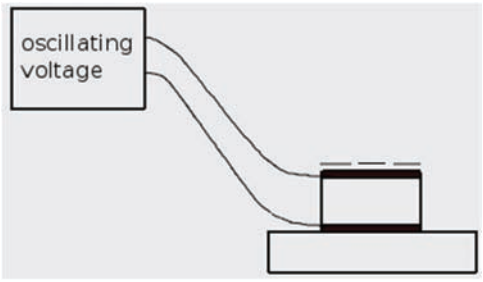

Figure 5.7 Longitudinal electromechanical effect.

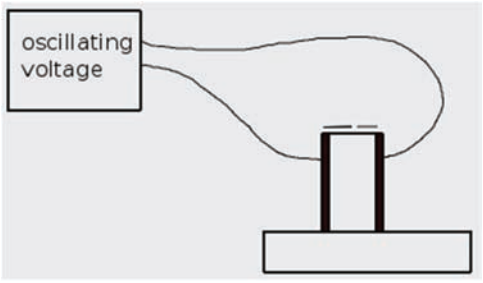

Figure 5.8 Transverse electromechanical effect.

One way to view these experiments is as observations of the way the form of a capacitor changes under the influence of an electric field. The measurement of these electromechanical cross-effects is not restricted to crystals and may be extended to other classes of dielectrics as well. Winkelhahn et al.[10,11] and Levitus et al.[12] report measurements on polymer electrets and polymer films, for example, using lock-in amplifiers in a Nomarski interferometer setup. The authors refer to the technique as electromechanical interferometry.

5.2.1 Piezoelectricity

The piezoelectric effect[13,14] is widely used in electromechanical actuators, and piezoelectric transducers[15] have found applications in many branches of technology. A straightforward way to measure piezoelectric coefficients with lock-in amplifiers is to put the piezoelectric sample at the end of one arm of an optical interferometer (Figs. 4.5 and 4.16) and to provide the sample with a mirror or a reflective layer. Oscillations of this sample under the influence of the applied AC voltage will then translate into a modulation of the path length difference, which can be measured with the interferometer.

5.2.2 Quadratic electrostriction and Maxwell stresses

Being a quadratic effect, electrostriction is measured at $2f$, i.e., at the second harmonic of the modulation frequency. In general, the observed strain signals are very small, and some effort must be made to recover them from noise.

In experimental practice, quadratic electrostriction is superimposed by another effect: Maxwell stresses.[16–18] Because this strain response of the dielectric also depends on the square of the electric field strength, it is, at least, difficult to separate it from quadratic electrostriction when a lock-in measurement at $2f$ is being performed. Therefore, some effort has been made to theoretically predict the contribution of electrostatic Maxwell stresses. A starting point is the Maxwell stress tensor, which displays a relatively intricate dependence on the dielectric properties of the material.

An account of the experimental details of electrostriction measurement is given by Yimnirun et al.[19] To compensate for spurious vibrations of the sample holder, an interferometric configuration that measures vibrations on two opposite sides has been proposed.[20]

5.3 Electro-Optic Effects

The physical phenomenon on which many electro-optic devices are based is double refraction (birefringence) in solid and liquid dielectrics in an electrostatic field. This electro-optic effect[21] is a change in the refractive index of a material under test in response to an applied electric field. The effect can be described as a change of the inverse dielectric constant tensor under the influence of the electric field. This tensor is also referred to as the impermeability tensor:

$$e_{ij} = \sum_{k=1}^{3} r_{ijk} E_k + \sum_{k=1}^{3} \sum_{l=1}^{3} g_{ijkl} E_k E_l, \tag{5.8}$$

where $e_{ij} = \Delta(1/n_{ij}^2)$ are coefficients of the impermeability tensor, E_k is the k^{th} component of the electric field strength vector, and Δ indicates a difference. It might seem surprising that the quantity $\Delta(1/n_{ij}^2)$ is used instead of a linear function of the refractive index. The reason for this choice is that this quantity has the property of a tensor, a fact that is helpful in the study of material anisotropy.

The applied field induces birefringence; i.e., the sample features different indices of refraction for light that is polarized parallel to or perpendicular to the applied electric field.

Two parts can be distinguished in Eq. (5.8), namely, a linear part that represents the Pockels effect and a quadratic part that represents the electro-optic Kerr effect. The first effect has found more applications in electro-optic modulators.

In conjunction with polarizers, devices based on the electro-optic effect can be used to modulate the phase, polarization, amplitude, or frequency of light. This explains why electro-optic modulators have many applications.

5.3.1 Linear electro-optic effect: the Pockels effect

The linear electro-optic effect is exhibited by crystals that lack a center of symmetry. The tensor of linear electro-optic coefficients has three indices.

To be able to note this three-dimensional object in the plane of a page, a contracted notation is often used in the technical literature. The equation in tensor notation,

$$\Delta\left(\frac{1}{n_{ij}^2}\right) = \sum_{k=1}^{3} r_{ijk} E_k, \tag{5.9}$$

is replaced by an equation in contracted notation:

$$\Delta\left(\frac{1}{n^2}\right)_\alpha = \sum r_{\alpha\beta} E_\beta. \tag{5.10}$$

After expansion, this equation takes the form

$$\begin{bmatrix} \Delta\left(\frac{1}{n^2}\right)_1 \\ \Delta\left(\frac{1}{n^2}\right)_2 \\ \Delta\left(\frac{1}{n^2}\right)_3 \\ \Delta\left(\frac{1}{n^2}\right)_4 \\ \Delta\left(\frac{1}{n^2}\right)_5 \\ \Delta\left(\frac{1}{n^2}\right)_6 \end{bmatrix} = \begin{bmatrix} r_{11} & r_{12} & r_{13} \\ r_{21} & r_{22} & r_{23} \\ r_{31} & r_{32} & r_{33} \\ r_{41} & r_{42} & r_{43} \\ r_{51} & r_{52} & r_{53} \\ r_{61} & r_{62} & r_{63} \end{bmatrix} \begin{bmatrix} E_1 \\ E_2 \\ E_3 \end{bmatrix}, \tag{5.11}$$

where the coefficients r_{11}, r_{22}, and r_{33} represent the longitudinal effect, while the coefficients r_{12}, r_{13}, r_{21}, r_{23}, r_{31}, and r_{32} are measures for the transverse effect. Equation (5.11) describes very small changes of the refractive indices of the material under the influence of an applied electric field. Let us denote the refractive indices in the "undisturbed" situation as n_{01}, n_{02}, and n_{03}. The refractive indices n_1, n_2, and n_3, which are observed if the electric field is applied, may then be denoted as follows:

$$\begin{bmatrix} \frac{1}{n_1^2} & 0 & 0 \\ 0 & \frac{1}{n_2^3} & 0 \\ 0 & 0 & \frac{1}{n_3^2} \end{bmatrix} = \begin{bmatrix} \frac{1}{n_{01}^2} & 0 & 0 \\ 0 & \frac{1}{n_{02}^2} & 0 \\ 0 & 0 & \frac{1}{n_{03}^2} \end{bmatrix} + \begin{bmatrix} \Delta\left(\frac{1}{n^2}\right)_1 & 0 & 0 \\ 0 & \Delta\left(\frac{1}{n^2}\right)_2 & 0 \\ 0 & 0 & \Delta\left(\frac{1}{n^2}\right)_3 \end{bmatrix}$$

$$+ \begin{bmatrix} 0 & \Delta\left(\frac{1}{n^2}\right)_6 & \Delta\left(\frac{1}{n^2}\right)_5 \\ \Delta\left(\frac{1}{n^2}\right)_6 & 0 & \Delta\left(\frac{1}{n^2}\right)_4 \\ \Delta\left(\frac{1}{n^2}\right)_5 & \Delta\left(\frac{1}{n^2}\right)_4 & 0 \end{bmatrix}. \tag{5.12}$$

Keep in mind that the mathematical objects that appear in this equation are matrices, not tensors. The first matrix on the right-hand side represents the constants in the absence of an applied electric field. The second matrix describes changes along the main axis of the chosen coordinate system. Finally, the traceless matrix, which is the third term in the sum, has coefficients as its entries that describe small changes that induce a lower material symmetry under the influence of the applied field. The values of the coefficients $\Delta(1/n^2)_\alpha$ are quite small, typically on the order of 10^{-5}. Therefore, lock-in techniques are an appropriate means to experimentally determine these coefficients.

Figure (5.9) shows a Pockels cell in longitudinal configuration, and Fig. (5.10) shows a Pockels cell in transversal configuration. Both types of cells are commercially available. An electro-optic modulator in longitudinal configuration has to be provided with transparent electrodes to let the light beam pass through the cell.

A Pockels cell is often used in laser experiments to modulate a light beam. This is a prerequisite to applying lock-in detection. An advanced experiment on circular dichroism[22] is sketched in Fig. 5.11. The light of the pump beam is

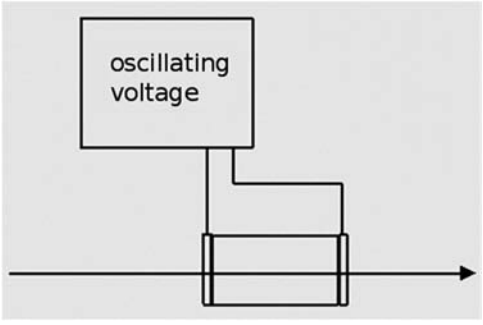

Figure 5.9 Pockels cell in a longitudinal configuration.

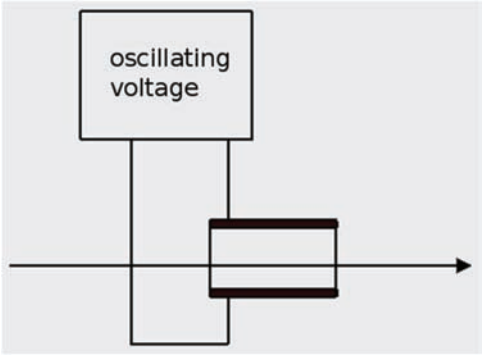

Figure 5.10 Pockels cell in a transversal configuration.

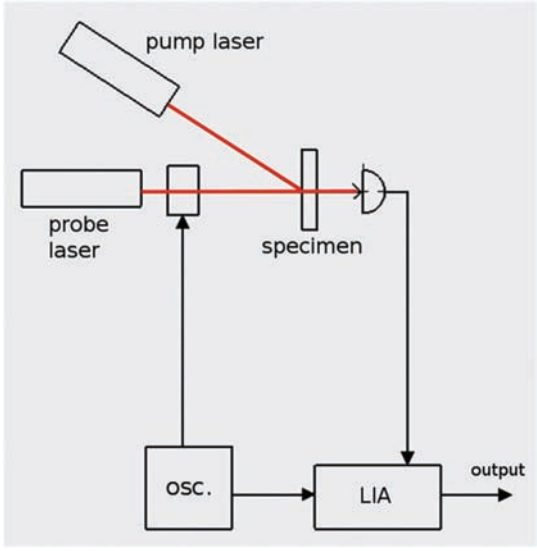

Figure 5.11 A Pockels cell modulates the probe beam. The light path of the pump beam and the light path of the probe beam are provided with a polarizer (not shown here).

linearly polarized. Under the influence of the Pockels cell, the polarization of the probe beam changes from left circularly polarized to right circularly polarized in a periodic way.

5.3.2 Quadratic electro-optic effect: the Kerr effect

In contrast to the Pockels effect, which is restricted to crystal classes of low symmetry, all crystals exhibit the quadratic electro-optic effect.[21] This is another physical effect and is named after the Scottish scientist.

Written in contracted notation, the dependence of the small deviations of the refractive indices on the applied electric field can be denoted as

$$\begin{bmatrix} \Delta\left(\frac{1}{n^2}\right)_1 \\ \Delta\left(\frac{1}{n^2}\right)_2 \\ \Delta\left(\frac{1}{n^2}\right)_3 \\ \Delta\left(\frac{1}{n^2}\right)_4 \\ \Delta\left(\frac{1}{n^2}\right)_5 \\ \Delta\left(\frac{1}{n^2}\right)_6 \end{bmatrix} = \begin{bmatrix} s_{11} & s_{12} & s_{13} & s_{14} & s_{15} & s_{16} \\ s_{21} & s_{22} & s_{23} & s_{24} & s_{25} & s_{26} \\ s_{31} & s_{32} & s_{33} & s_{34} & s_{35} & s_{36} \\ s_{41} & s_{42} & s_{43} & s_{45} & s_{46} & s_{46} \\ s_{51} & s_{52} & s_{53} & s_{54} & s_{55} & s_{56} \\ s_{61} & s_{62} & s_{63} & s_{64} & s_{65} & s_{66} \end{bmatrix} \begin{bmatrix} E_1 \\ E_2 \\ E_3 \end{bmatrix}. \tag{5.13}$$

To measure the quadratic effect, the signal is detected at the second harmonic of the modulation frequency ($2f$ detection). The effect is not limited

to crystals, but can be observed in liquids as well. A sophisticated experimental setup to accomplish this using lock-in amplification was presented by Bartolini et al.[23]

References

1. J. McCord, "Progress in magnetic domain observation by advanced magneto-optical microscopy," *J. Physics D: Applied Physics* **48**, 333001 (2015).
2. W. Voigt, "Doppelbrechung von im Magnetfeld befindlichem Natriumdampf in der Richtung normal zu den Kraftlinien" ("Birefringence of sodium vapor in a magnetic field along a direction perpendicular to the lines of force"), *Nachr. Kgl. Ges. Wiss. Göttingen*, 355–359 (1898) [cited according to https://de.wikipedia.org/wiki/Voigt-Effekt, accessed 19th August 2016].
3. A. A. Cotton and H. Mouton, "Nouvelle propriété optique (biréfrigence mgnétique) de certains liquids organiques non colloidaux," *Comptes Rendus hebdomadaires des Séances de l'Académie des Sciences Paris* **145**, 229–231 (1907) [cited according to https://de.wikipedia.org/wiki/Cotton-Mouton-Effekt, accessed 19th August 2016].
4. A. A. Cotton and H. Mouton, "Sur la biréfringence magnétique des liquids organiques," *Comptes Rendus hebdomadaires des Séances de l'Académie des Sciences Paris* **145**, 870–872 (1907) [cited according to https://de.wikipedia.org/wiki/Cotton-Mouton-Effekt, accessed 19th August 2016].
5. M. Faraday, "On the magnetization of light and the illumination of magnetic lines of force," *Phil. Trans.* **136**, 1–20 (1846) [cited according to McCord].
6. J. Kerr, "On rotation of the plane of polarization by reflection from the pole of a magnet," *Phil. Mag.* **3**, 321–343 (1877) [cited according to McCord].
7. P. Weinberger, "John Kerr and his effects found in 1877 and 1878," *Philosophical Magazine Letters* **88**(12), 897–907 (2008).
8. A. B. Marchant, *Optical Recording: A Technical Overview*, Addison-Wesley Publishing Company, Reading-Menlo Park-New York (1990).
9. T. W. McDaniel and R. H. Victora, *Handbook of Magneto-optical Data Recording: Materials, Subsystems, Techniques*, Noyes Publications, Wetwood, New York (1997).
10. H.-J. Winkelhahn, H. H. Winter, and D. Neher, "Piezoelectricity and electrostriction for dye-doped polymer electrets," *Applied Physics Letters* **64**(11), 1347–1349 (1994).
11. H.-J. Winkelhahn, T. Pakula, and D. Neher, "Investigations of the viscoelastic properties of thin polymer films by electromechanical interferometry," *Macromolecules* **29**(21), 6865–6871 (1996).

12. M. Levitus, G. Glasser, D. Neher, and P. F. Aramendía, "Direct measurement of the dipole moment of a metastable merocyanine by electromechanical interferometry," *Chemical Physics Letters* **277**, 118–124 (1997).
13. W. P. Mason, *Piezoelectric Crystals and their Applications to Ultrasonics*, Van Nostrand, Princeton, New Jersey (1956).
14. H. F. Tiersten, *Linear Piezoelctric Plate Vibrations*, Plenum Press, New York (1969).
15. A. Arnau, Ed., *Piezoelectric Transducers and Applications*, Springer-Verlag GmbH, Berlin-Heidelberg-New York (2004).
16. W. K. H. Panofsky and M. Phillips, *Classical Electricity and Magnetism*, Dover Publications, Mineola, New York (2005).
17. G. Kloos, "The correction of interferometric measurements of quadratic electrostriction for cross effects," *J. Physics D: Applied Physics* **28**, 939–944 (1995).
18. G. Kloos, *Maxwell Stresses and Dielectric Materials*, Trans Tech Publications, Zurich (2008).
19. R. Yimnirun, P. J. Moses, R. J. Meyer, Jr., and R. E. Newnham, "A single-beam interferometer with sub-angström displacement resolution for electrostriction measurements," *Measurement Science and Technology* **14**, 766–772 (2003).
20. G. Kloos, "Design of a Mach–Zehnder interferometer for the measurement of electrostrictive strains," *Measurement Science and Technology* **7**, 1–5 (1996).
21. T. A. Maldonado, "Electro-optic Modulators," in *Handbook of Optics II: Devices, Measurements, and Properties*, M. Bass, Ed., McGraw-Hill, New York (1995).
22. T. Dartigalongue and F. Hache, "Precise alignment of a longitudinal Pockels cell for time-resolved circular dichroism experiments," *J. Optical Society of America B* **20**(8), 1780–1787 (2003).
23. P. Bartolini, A. Taschin, R. Eramo, and R. Torro, "Optical Kerr effect experiments in complex fluids," Chapter 2 in *Time-Resolved Spectroscopy in Complex Liquids: An Experimental Perspective*, R. Torre, Ed., Springer Science+Business Media, New York, pp. 73–127 (2008).

Chapter 6
Infrared Thermography

6.1 Photothermal Radiometry

A classical experimental configuration for a photothermal radiometry[1] setup is depicted in Fig. 6.1. A laser is directed to a sample that is to be measured. The laser intensity is modulated mechanically using a chopper wheel. A signal derived from this chopper wheel serves as the reference signal for the lock-in amplifier.

The lens images the surface of the sample onto a detector. This allows for remote measurement of the sample temperature, which is modulated by the incident laser radiation. Lock-in amplification provides information on the amplitude and phase of this variation in temperature. The specimen under test is mounted on a translation stage so that different points on the surface of the sample can be measured in subsequent steps.

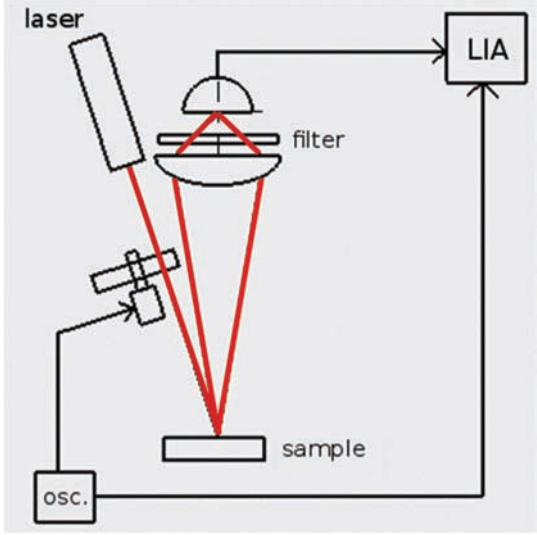

Figure 6.1 Experimental setup for photothermal radiometry.

6.2 Optically Induced Lock-in Thermography

Modern instrumentation makes it possible to take pictures of an irradiated surface. These instruments are employed in the field of nondestructive testing. Optical radiation is provided using halogen lamps (Fig. 6.2). The temperature on the surface is recorded by an infrared camera. Unlike the instrumentation previously described, the images are then processed by applying discrete Fourier transforms (DFTs) to the data. In this way, amplitude images and phase images, which describe the changing temperature distribution, are generated as output.

This method is called optically induced lock-in thermography, or phase-sensitive thermography, and is a tool used for quality control in industrial applications. An example of products being investigated with this method are fiber compounds.

6.3 Ultrasonic Lock-in Thermography

Ultrasonic lock-in thermography is similar to optically induced lock-in thermography. The difference is the process of periodic excitation: An ultrasonic transducer fixed to the specimen is used to modulate the sample under study (Fig. 6.3). The amplitude image and the phase image can provide information on delamination or on defects below the surface.

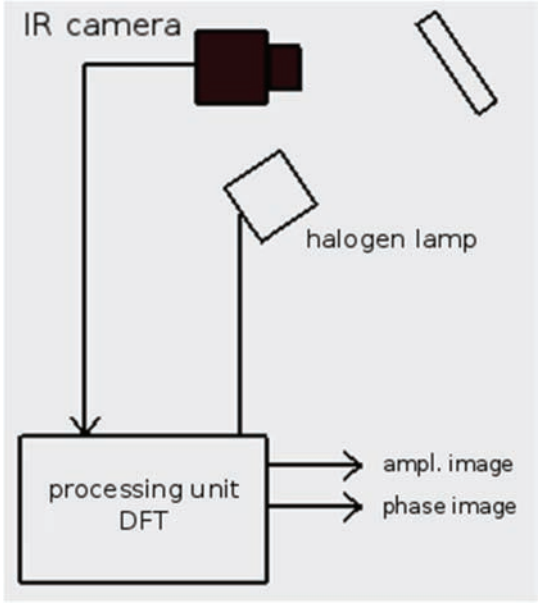

Figure 6.2 Optically induced lock-in thermography setup. Halogen lamps illuminate a sample, which is measured using an infrared camera. Using discrete Fourier transforms, an amplitude image and a phase image are generated.

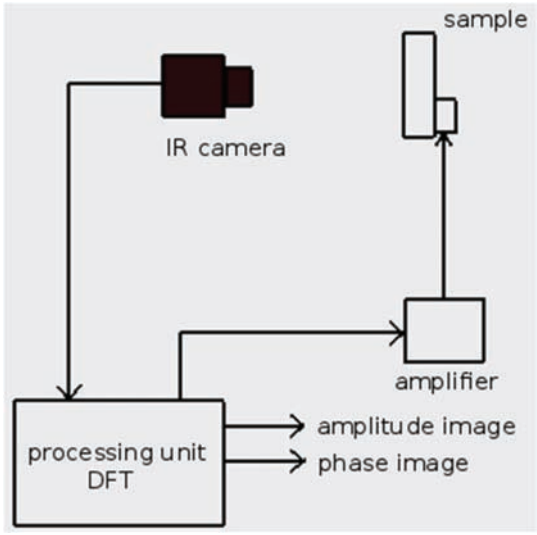

Figure 6.3 Setup for ultrasonic lock-in thermography. An ultrasonic transducer is fixed to the sample, which is measured using an infrared camera. Discrete Fourier transforms are applied to process the input images.

References

1. P.-E. Nordal and S. O. Kanstad, "Photothermal radiometry," *Physica Scripta* **20**, 659–662 (1979).

Chapter 7
Laser Wavelength Stabilization

Figure 7.1 depicts the scheme of a feedback loop that underlies many servo systems used to stabilize the frequency of optical lasers. This chapter presents examples of the ways this stabilization can be realized. Basically, the scheme consists of a wavelength comparator that generates the error signal for the feedback loop by processing a reference wavelength and the actual wavelength of the laser. This error signal is fed back to the loop, and a transducer is employed to change the laser cavity slightly to bring the error in frequency to zero.

7.1 Laser Stabilization Using a Fabry–Pérot Cavity

A generic scheme of the feedback loop for stabilization of the wavelength[1] can be recognized in the experimental configuration of Fig. 7.2. Here, a Fabry–Pérot interferometer serves as the reference. Its wavelength is modulated around its reference value, making use of a piezoelectric component in the longitudinal configuration (Fig. 5.7). The induced sinusoidal modulation is

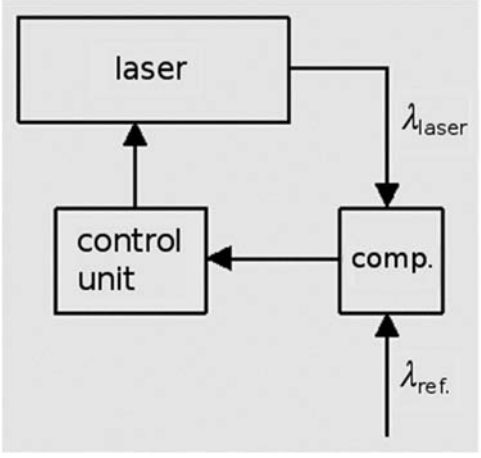

Figure 7.1 Feedback loop to stabilize the wavelength of the laser by comparing it to a reference wavelength.

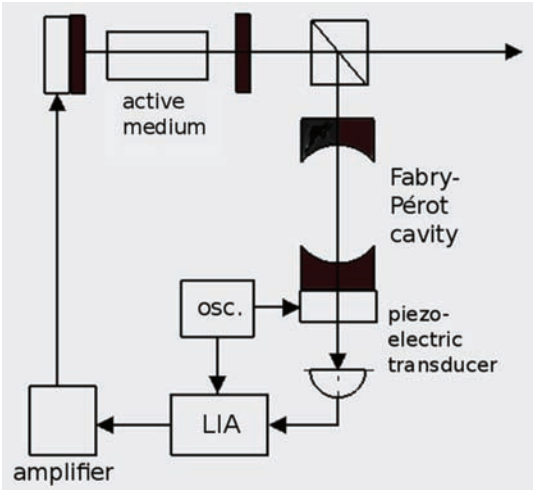

Figure 7.2 Laser wavelength stabilization setup comprising two resonator mirrors and an active medium. A Fabry–Pérot interferometer serves as a wavelength reference. A piezo-electric transducer mounted on one of the resonator mirrors closes the feedback loop.

helpful when applying lock-in techniques. The feedback loop is finally closed by another piezoelectric transducer that moves one mirror of the laser resonator and reduces the difference between the wavelength of the Fabry–Pérot interferometer and the wavelength of the laser until the laser resonator operates at the wavelength of the interferometer.

The piezoelectric transducer is shown in Fig. 7.3, which is not to scale. The figure displays an electromechanical configuration with cylindrical symmetry, in which the transversal effect is exploited.

To better understand the operation of the interferometer, it is helpful to think of its intensity-versus-wavelength function in the vicinity of the reference wavelength as a peak described by a quadratic function. Let us recall that the lock-in amplifier allows us (in an approximation) to measure the n^{th} derivative. If the lock-in amplifier is tuned to the modulation frequency, we measure the first derivative of the quadratic curve, i.e., a straight line. The point of operation is at the wavelength of the unmodulated Fabry–Pérot interferometer.

This property of a Fabry–Pérot cavity—its ability to provide a wavelength reference—is also exploited in the configuration shown in Fig. 7.4, which shows an approach often referred to as the Pound–Drever–Hall technique.[2] Periodic modulation is introduced into the optical setup with the help of a phase modulator. The phase modulator can be a Pockels cell, for example.

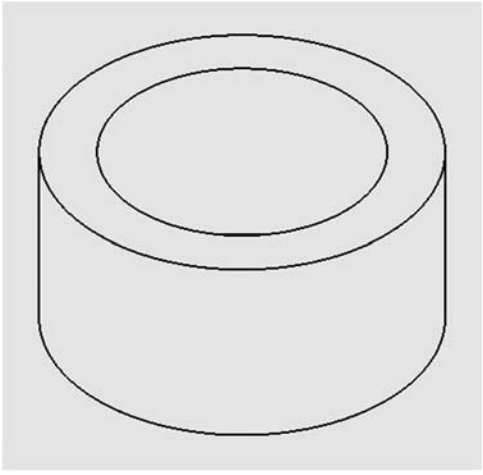

Figure 7.3 Piezoelectric transducer with cylindrical symmetry. The electrodes are on the inner and on the outer side of the cylinder.

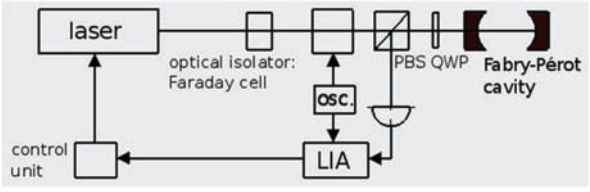

Figure 7.4 An oscillator drives a phase modulator and also provides the reference signal to the lock-in amplifier. Before the light enters the Fabry–Pérot cavity, it passes through a polarizing beamsplitter (PBS) and a quarter-wavelength plate (QWP).

7.2 Laser Containing a Gas Absorption Cell

Locking a gas laser to a specific frequency is an example illustrating an application of detection at $3f$, i.e., at the third harmonic of the modulation frequency, with lock-in amplifiers. The laser cavity contains an absorption cell filled with a gas, e.g., iodine vapor. Let us assume that, as a result of selective absorption, small peaks—which are characteristic of the gas—appear in the laser intensity function, which is recorded as a function of the cavity length. The aim now is to lock the laser to the frequency represented by one of these characteristic peaks.

In the close vicinity of the peak, this intensity function can be modeled as the sum of a Lorentzian function for the absorption peak and a quadratic function for the background:

$$I(x) = \frac{\gamma^2}{x^2 + \gamma^2} + ax^2 + bx + c, \tag{7.1}$$

where γ represents the full-width at half-maximum (FWHM) of the Lorentz curve.

What we need to close the feedback loop is an appropriate error signal that allows for stable locking of the frequency. A function that crosses the horizontal axis at zero provides such an error signal. It features well-defined positive and negative regions. In contrast to a quadratic function, for example, this function provides direct information to the servo system concerning the correct direction in which the control circuit has to react to bring the deviation to zero.

If we look at the third derivative of the intensity function, we have

$$\frac{d^3I}{dx^3} = 24\gamma^2 x \frac{\gamma^2 - x^2}{(x^2 + \gamma^2)^4}. \tag{7.2}$$

This is a function that is point symmetric with respect to the point of operation:

$$\frac{d^3I(-x)}{dx^3} = -\frac{d^3I(x)}{dx^3}. \tag{7.3}$$

It is also worth noting that in Eq. (7.2) there is no dependence on the background, as described by the quadratic function.

The next step involves considering how to obtain this third derivative of the intensity function. Referring to Chapter 2, we can make use of the result that (in a certain approximation) the third derivative can be realized by lock-in detection at $3f$, i.e., at the third harmonic of the fundamental frequency. This method is sometimes called third-derivative locking[3] and is applied in iodine-stabilized lasers, for example.

References

1. W. Demtröder, *Laser Spectroscopy: Basic Concepts and Instrumentation* Springer-Verlag GmbH, Berlin-Heidelberg-New York (1996).
2. E. D. Black, "An introduction to Pound–Drever–Hall laser frequency stabilization," *American J. Physics* **69**(1), 79–87 (2001).
3. D. P. Blair and P. H. Sydenham, "Phase sensitive detection as a means to recover signals buried in noise," *J. Physics E: Scientific Instruments* **8**, 621–627 (1975).

Chapter 8
Advanced Microscopy

In a traditional field of optics, lock-in amplifiers are used if the signal-to-noise ratio can be improved by modulation techniques. Application examples from different branches of optics are provided in this chapter to illustrate this idea.

8.1 Scanning Tunneling Optical Microscope and Fabry–Pérot Interferometer

In the experimental setup in Fig. 8.1, modulation is introduced into the experiment by modulating the laser at 10 kHz using an acousto-optic modulator.[1,2] In this example, a helium neon laser is used as a light source, and the laser light is directed to the prism shown in the figure. The purpose of this prism is to fold the optical path inside the Fabry–Pérot cavity that is formed by the semitransparent plate and the reflecting mirror, on which a piezoelectric transducer is mounted. Another piezoelectric transducer (not shown in the figure) is fixed to the apex of the prism.

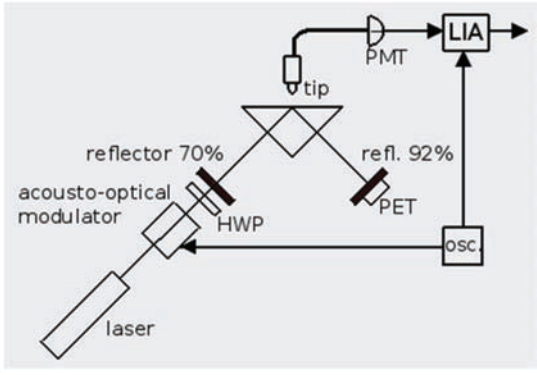

Figure 8.1 A prism is positioned inside the interferometer formed by two mirrors with different reflectivities. An acousto-optical modulator modulates the laser intensity that enters the interferometer cavity after passing through a half-wavelength plate (HWP). The position of one mirror of the interferometer can be varied using a piezoelectric transducer (PET). Using an optical fiber, the light is guided to a photomultiplier tube (PMT).

The instrument in Fig. 8.1 can be considered as a combination of a scanning tunneling optical microscope and a Fabry–Pérot interferometer. The tunneling microscope has a thin dielectric tip, which is used as a means to look inside the Fabry–Pérot resonator. The microscope detects the evanescent field over the prism surface. Equipped with piezoelectric transducers, this instrument allows for mapping of the evanescent field. Making use of a tapered fiber, the light is guided to a cooled photomultiplier tube, where it is detected. The detected light serves as an input signal to the lock-in amplifier, while the signal fed to the acousto-optic modulator serves as a reference.

8.2 Polarization-Contrast Confocal Microscope

Figure 8.2 displays the configuration of a confocal microscope that has been modified to perform polarization–optical measurements.[3] The instrument analyzes the state of polarization of the light that quantitatively impinges on the photomultiplier tube.

The Soleil–Babinet compensator acts as a quarter-wave plate that has two functions: (1) to provide circularly polarized light and (2) to be the first component of the electro-optic rotating analyzer. Other polarization–optical components used in this instrument are an electro-optical modulator, which is realized as a Pockels cell, and a polarizer. Unlike the instruments in the previously shown configurations, a saw-tooth wave is used here instead of a sinusoidal wave.

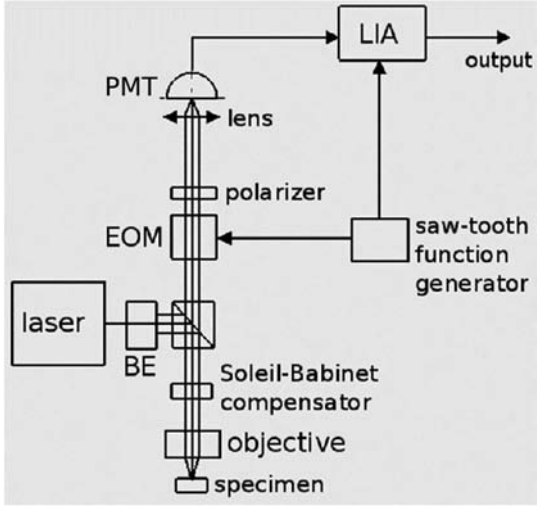

Figure 8.2 A laser used as a light source. Before the laser light enters the microscope, it passes through a beam expander (BE). A saw-tooth function generator drives an electro-optical modulator (EOM) and provides a reference signal to the lock-in amplifier.

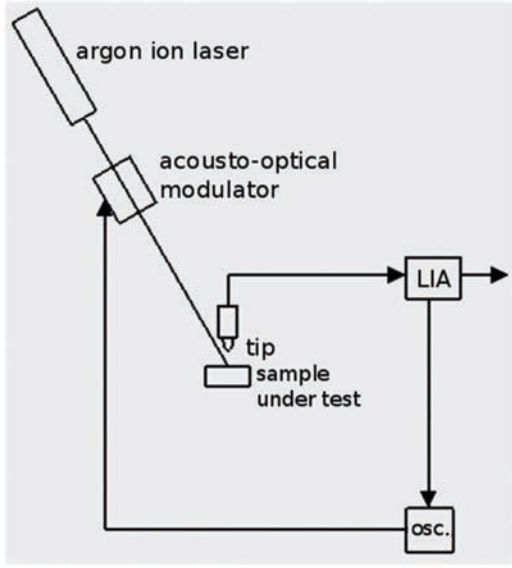

Figure 8.3 The light of the argon ion laser induces photothermal displacements in the specimen, which are detected using a lock-in amplifier.

8.3 Scanning Tunneling Microscope and Photothermal Displacements

The purpose of the instrument shown in Fig. 8.3 is to measure photothermal displacements (of a sample under test) that are induced by the irradiation of the sample with an argon ion laser.[4] To introduce modulation into the experiment (as a prerequisite to applying the lock-in technique), intensity modulation is performed using an acousto-optic cell.

Periodic thermal expansion is observed with a scanning tunneling microscope that is operated in constant-current mode. This implies that the distance from the tip to the specimen is kept constant by the feedback loop. The voltage of the piezoelectric tube, which is used as the actuator to close the feedback loop, can therefore serve as a direct measure for the displacement of the specimen.

References

1. D. Courjon, C. Bainier, and F. Baida, "Seeing inside a Fabry–Pérot resonator by means of a scanning tunneling optical microscope," *Optics Communications* **110**, 7–12 (1994).
2. F. Baida, C. Bainier, and D. Courjon, "Interférometrie haute resolution par microscopie optique en champ proche," *Microscopy, Microanalysis, Microstructures* **5**, 409–425 (1994).

3. F. Massoumian, R. Juskaitis, M. A. A. Neil, and T. Wilson, "Quantitative polarized light microscopy," *J. Microscopy* **209**(1), 13–22 (2003).
4. F. Depasse, N. Trannoy, and P. Grossel, "Fourier transform applied to alternating temperature calculation," *Microscopy, Microanalysis, Microstructures* **8**, 21–36 (1997).

Chapter 9
Other Applications

There are many applications of lock-in amplifiers that were not considered in this introductory text. Some of these are briefly mentioned here. One such application is experiments in the field of photoacoustic spectroscopy,[1] which are often based on lock-in techniques. Photoelastic modulators[2] provide many possibilities in the design of experiments that use periodic modulation as a prerequisite to detecting small or weak signals in noise. Magnetostriction is a physical effect that is studied using lock-in amplifiers. Being a quadratic effect as well, magnetostriction can be considered as analogous to electrostriction from a macroscopic point of view and is therefore also measured at the second harmonic of the modulation frequency. Finally, there is the vast and growing field of applications of lock-in amplifiers in laser spectroscopic systems.[3] One aim of this tutorial text is to provide an introduction to the technical literature on these subjects.

References

1. D. A. Skoog, *Principles of Instrumental Analysis*, Saunders College Publishing, Philadelphia (1985).
2. J. M. DiNitto and J. M. Kenney "Novel technique for improvement in calibration of the photoelastic modulator in circular and linear dichroism spectroscopy," *Applied Spectroscopy* **67**(1), 40–48 (2013).
3. W. Demtröder, *Laser Spectroscopy: Basic Concepts and Instrumentation* Springer-Verlag GmbH, Berlin-Heidelberg-New York (1996).

Index

Dr. Gerhard Kloos is a physicist. He received his Ph.D. from Eindhoven University of Technology, where he worked on modulation laser interferometry and electromechanics. He has published several scientific papers on optical technology and materials science, and three books on optical design, including *Matrix Methods for Optical Layout* (SPIE Press, 2007). He does research at an industrial enterprise where he develops optical systems.